[redacted]

CLASSIFICATION CHANGE
To UNCLASSIFIED
By authority of GSI - Ex 11652
Changed by L Burley Date 12/3/62
Classified Document Master Control Station, NASA
Scientific and Technical Information Facility

14827

Copy No. 07

Copy #1

SID 62-1151

PRELIMINARY REPORT OF TRANSIENT PRESSURES MEASURED ON THE 0.055 SCALE APOLLO PRESSURE MODEL (PSTL-1) IN NAA TRISONIC WIND TUNNEL [U]

NAS9-150

September 1962

4.5.5.1

Approved by

D. J. Gildea

D. J. Gildea
Manager,
Flight Technology

[redacted]

This document contains information affecting the national defense of the United States within the meaning of the Espionage Laws, Title 18 U.S.C. Sections 793 and 794. Its transmission or revelation of its contents in any manner to an unauthorized person is prohibited by law.

Downgraded at 3 year intervals; declassified after 12 years; DOD DIR 5200.10.

NORTH AMERICAN AVIATION, INC.
SPACE and INFORMATION SYSTEMS DIVISION

[redacted]

[redacted]

FOREWORD

The work on this report was done under the NASA Apollo contract NAS9-150.

This report was prepared by the System Dynamics Group of Applied Sciences, Space and Information Systems Division.

ABSTRACT

This report contains information on the transient pressure loads to be expected on a Saturn C-1 vehicle with an Apollo payload. The measurements were made on a 0.055 scale wind tunnel model in the Mach number range from 0.7 to 3.5 at 0, 2, 4 and 6 degrees angle of attack. The program included tests on four model configurations, which included two proposed Launch Escape System configurations, one a supersonic noise probe replacing the LES and one with no LES. The reduced data contained in this report are for a full scale vehicle on a 300 mile orbit trajectory. The data are presented as equivalent overall sound pressure levels for all data points and as 1/3 octave band spectrums levels (1 to 1000 cps) for certain selected points.

CONTENTS

CONFIDENTIAL

ILLUSTRATIONS

CONFIDENTIAL

TABLES

I. INTRODUCTION

Analyses of structural vibration in aircraft and in spacecraft during atmospheric portions of flight, have proven that sonic excitation is the predominate source of local vibration. The excitation may be from an acoustic source (noise radiated from booster engine exhaust at launch) or from a psuedo-acoustic source (unsteady aerodynamic flow during atmospheric flight). Calculated estimates by NAA and preliminary wind tunnel model tests by NASA (Reference 2) indicated that the "acoustic" environment created by the unsteady aerodynamic flow would be an order of magnitude greater than that caused by the booster engines at launch. The NASA study also indicated that during transonic flight, in the vicinity of the shoulder between the command module and service module, the boundary layer might detach and then re-attach to the spacecraft surface in a random manner and would cause localized, large magnitude, fluctuations in static pressure.

A wind tunnel test program was established to study the phenomena and to further define the acoustic and buffet loads. The program utilized a 0.055 scale model of the C-1 launch configuration as described in Reference 1. The model was designated as number PSTL-1 and is shown in Figure 1. The program objectives were to: (1) determine the magnitudes and spectral distribution the broad band, random fluctuating pressures on the spacecraft and booster stages; (2) study the characteristics of pressure pertubations on the surface due to boundary layer detachment; and (3) evaluate the effect of Mach number and angle of attack on both. The objectives were expanded to evaluate the effect of a proposed drag washer, to be located on the launch escape engine for stability purposes, on the transient pressures; and, at the request of NASA-MSFC, to evaluate the transient pressure distribution on the S-IV booster stage as influenced by local surface structure.

The first part of the program was conducted in the NAA-Los Angeles Division, Trisonic Wind Tunnel. Subsequent tests will be conducted in the Ames Research Center 14' x 14' and 9' x 7' wind tunnels.

This report includes only those data from measurements made on the Apollo Section of the model, on the surface of the S-IV and S-I stages immediately aft of interface shoulders, and from the noise probe (Meas. 1-13 and 20, Table 1). Subsequent tests will be reported individually but will include data from the first test which are not included in this report. A final report will summarize and relate the data from all PSTL-1 tests.

[redacted]

II. MODEL DESCRIPTION

The model consists of a 0.055 scale replica of the Saturn C-1 booster minus the aft end of the S-I stage (Reference 1) with the Apollo payload. The model was sting mounted and instrumented with pressure transducers per Figure 2. Tests were conducted with the following configurations:

A. No Launch Escape System (LES)

B. Noise Probe (substituted for LES)

C. Launch Escape System (LES)

D. LES with Washer

[redacted]

III. INSTRUMENTATION - TRANSIENT PRESSURE

A. GENERAL

The objectives required that a measurement system be utilized which would provide frequency response from dc to an estimated 200 kc. The dc response was required to measure local static pressure and the extremely low frequency changes in local static pressure that would occur around the model shoulders in event of boundary layer detachment. The required high frequency response was determined from calculated noise spectrums for the full scale Apollo which indicated significant transient pressure levels in frequency bands above 10 kc, and by the model scaling ratio of 0.055. A survey of equipment manufacturers revealed that a single system with the required frequency response capability was not available.

A system manufactured by Photocon Research Products of Pasadena, California was chosen as the best compromise. It has a frequency response which is essentially flat from dc to 10 kc. The decision to compromise the high frequency spectrum (above 20 kc) rather than the dc response was made after a review of the test objectives and available data. This review indicated that data were not available to define the absolute magnitude of the local static pressure during intervals of boundary layer detachment and relate it to the local mean static pressure (as normally determined from a static pressure orifice). However, the calculated broad band noise spectrum for the full size vehicle and the data from Reference 2 indicated that the maximum levels would occur in the 32 and 63 cps (mean center frequency) octave bands. On the model, the equivalent maximum levels would occur in the 300 and 1000 cps octave bands. The usuable 30 kc response of the Photocon system would provide data at frequencies several octaves above the peak in the distribution curve and the lack of data at higher frequencies would not seriously impair the program objectives.

The transducer sensitivity, ±15 psi, was selected after analysis of the tunnel operating characteristics and the calculated pressure distributions on the model which indicate that local static pressures ranging from -13.7 to +12.1 psig would occur (Reference 1).

B. LOCATIONS

A total of twenty-three points were instrumented during the tests. These included: twenty flush mounted transducers on the model for measuring surface pressures, which were located as shown in Figure 2

and Table 1; one transducer in the Noise Probe for measuring the free stream background noise in the tunnel; one transducer in the tunnel wall to detect and evaluate reported intermittent tunnel acoustic resonances; and one transducer rigidly mounted within the model, oriented with its axis perpendicular to the model longitudinal axis, to evaluate the vibration sensitivity of the transducers. All transducers systems were manufactured by Photocon Research Products except for transducer number 21, a Kistler microphone, which was furnished, installed, and evaluated by NASA-MSFC personnel.

C. DESCRIPTION

Each system, except for numbers 20 and 21, included a Model 524 pressure tranducer, a model 2573 cable termination network, and a model 605 Dynagage power supply. Measurement 20 used a Photocon model 374, ±5 psi transducer instead of model 524. The Model 524 transducer is a capacitive type with a one-quarter inch flush diaphragm in a one-half inch threaded housing as shown in Figure 3. The diaphragm has a nominal resonant frequency of 27 kilocycles, with five to six percent damping, as measured in a shock tube. A small, ceramic core, r-f inductor is also mounted in the transducer housing. The Dynagage power supply consists of a tunable r-f oscillator, an r-f detector, and a direct current cathode follower. The principle of operation is as follows: The diaphragm of the transducer in conjunction with an insulated electrode form an electrical capacitor which is connected to the transducer inductor to form a parallel tuned circuit. This tuned circuit is link coupled via a 50 ohm line to the oscillator and detector circuits in the Dynagage. A pressure applied to the transducer diaphragm causes a change in the associated capacitance and a corresponding change in the impedance of the tuned circuit at the excitation frequency. This variation in impedance is link coupled to the detector circuit and causes a change in the detector output voltage. The detector output is then cathode follower coupled to a low-pass filter to provide an audio output signal which is an analog of the pressure changes on the transducer diaphragm. The cable termination network is used to electrically tune the transducer-Dynagage link to a one-quarter wave length which minimizes cable losses and allows long cable lengths to be used.

Figure 4 shows the block diagram of a typical measurement and data recording circuit with provisions for pressure calibration and electrical frequency response checks. The principles of operation of the systems and the flat response at low frequencies permitted end to end sensitivity checks of the systems by application of an alternating pressure to the transducer, using the pressure calibrator as shown in Figure 5, or by the application of static pressure. During the tests the former method was used for the background noise measurements, transducers number 20 and 22, and the latter method proved more convenient for all flush mounted transducers since it did not require their removal from the model.

[redacted]

The Frequency Calibrator (Model FC-110), when substituted for the transducer, provides a means for evaluating the electrical frequency response of the system from 100 to 50,000 cps. Its circuitry includes a transducer coil and fixed capacitor with a reactance tube connected in parallel. Audio input voltages cause analogous capacitive changes in the reactance tube and a suitable input signal for the system.

The pressure and equivalent acoustic sensitivity for each Photocon system is shown in Table 2 and the relative composite frequency response of the system is shown in Figure 5.

An Ampex Model CP-100, one-inch tape recorder, which had a flat frequency response from dc to 20 kc in the FM record mode, was used for recording the signals from transducers 1 through 13 and 20. Signals from transducers 14 through 19 were recorded on an Ampex Model FR-100 one-inch recorder, utilizing simultaneous recording of each signal in an FM and direct record mode in order to obtain the required frequency response. The signals from the transducer used to monitor intermittent tunnel resonances and the transducer vibration sensitivity were recorded on a portable, two channel tape recorder. A multicircuit switch was inserted in the system between the Dynagage and the tape recorder (Cal. - Opr. Switch, Figure 4) to provide means for recording a 1 volt, 400 cps reference signal on all tape channels simultaneously. One channel on each one-inch recorder was used for voice notations prior to the test run and for recording a tunnel timing pip during the run.

D. SPECIAL PROCEDURES

The tape recorder specifications limit the allowable input voltage to ±1.5 volts dc or 1 volt rms to prevent overload distortion. The output voltage from the Dynagage with a static pressure on the transducer over 10 to 15 percent of the nominal transducer rated pressure would exceed this limitation. Simple attenuation of the Dynagage output would have severely limited the resolution of high frequency data because the dc pressure levels were normally considerably greater than the fluctuating pressure levels. It was known that a positive pressure on the transducer caused a negative voltage from the Dynagage and vice versa. Therefore, to retain maximum high frequency sensitivity, the local static pressure at each measurement point was determined from tunnel operating conditions and calculated static pressure distributions on the model. The calculated local static pressure was translated to an equivalent Dynagage output voltage. If this voltage exceed two volts, the Dynagage attenuator was adjusted accordingly. Then the output of the Dynagage was biased up to 1.5 volts dc with polarity opposite to the expected signal voltage. Then during the test run, the static pressure on the transducer caused the Dynagage dc output voltage to be near the center of the tape recorder input voltage range and retained the majority of the range for recording fluctuating pressure without distortion.

[redacted]

IV. OPERATIONS

A. TUNNEL OPERATING CONDITIONS:

The NAA-LAD trisonic wind tunnel is of the blow-down type. Eight large spheres are filled with compressed air which is released through a valve to provide the required flow conditions in the tunnel. A test run can be made every half hour, this being the time required to fill the spheres. A Mach range of 0.40 to 3.50 is obtainable, Mach number being controlled by adjusting the side walls to vary the nozzle shape just ahead of the test section. A total run time of approximately 17 seconds is normally achived, which allows a stabilized test time of 12 to 14 seconds.

Following are the tunnel operating conditions:

*$R_e(10^6)$	Mach Number	P_{T_o} psia	P_o psia	q psf	Estimated run time - secs
5.0	0.40	29	25.8	420	32
7.3	0.60	305	23.7	860	17
7.8	0.80	27	17.8	1140	17
8.0	0.90	26.3	15.3	1270	17
8.0	0.93	26	14.9	1300	17
8.1	0.96	26	14.4	1340	17
8.2	1.00	26	13.8	1385	17
8.4	1.06	26.2	12.7	1470	17
8.5	1.20	26.5	10.8	1600	17
10.0	1.50	32.5	8.9	2000	17
10.0	1.75	35		2020	17
11.0	2.00	41.7	5.5	2170	17
12.0	2.50	58	3.5	2145	17
12.0	3.00	74.6	2.1	1842	17
12.0	2.40	96.5	1.3	1565	11

*Reynolds numbers are based on command module diameter (8.47 in.)

B. PRELIMINARY OPERATIONS

The model, with all transducers, was installed in the tunnel. The continuity and the electrical frequency response of all transducer systems, excluding the transducer, was measured utilizing the Model FC-110,

[redacted]

Frequency Calibrator. The overall pressure sensitivity and linearity of each system was then checked. Static pressure was used for checking the sensitivity of the boundary layer transducers and the Model PC-120, Pressure Calibrator was used with the background noise transducers. The pressure sensitivity was re-checked at intervals during the test program to detect any changes. (Note: no significant changes were noted.) The ambient electrical noise level in each system was recorded at intervals during the program for subsequent evaluation.

[redacted]

V. TEST PROGRAM

A. DATA POINTS

Tests were conducted with the following model configurations: No tower, noise probe (replaced tower during these tests), plain tower, and tower with washer. Data were recorded at Mach numbers from 0.7 to 3.5 and angles of attack from 0 to +4 degrees as shown in Tables 3 through 6.

B. TEST CONDUCTION AND PROCEDURES

A fifteen second duration reference signal at one volt, 400 cps was recorded on all tape channels. Each Dynagage was balanced, its attenuator set and output biased in accord with calculated local static pressure levels. Tape recorders were started and then tunnel was started. Data samples of approximately seven seconds duration were obtained at two angles of attack during each run.

C. PROBLEM AREAS

No measurement systems were lost during the program, however erratic operation on measurement system 1 was traced to a loose cable connection and repaired. Some data were lost during early runs due to exceeding tape recorder input voltage limitations. In some cases this was due to incorrect estimation of local static pressure and in others to incorrect bias polarity.

VI. DATA REDUCTION

A. GENERAL

The data reduction procedures included the evaluation of static pressure levels (p), the overall rms level of fluctuating pressure ($\overline{p}$) and one-third octave band spectrums. Power spectral density plots were to be made of selected data samples, predominately those which exhibited erratically shaped one-third octave band spectrums. Such erracticness is usually an indication of a discrete frequency occurrence within that band such as would be caused by an oscillating shock wave. Data samples were visually inspected with an oscilloscope and low frequency oscillographic recordings were made of those which exhibited intermittent changes in dc level indicating detachment of the boundary layer.

B. DATA REDUCTION SYSTEM

One-third octave band spectrums were chosen as the primary form for analysis of fluctuating pressures, however, the quantity of data samples to be reduced and the length of the data sample (less than 7 seconds) required a unique analyzer to minimize data reduction time. The system, block diagramed in Figure 6, was fabricated by the Engineering Development Laboratories for this purpose. The signal voltages from the tape recorder, analogous of fluctuating pressures, were amplified and coupled to a Bruel & Kjaer, 1/3 octave band filter set which had mid-frequency filters from 12.5 cps to 40 KC. The signal was simulataneously coupled to all filters in parallel and the outputs individually rectified and averaged and connected to a multi-position, motor driven commutator. The averaged, filter outputs were then sequentially sampled and recorded on a dc recorder. The system provided a complete spectrum in 5 seconds. As noted in Figure 5, the time sequence of sampling filter outputs was from high frequency to low frequency. This arrangement was chosen to provide the longest averaging time before sampling the output of the lowest frequency filter. The linear dynamic range of the system was limited to 30 db by the rectifier and signal levels of less than 35 mv overall at the input could not be reduced. The accuracy of the system (within its linear range) was evaluated as equivalent to that achieved with a B & K, 1/3 octave band spectrum analyzer used in a standard operational mode. However, the Model 2305 Level Recorder in a dc record mode has very low frequency response and will not follow rapid level changes accurately. Fortunately, the spectrum shape of the fluctuating pressures were gradually sloped, so the recorder response did not degrade the program accuracy. The commutator had a

[redacted]

second circuit (not shown) which provided a position correlation pip to the recorder events channel for frequency identification of the recorded spectrum.

The dc and overall fluctuating levels (rms) were manually tabulated for each data sample.

[redacted]

VII. DATA PRESENTATION AND DISCUSSION

A. TUNNEL OPERATIONAL NOISE

The operational background noise in the tunnel was measured to evaluate its influence on the model boundary layer measurements. This noise was measured with a transducer mounted in a supersonic probe (Figure 1) which was substituted for the Launch Escape System on the model. Data were taken at zero angle of attack and Mach numbers from 0.7 to 3.5 as noted in Table 4. The tunnel noise was below the level of interference with the boundary layer measurements. At some subsonic velocities, a significant noise level was measured but analysis showed that it was all high frequency noise and was attributed to local effects on the noise probe and not tunnel noise.

A second transducer was mounted in the tunnel wall to detect a reported intermittent acoustic resonance in the tunnel and to evaluate the effect of such a discrete frequency noise on the model measurements. No such resonance condition was experienced during the program so the data from this transducer were not considered pertinent to the program and were not reduced.

B. TRANSIENT BOUNDARY LAYER PRESSURES

The predominate source of transient pressures on the Apollo Spacecraft will be the turbulent wake from the Launch Escape System (LES) impinging on the spacecraft structure. Data were recorded during test runs using the four model configurations listed in Section II. The data from model configurations A and B were for reference purposes in the study of the boundary layer detachment-reattachment (buffet) problem. The difference between configurations C and D was the drag washer located on the LES just forward of the engine nozzle fairing, as shown in Figure 1. The influence of the larger diameter of the washer, as compared to the nozzle engine fairing (ratio of 1.19 to 1), was to be evaluated.

Configurations C and D were tested at α = 0, 2, 4 and 6 degrees and at Mach numbers from 0.7 to 3.5 as shown in Tables 5 and 6.

The model transient pressures were evaluated as overall and one-third octave band pressures (psi, rms), corrected for the frequency response of the system (Figure 5) and translated to equivalent values for a full scale

[redacted]

vehicle. The model data above 18 KC were not included in the analysis because of limitations in accuracy of system calibration at higher frequencies. This in turn, limited equivalent full scale data to nominally 1000 cps. The tunnel free stream velocity (v) and dynamic pressure (q) at each Mach number and the equivalent parameters for a C-1 vehicle on a calculated trajectory to a 300 mile orbit are given in Tables 5 and 6. These values were used to scale the model data using following relationships:

$$\text{Frequency - } f_{FS} = f_M \left(\frac{d_M}{d_{FS}}\right)\left(\frac{v_{FS}}{v_M}\right)$$

$$\text{Power Spectral Density - } P(f)_{FS} = P(f)_M \left(\frac{q_{FS}}{q_M}\right)^2 \left(\frac{d_{FS}}{d_M}\right)\left(\frac{v_M}{v_{FS}}\right)$$

Overall and percentage band width levels (octave, 1/3 octave, etc.)-

$$+ \ \overline{p}_{FS} = \overline{p}_M \left(\frac{q_{FS}}{q_M}\right)$$

Where

f - frequency, cps

d - dimension, feet or inches

v - velocity, feet/sec

q - aerodynamic pressure, psi

P(f) - power spectral density, $\overline{p}$/cps

$\overline{p}$ = root means square pressure, psi

Subscripts M and FS denote respective model and full scale parameters.

The scaled pressures were then translated to equivalent sound pressure levels to facilitate plotting and data comparison.

SPL = 10 log 10 $\frac{\overline{p}^2}{p_r^2}$ db, where p_r is the acoustic reference pressure, 0.0002 dynes/cm^2 or 2.94 (10^{-9}) psi.

The variation in overall sound pressure level with velocity for a C-1 vehicle on a 300 mile orbit trajectory is shown in Figure 7 (M=0.7 to 1.2) and Figure 8 (M=1.0 to 3.5) for the washer off configuration and in Figures 9 and 10 for the washer on configuration. The velocity range was divided into two parts to allow better resolution in the transonic region.

Discontinuities in the curves indicate the loss of data points due to the signal overdriving the tape recorder.

The relative flatness of the curves (Figure 7 to 10), indicates that the spacecraft and booster will be subjected to high level, transient pressure loads during the entire period of subsonic, transonic and low supersonic flight with peak loads occurring in the transonic region. Variations in angle of attack will cause only minor increases in the levels on the leeward side of the vehicle and minor decreases in the levels on the windward side.

The maximum transient pressure loads at each measurement position, regardless of Mach number or angle of attack, for both configurations, are plotted as equivalent sound pressure levels in Figure 11. The figure shows that the maximum loads on the spacecraft will occur on the aft portion of the C/M and the forward portion of the S/M and that the maximum levels with washer on and washer off are 168 db and 166 db respectively. An average increase of 2 db in maximum transient pressure loads is evidenced all along the spacecraft, with the washer on, except in the nose cone area of the C/M. However, further analysis of Figures 7 through 10 shows that it is only around the C/M and the forward portion of the S/M that the increased levels are directly attributable to the increased wake turbulence caused by the washer. On the aft end of the S/M and on the adapter section (Positions 4-8), it is the influence of the washer on the spatial characteristics of the flow and the resultant relative magnitude and position of oscillating shock waves which cause the indicated difference. On the after portion of the S/M and on the adapter section, the levels show a tendency to be independent of the washer influence on the wake turbulence because of the isolation provided by a normal shock wave. However, the position and the magnitude of the shock wave is related to the flow conditions established with and without the washer and hence effect the local transient pressure loads, especially in the vicinity of measurement positions 4, 5 and 6. A complete analysis of the influence of the flow conditions on shock wave position and the effect on local transient pressure loads requires real time correlation between shock wave position (motion pictures) and measured characteristics, which were not available at subsonic and transonic velocities during this program.

The local transient pressure coefficients along the vehicle associated with the maximum loads of Figure 11 and the distribution of the transient pressure coefficient at $M = 1, \alpha = 0$ are shown in Figure 12.

The comparative influence of the washer on the frequency distribution of transient pressures is shown in Figure 13, One-third Octave Band Spectrums of Maximum Sound Pressure Levels and Figure 14, One-third Octave Band Spectrums of Sound Pressure Levels at $M = 1$, $\alpha = 0$. The direct influence of the washer on the vortice size within the turbulent wake and the associated spectrum distribution, is evident in the curves from transducers 1,

2 and 3 in Figure 14. These curves show a slight shift to lower frequencies with the washer on, in approximate proportion to that expected from the ratio of the nozzle fairing diameter to the washer ($d_n/d_w = 0.84$). This difference is less evident on transducer 1 than on 2 and 3, because of the relative position with respect to the vehicle center line. With the washer off, the spectrum shapes at measurement positions on the S/M, aft of Position 3, are very similar to those for transducers 1, 2 and 3. However, with the washer on, the peaks in the spectrums shift to a much lower frequency which indicates that the overall flow pattern and the spatial orientation of shock waves have changed and influence the spectral distribution. Further evidence of the influence of flow pattern on spectral distribution is provided in Figure 13, where the spectrums are associated with flow conditions which caused maximum overall levels, with and without washer. These curves cannot be directly compared because of differences in Mach number and angle of attack, but definite patterns, with and without washer, can be established.

Measurement 11 was located behind a simulated clamp for evaluating the effect of the clamp on local noise. The maximum overall levels, with and without washer, were the same (Figure 7) and the associated spectrum distributions (Figure 13) showed little dependence on the tower configuration. Comparison of measurements 11 and 5 at $\alpha = 0$ (Figure 14) provide the best indication of the local effects of the clamp on spectrum shape.

C. BOUNDARY LAYER DETACHMENT

All data, and especially that from measurements in the vicinity of the spacecraft shoulder, were visually inspected for occurrance of step changes in local static pressure indicative of boundary layer detachment and re-attachment. No evidence of this phenomona was found on configurations C and D, however the data from configurations A and B did provide examples which could be used for reference purposes. A typical example of this phenomona is shown in the oscillographic trace of Figure 15. This trace is the filtered signal (dc to 40 cps) from transducer 3 during a test with configuration B at Mach 0.89 and $\alpha = 0$. It is noted that the pressure decreases when the boundary layer detaches and returns to the original value when re-attachment occurs. In this instance the pressure fluctuation was equivalent to 46% of the aerodynamic pressure. The magnitude of the pressure fluctuation, the frequency of occurrence, and the relative position on the vehicle are dependent on flow condition and angle of attack (Ref. 2, 3 and 4). Since this phenomona was not noted on configuration C and D, it is assumed that the programed test conditions did not include the specific conditions required to induce boundary layer detachment on the vehicle with a tower attached.

The pressure fluctuations, which occur during boundary layer detachment, have little significance from a static stress standpoint because the

absolute magnitudes do not exceed those depicted by a static pressure distribution. However, they do have dynamic significance since they represent a local shock input which could excite structural vibration modes.

D. STATIC PRESSURE DISTRIBUTION

The static pressure distributions on the model were evaluated for all test conditions by standard procedures using static pressure orifices and manometers. The faired curves of these distributions at Mach 0.7 and 1.0 for $\alpha = 0$, are plotted in Figure 16 in terms of the static pressure coefficient, Cp. For comparison, the static pressure coefficients derived from the transient pressure transducers at M=0.89 and 1.0 are plotted as points. Displacement of the M=1.0 points from the M=1.0 curve can be attributed to measurement errors in the transient pressure system (due to erroneous bias settings, unbalance of tape recorder electronics and dc drift of system), local pressure pertubations not reflected in the static pressure distribution curve (curve was faired through regions in which static pressure orifices were not located) and because of the relative large area covered by the transducer diaphram.

VIII. SUMMARY AND CONCLUSIONS

The tests show that the spacecraft and the booster stages will be subjected to severe transient pressure loads throughout the periods of subsonic, transonic and low supersonic flight. These loads will be greatest in the vicinity of the shoulder on the spacecraft and will reach equivalent sound pressure levels of 168 db with the washer on the LES and 166 db with the washer off. The one-third octave band spectrums associated with these maximum levels indicate peak energy between 20 and 30 cps with the washer on and between 60 and 80 cps with the washer off.

The predominate effect of the washer is its influence on overall flow characteristics around the spacecraft which effects the spatial orientation and magnitude of normal shock waves and the frequency distribution of transient pressures on the S/M at $\alpha = 0$ and on the entire spacecraft when $\alpha \neq 0$.

The intermittent occurrance of the boundary layer detachment-reattachment (buffet) in the vicinity of the spacecraft shoulder at transonic speeds were not detected during tests with model configurations which included the LES. Data from tests with the LES removed were used to study the phenomona. Characteristic changes in local static pressure during "buffet" were compared to the static pressure distribution and it was observed that the buffet pressures were within the static pressure envelope and, hence, constitutes a dynamic load problem, but is not a static load factor.

Additional tests are required which provide finer Mach number steps and with complete photographic coverage to further define the overall flow characteristics, with and without the washer; the influence of the washer on the spatial orientation of normal shock waves; the influence of the shock waves on the magnitude and frequency spectra of transient pressures behind the shock waves; and to determine if "buffet" does occur at some Mach number not yet tested.

The severe acoustic environments predicted from these tests are not expected to constitute a structural fatigue problem because of the distribution of energy throughout a broad frequency spectrum and because of the short exposure time depicted for a trajectory to a 300 mile orbit. However, the response of the spacecraft structure to these loads will represent severe vibration environments for internal equipment which could cause intermittent malfunctions and/or failures necessitating mission abort.

IX. REFERENCES

1. SID 62-745, Pretest Report for the 0.055 Scale Apollo Pressure Model (PSTL-1) in the NAA Trisonic Wind Tunnel, 5 July 1962.

2. NASA TMX-607, Launch Vehicle Dynamics, A.G. Rainey and H.L. Runyon, December 1961.

3. NASA TMX-503, Steady and Fluctuating Pressures at Transonic Speeds on Two Space Vehicle Payload Shapes, C.F. Coe, March 1961.

4. NASA TMX-646, The Effects of Some Variations in Launch Vehicle Nose Cone Shape on Steady and Fluctuating Pressures at Transonic Speeds, C.F. Coe, March 1962.

[redacted]

Table 1. Pressure Transducer Locations on Model PSTL-1

Location				
Transducer Number	Model Station (Inches)	NASA (C-1) (Inches)	X_a (Inches)	ϕ (Degrees)
1	22.00	1844	1100	0
2	25.30	1784	1040	0
3	26.84	1756	1012	0
4	28.16	1732	988	0
5	29.48	1708	964	0
6	30.80	1684	940	0
7	32.12	1660	916	0
8	33.44	1636	892	0
9	26.84	1756	1012	180
10	28.16	1732	988	180
11	29.48	1708	964	270
12	52.957	1280	536	0
13	72.121	947	203	22.5
14	61.999	1116	372	0
15	67.647	1013	269	0
16	69.765	975	231	0
17	69.765	975	231	180
18	59.175	1167	423	22.5
19	67.647	1013	269	22.5
20	Noise Probe			
*21	67.647	1013	269	180
**22	Internal			

*All transducers were Photocon Model 524, ±15 psi with Dynagage power supplies, except for number 21 which was a Kistler Transducer furnished by NASA-MSFC for evaluation purposes.

**Vibration effect only, not exposed to pressure.

LOCATION REFERENCE

1. Model Station orgin is imaginary point ahead of L.E.S. Nose Cone.

2. NASA body station orgin is nozzle exit plane of S-1 stage in C-1 configuration.

3. Xa reference orgin is 1000 inches aft of Apollo C/M heat shield mold line.

4. The following body stations are coincident:

   Xa = 1000 inches
   NASA (C-1 B.S.) = 1744 inches
   Model Station = 27.5 inches

[redacted]

Table 2. Pressure and Equivalent Acoustic Sensitivity of Photocon Pressure Transducers

All sensitivities related to output of Dynagage with 200 ft.

R6-58 A/U cable and Model 2573 Cable Termination Network.

Transducer Number	Pressure Sensitivity psi/volt	Acoustic Sensitivity re 0.0002 M Bar
1	2.21	-103.5
2	2.5	-104.6
3	2.5	-104.6
4	2.17	-103.4
5	2.74	-105.4
6	2.06	-102.9
7	2.12	-103.2
8	2.64	-105.1
9	2.16	-103.3
10	2.24	-103.6
11	2.15	-103.3
12	2.3	-103.9
13	2.25	-103.7
20	.71	-104.2

Table 3. Configuration A

Mach Number	Velocity Model FPS	Velocity Full FPS	q Model PSF	q Full Scale PSF	Mach Number	Velocity Model FPS	Velocity Full FPS	q Model PSF	q Full Scale PSF
0.7	755	702	1033	387	1.2	1185	1200	1594	682
0.92	961	998	1363	610	1.998	1674	1950	2182	582
1.0	1042	1062	1403	630	3.014	2032	2880	1843	288

Table 4. Configuration B

Mach Number	Velocity Model FPS	Velocity Full FPS	q Model PSF	q Full Scale PSF	Mach Number	Velocity Model FPS	Velocity Full FPS	q Model PSF	q Full Scale PSF
0.7	747	702	988	387	1.2	1196	1200	1595	682
0.89	933	970	1255	595	1.505	1415	1490	2035	718
0.92	957	1005	1298	608	1.758	1560	1700	1941	670
0.96	984	1022	1324	615	1.998	1686	1950	2135	582
1.0	1031	1085	1405	634	2.494	1880	2400	2165	425
1.06	1099	1090	1485	647	3.014	2028	2880	1830	288
1.10	1132	1110	1520	659	3.464	2128	3500	1612	160

Table 5. Simple Tower Configuration C

Mach Number	Velocity Model FPS	Velocity Full FPS	q Model PSF	q Full Scale PSF	Mach Number	Velocity Model FPS	Velocity Full FPS	q Model PSF	q Full Scale PSF
0.70	755	703	1035	388	1.20	1205	1200	1590	682
0.89	940	974	1265	596	1.505	1415	1490	2010	718
0.92	965	997	1350	606	1.758	1555	1700	1970	670
0.96	1000	1020	1333	614	1.998	1680	1950	2125	582
1.0	1045	1066	1405	633	2.494	1880	2400	2170	435
1.06	1080	1090	1450	647	3.014	2030	2880	1440	288
1.10	1117	1110	1500	659	3.467	2120	3500	1630	160

Table 6. Tower & Washer Configuration D

Mach Number	Velocity Model FPS	Velocity Full FPS	q Model PSF	q Full Scale PSF	Mach Number	Velocity Model FPS	Velocity Full FPS	q Model PSF	q Full Scale PSF
0.70	770	703	1030	388	1.20	1205	1200	1590	682
0.89	945	971	1270	594	1.505	1410	1490	1960	718
0.92	960	1000	1350	608	1.758	1560	1700	1950	670
0.96	1000	1022	1335	615	1.998	1675	1950	2175	582
1.0	1047	1082	1410	635	2.494	1875	2400	2170	425
1.06	1085	1090	1455	647	3.014	2027	2880	1840	288
1.10	1125	1110	1505	659	3.467	2125	3500	1615	160

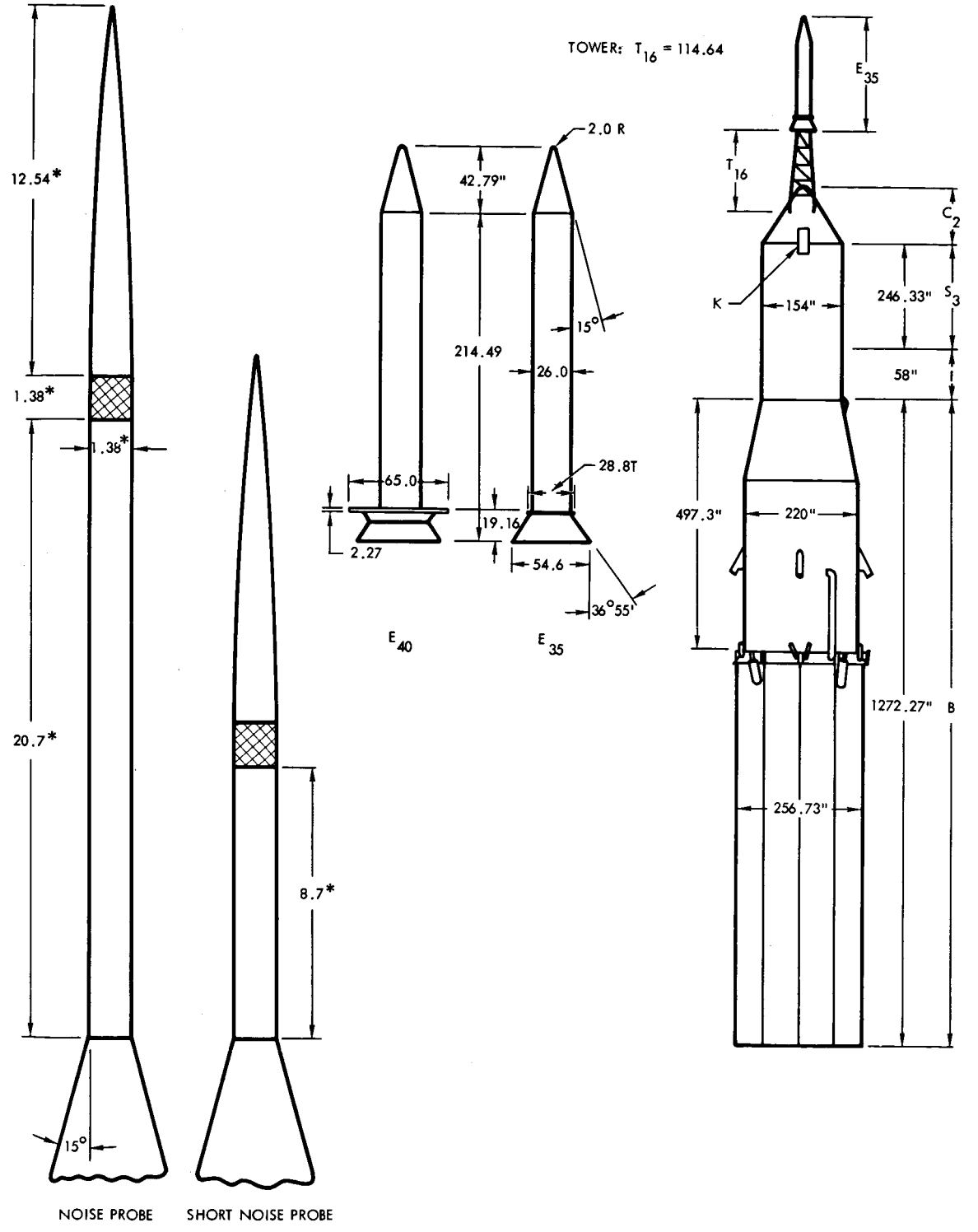

Figure 1. Model Description

CONFIDENTIAL

CONFIDENTIAL

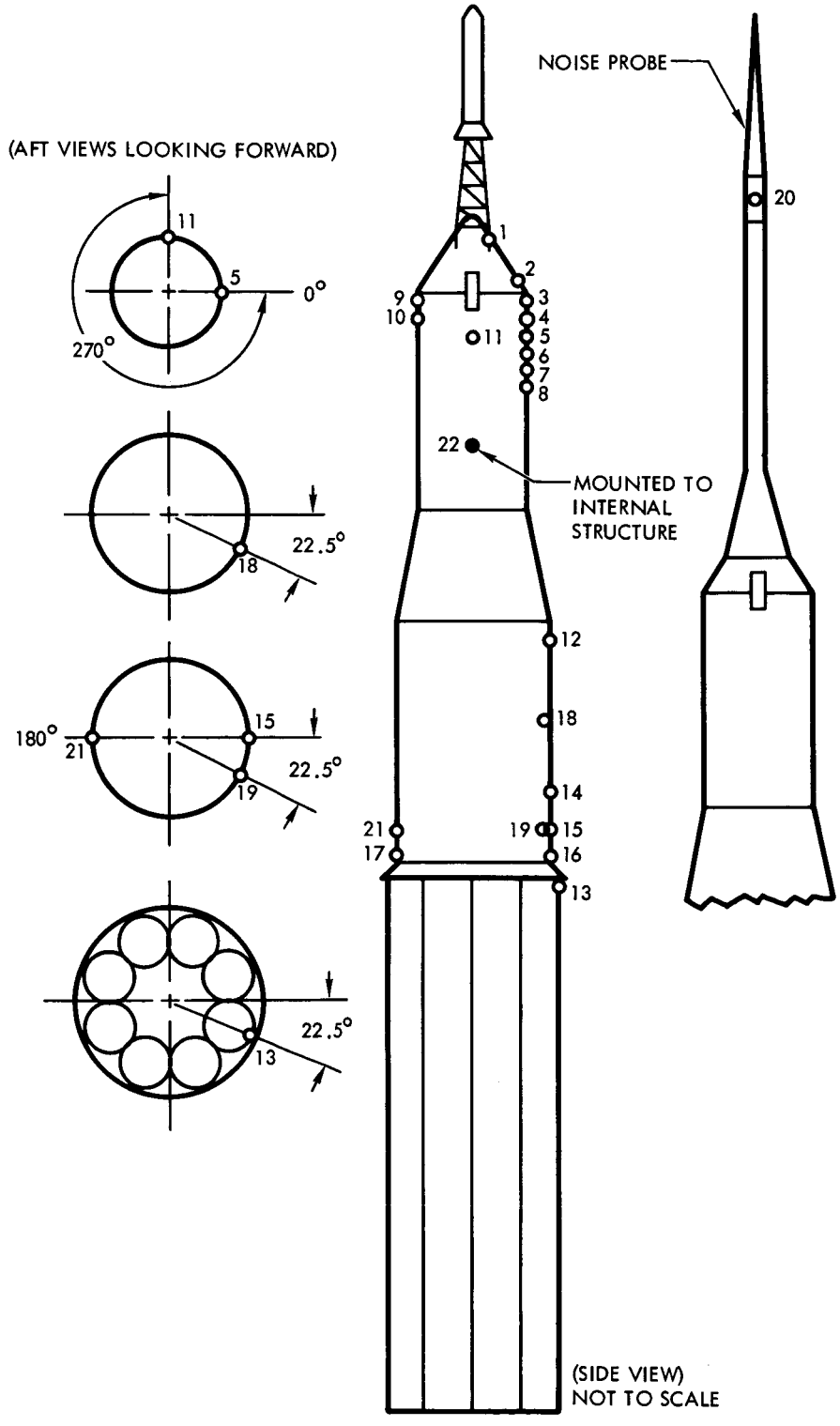

LOCATION OF PRESSURE TRANSDUCERS

Figure 2. Location of Pressure Transducers

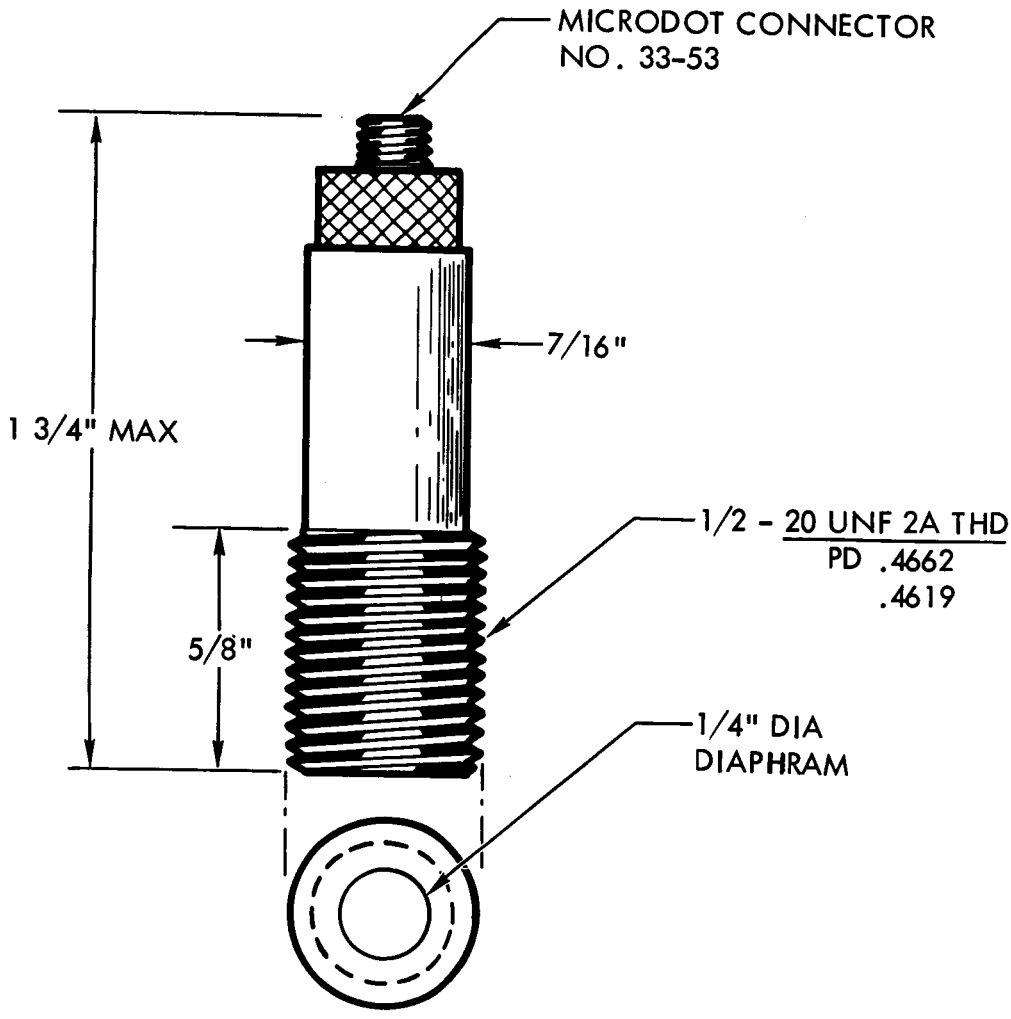

NOTES
1. SUPPLIED WITH CBM 10 FT CABLE WITH NO. 32-15 RIGHT ANGLE CONNECTOR
2. 1 HEX LOCK NUT 3/32 X 3/4 O.D.

Figure 3. Pressure Transducer

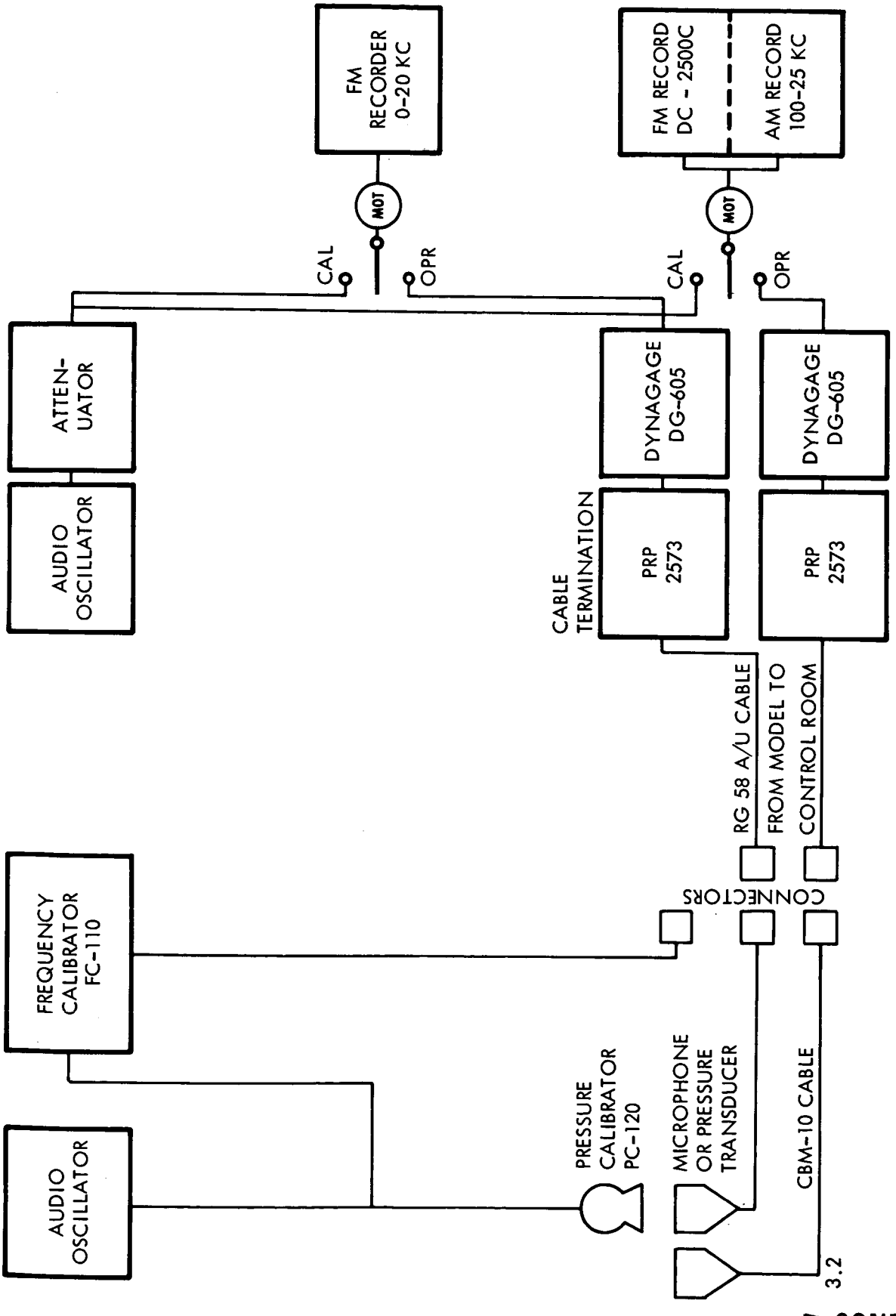

Figure 4. Data Gathering Circuit - Block Diagram

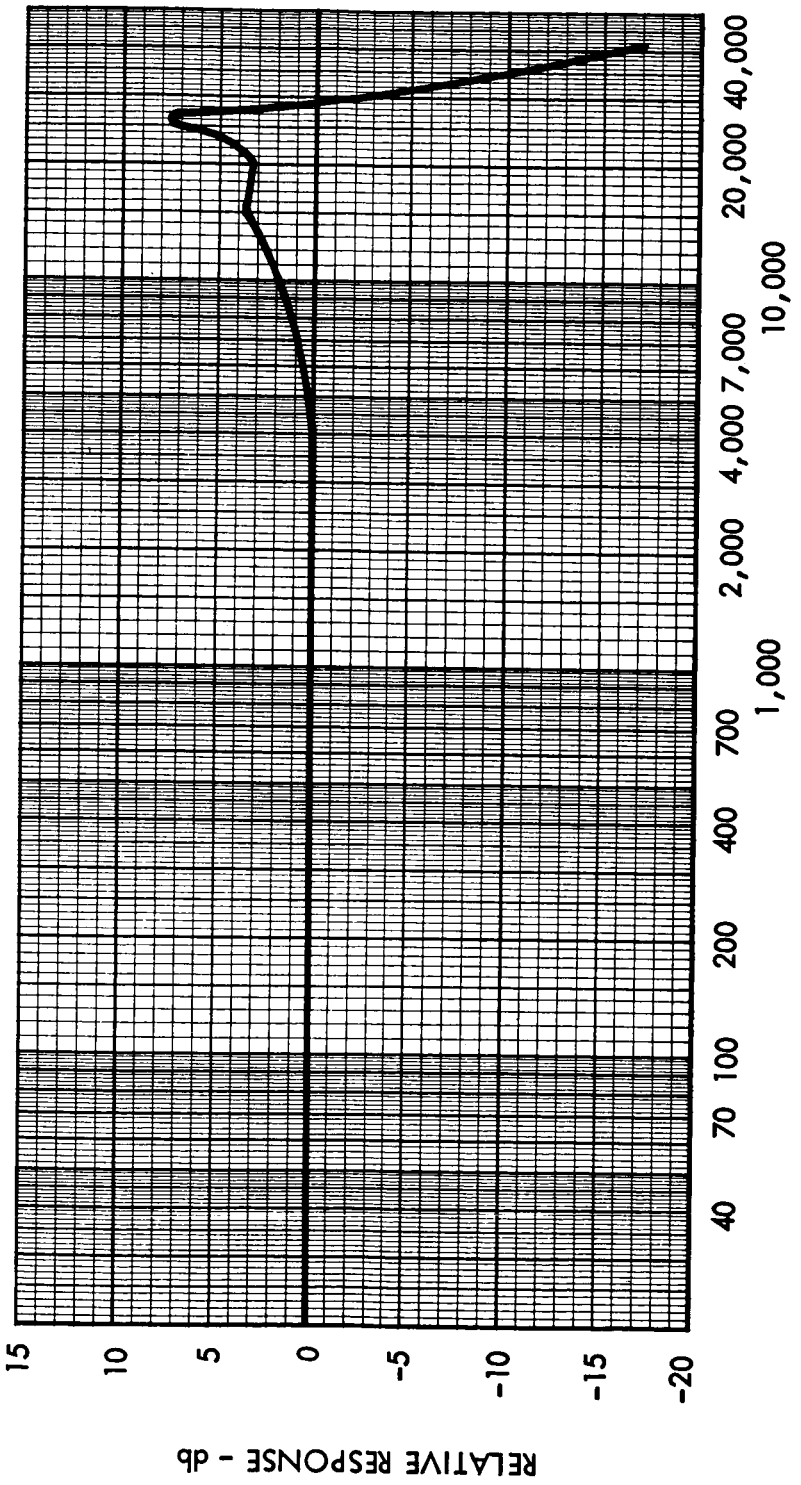

Figure 5. Relative Frequency Response of Photocon System

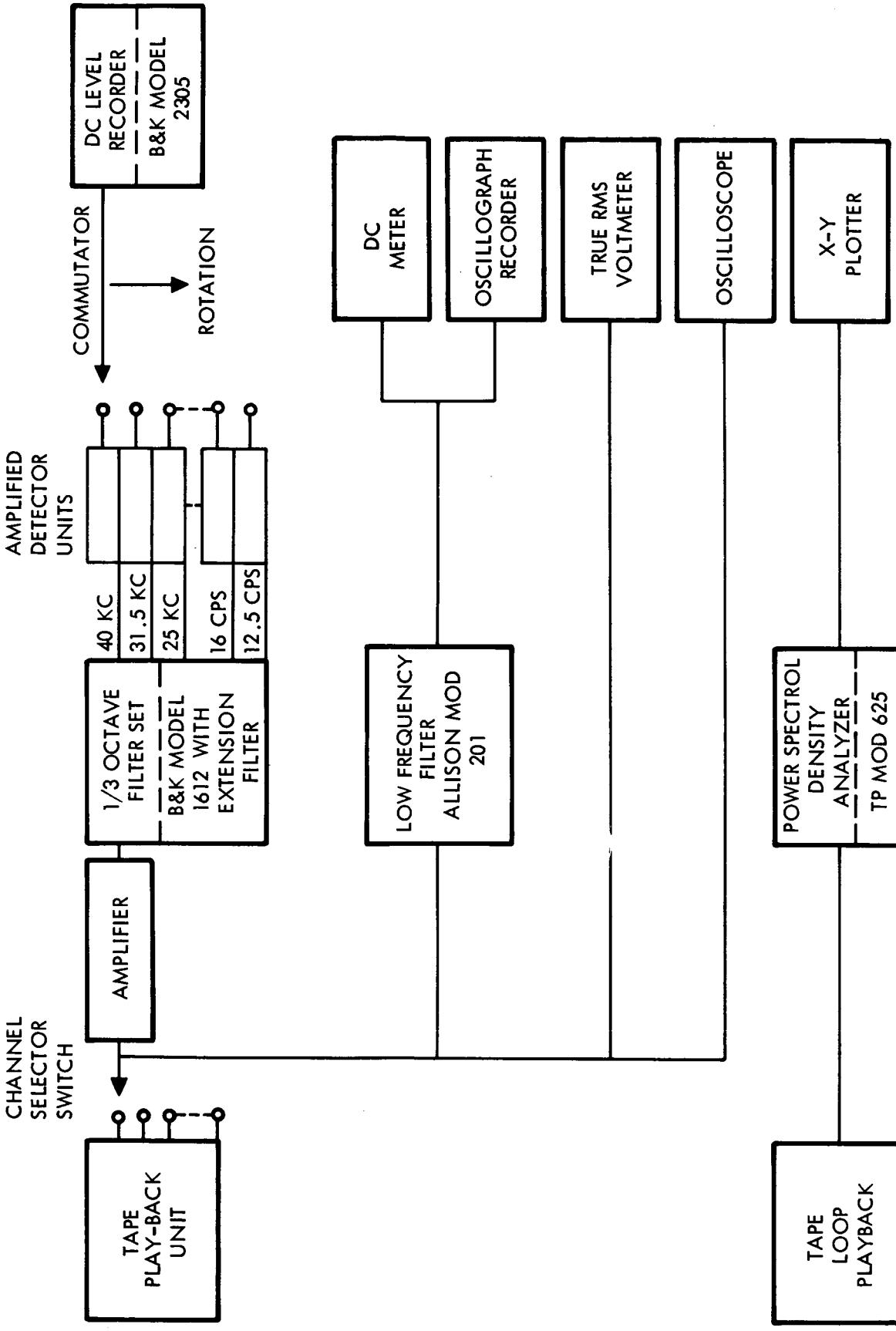

Figure 6. Data Reduction System

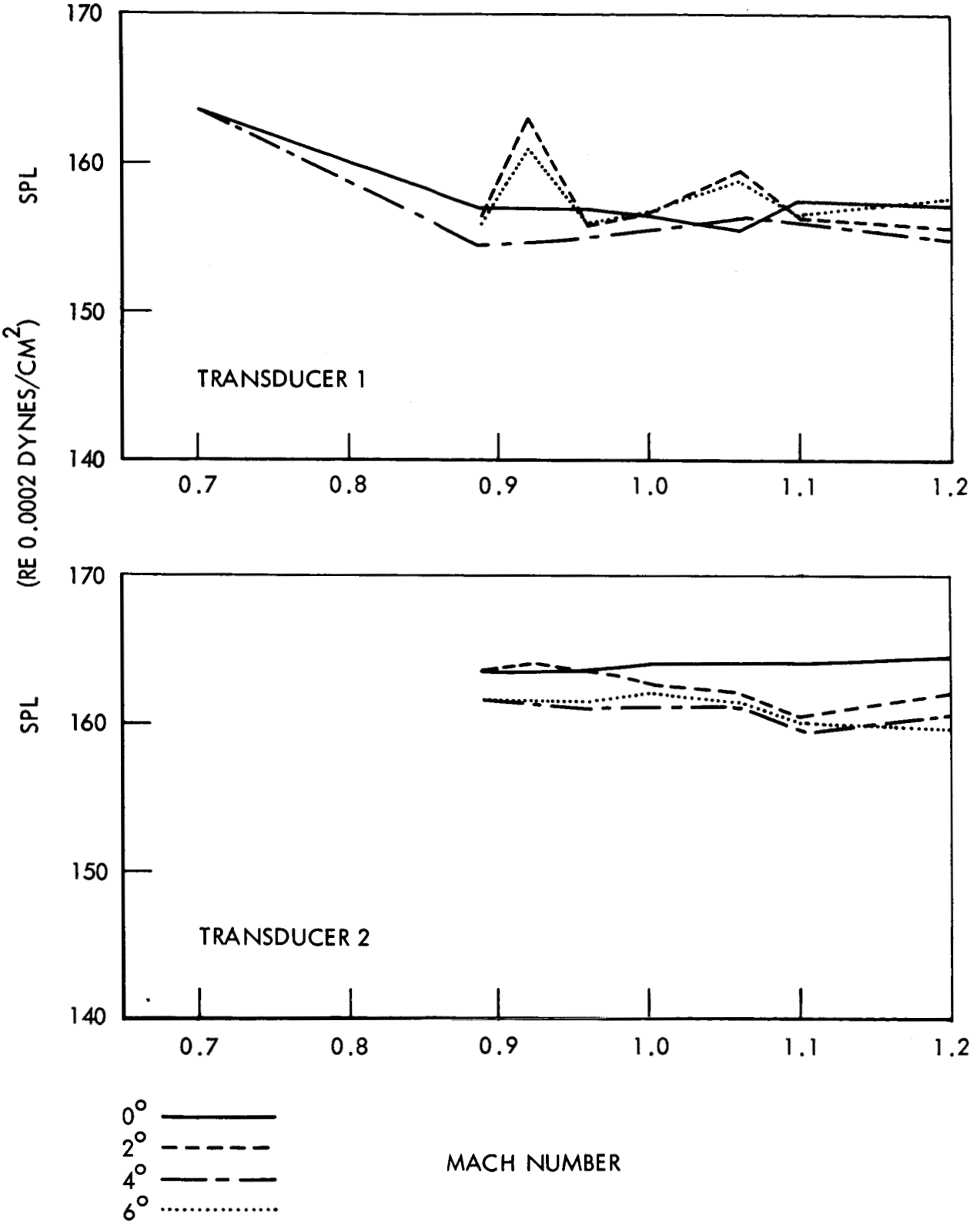

Figure 7. Overall Sound Pressure Level Versus M, Configuration C (M=0.7 to 1.2) (Sheet 1)

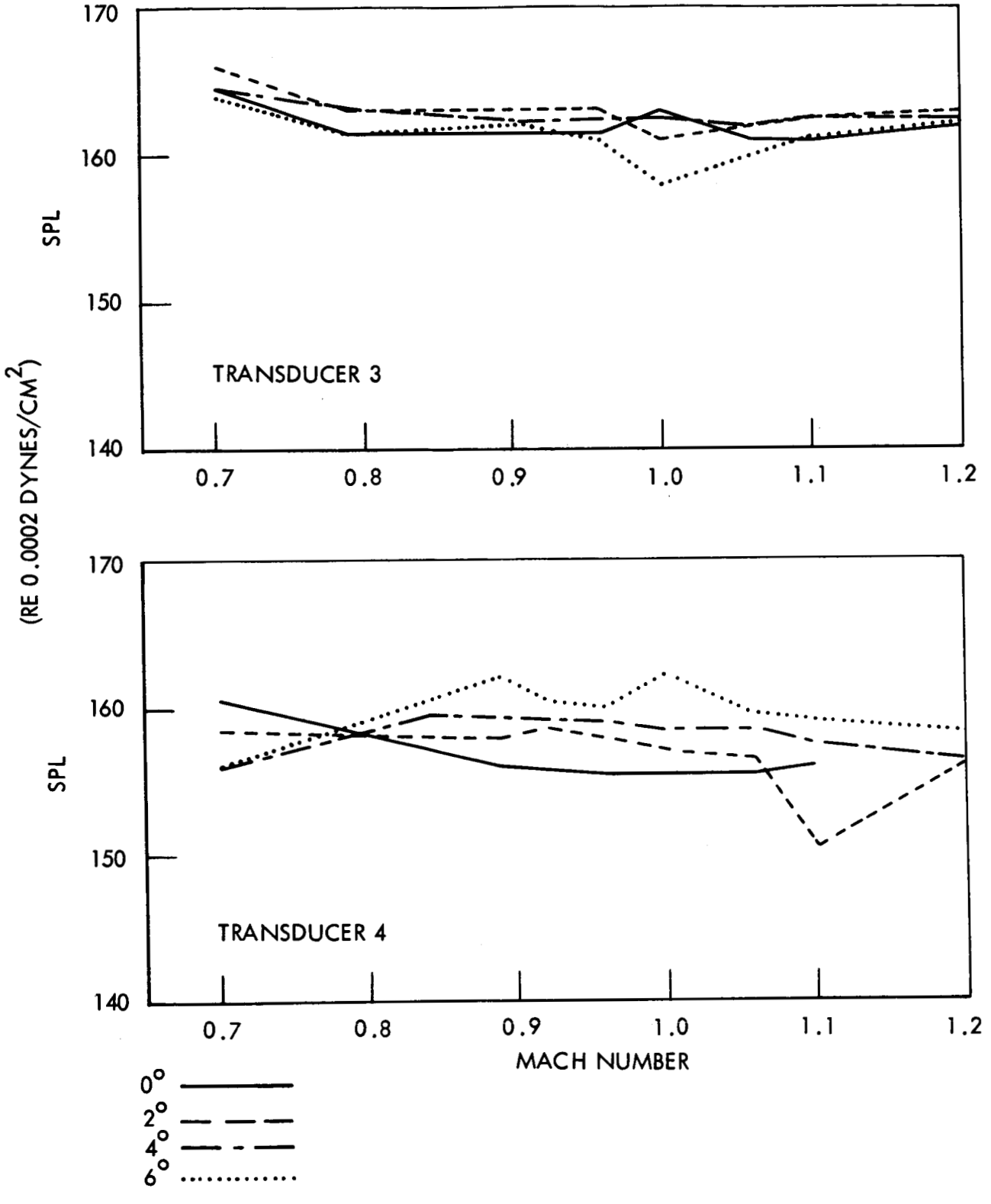

Figure 7. Overall Sound Pressure Level Versus M, Configuration C (M=0.7 to 1.2) (Sheet 2)

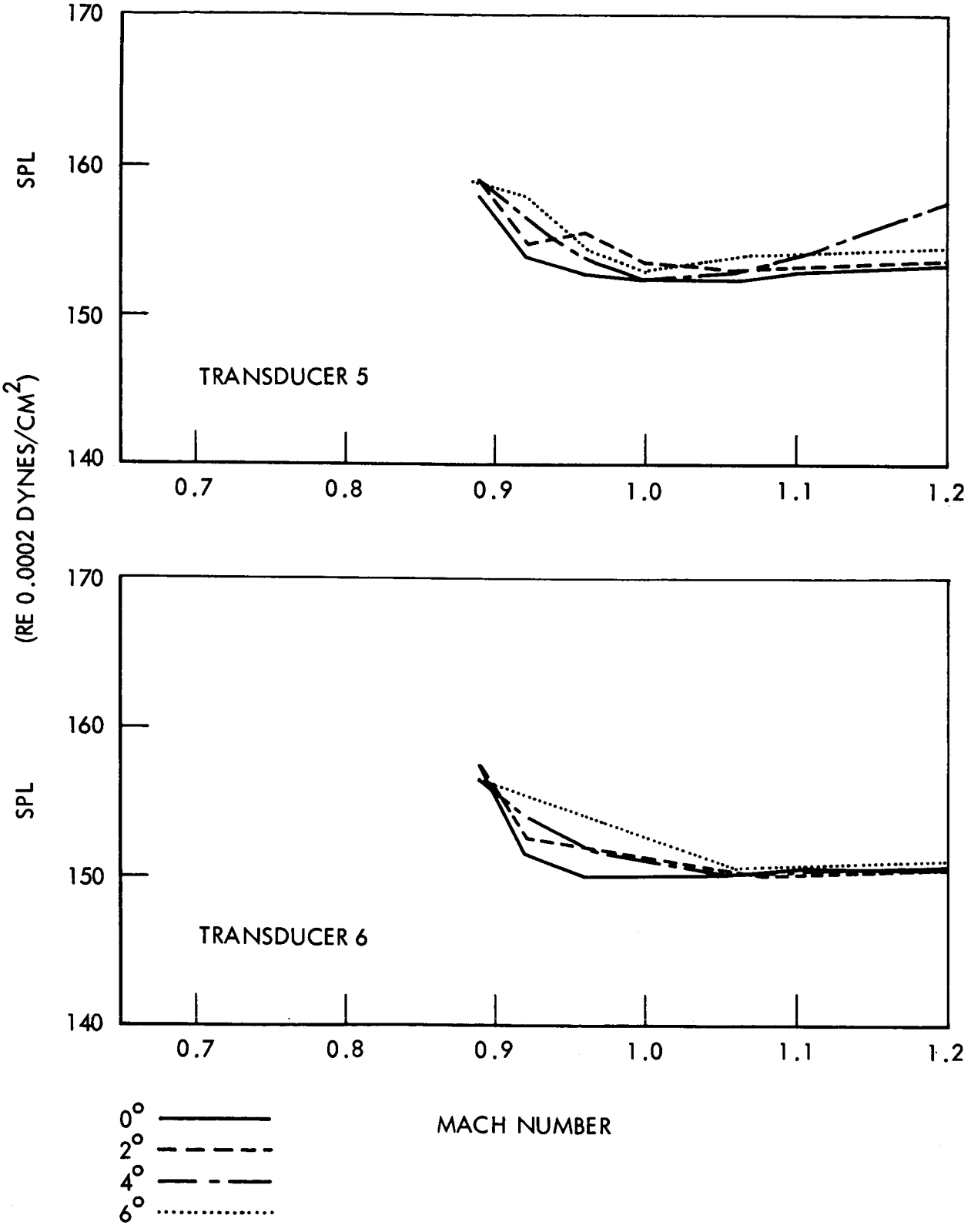

Figure 7. Overall Sound Pressure Level Versus M, Configuration C (M=0.7 to 1.2) (Sheet 3)

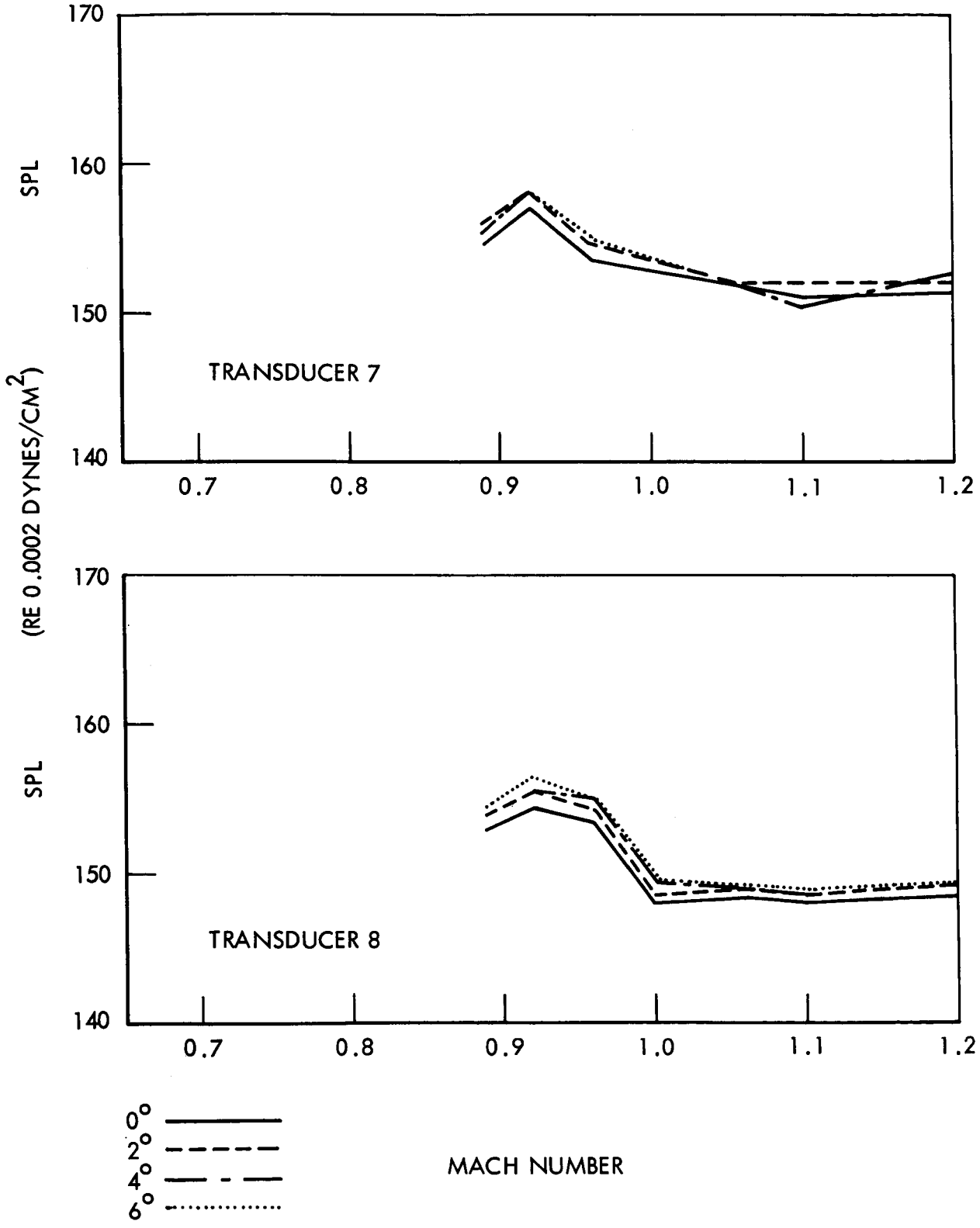

Figure 7. Overall Sound Pressure Level Versus M, Configuration C (M=0.7 to 1.2) (Sheet 4)

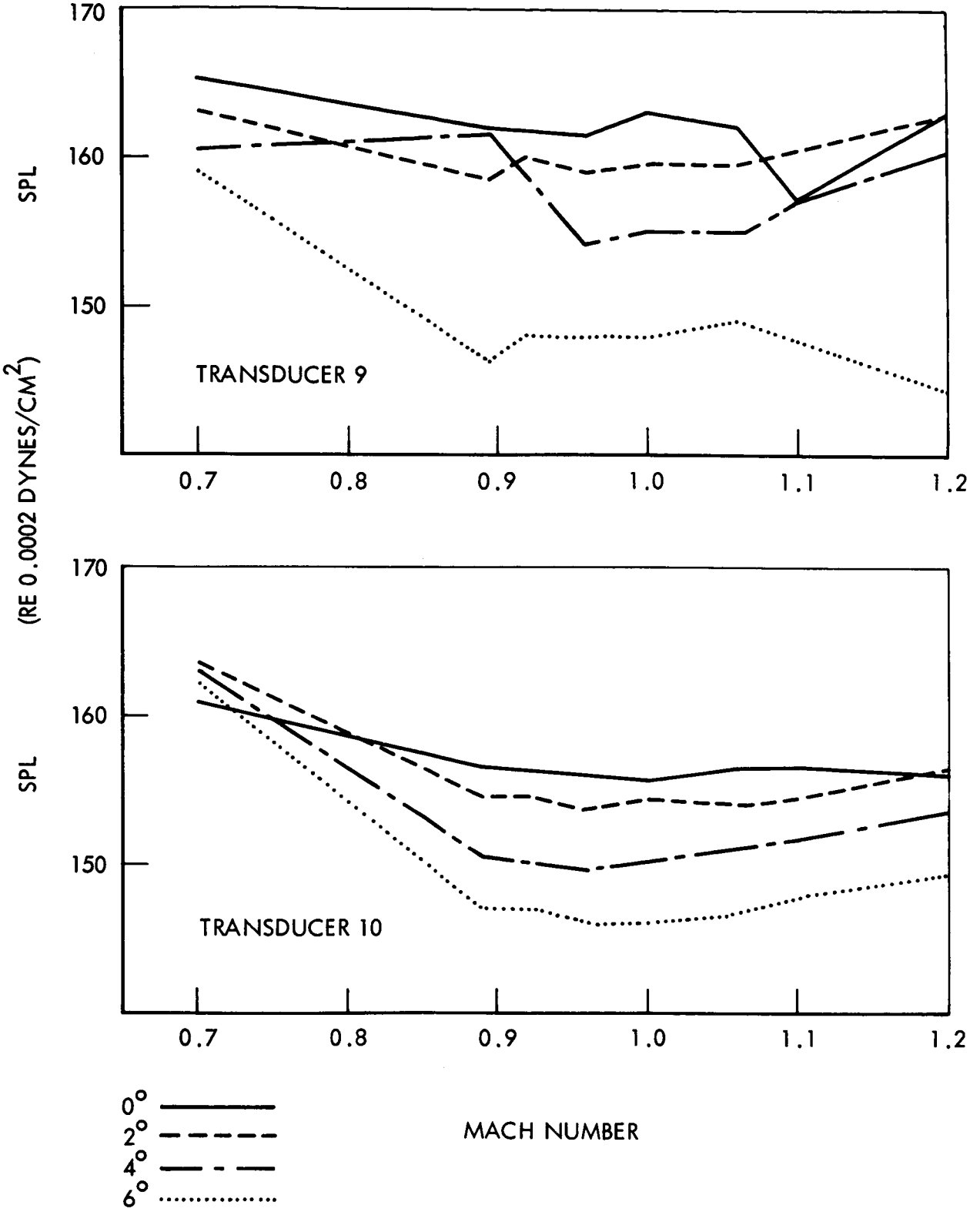

Figure 7. Overall Sound Pressure Level Versus M, Configuration C (M=0.7 to 1.2) (Sheet 5)

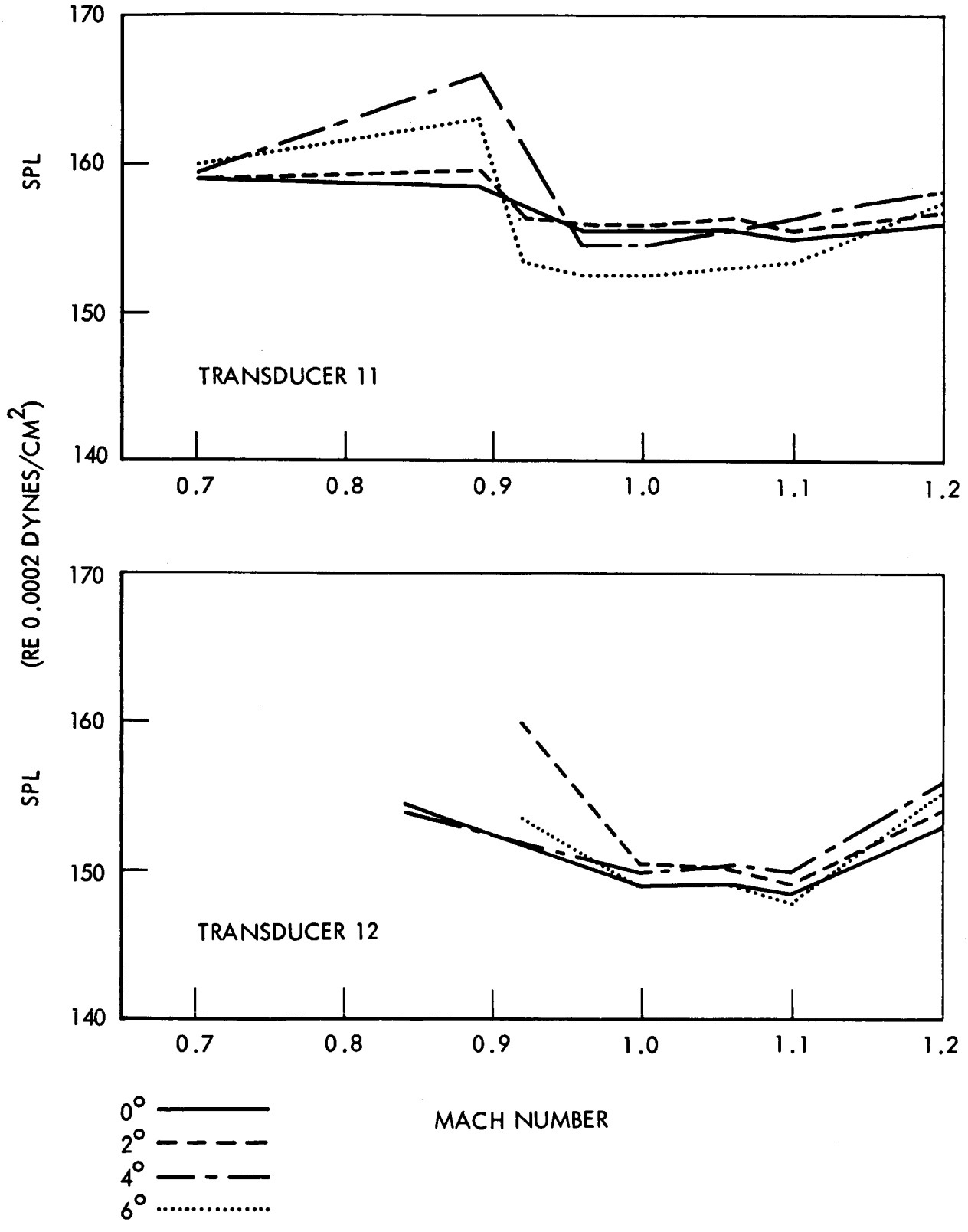

Figure 7. Overall Sound Pressure Level Versus M, Configuration C (M=0.7 to 1.2) (Sheet 6)

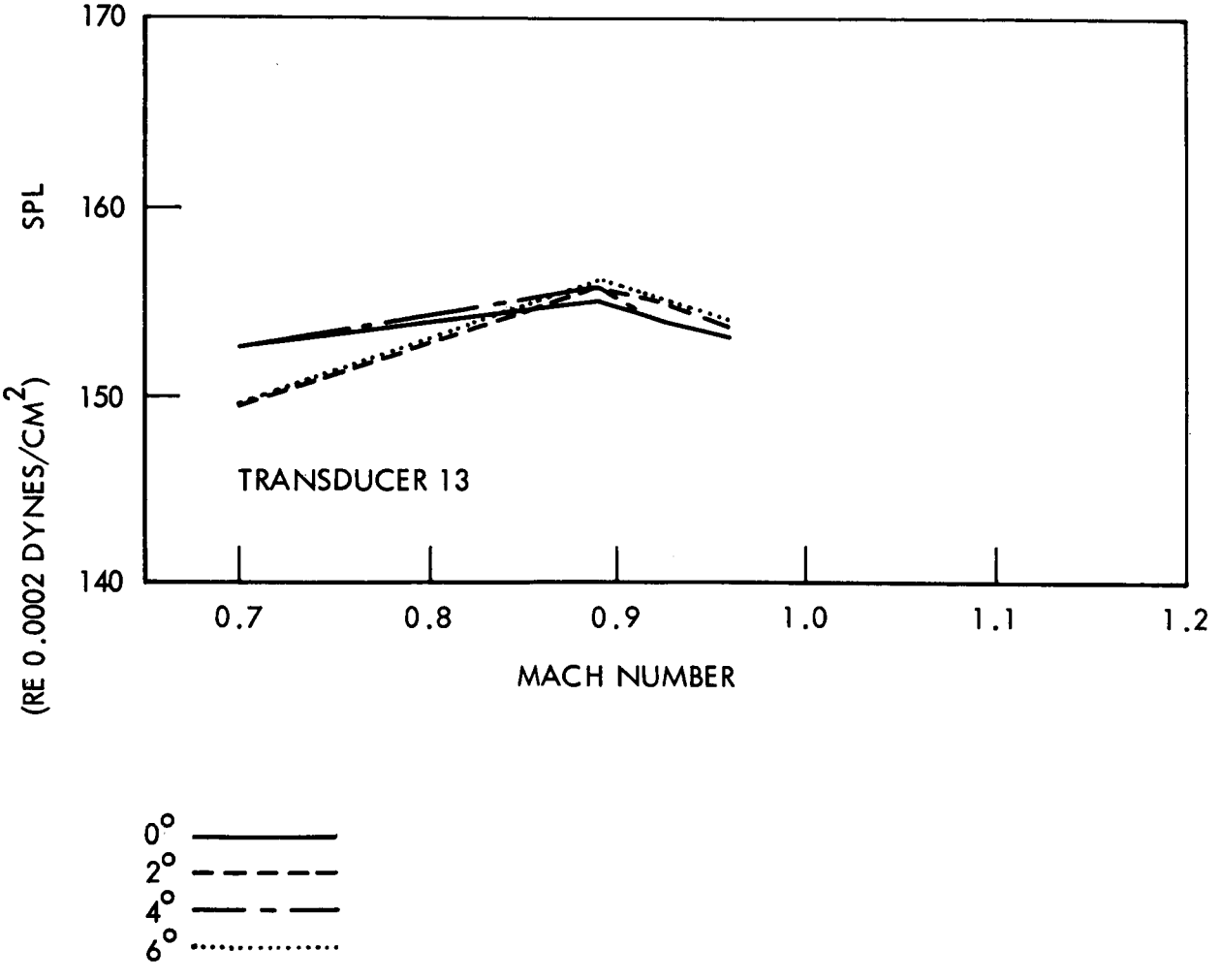

Figure 7. Overall Sound Pressure Level Versus M, Configuration C (M=0.7 to 1.2) (Sheet 7)

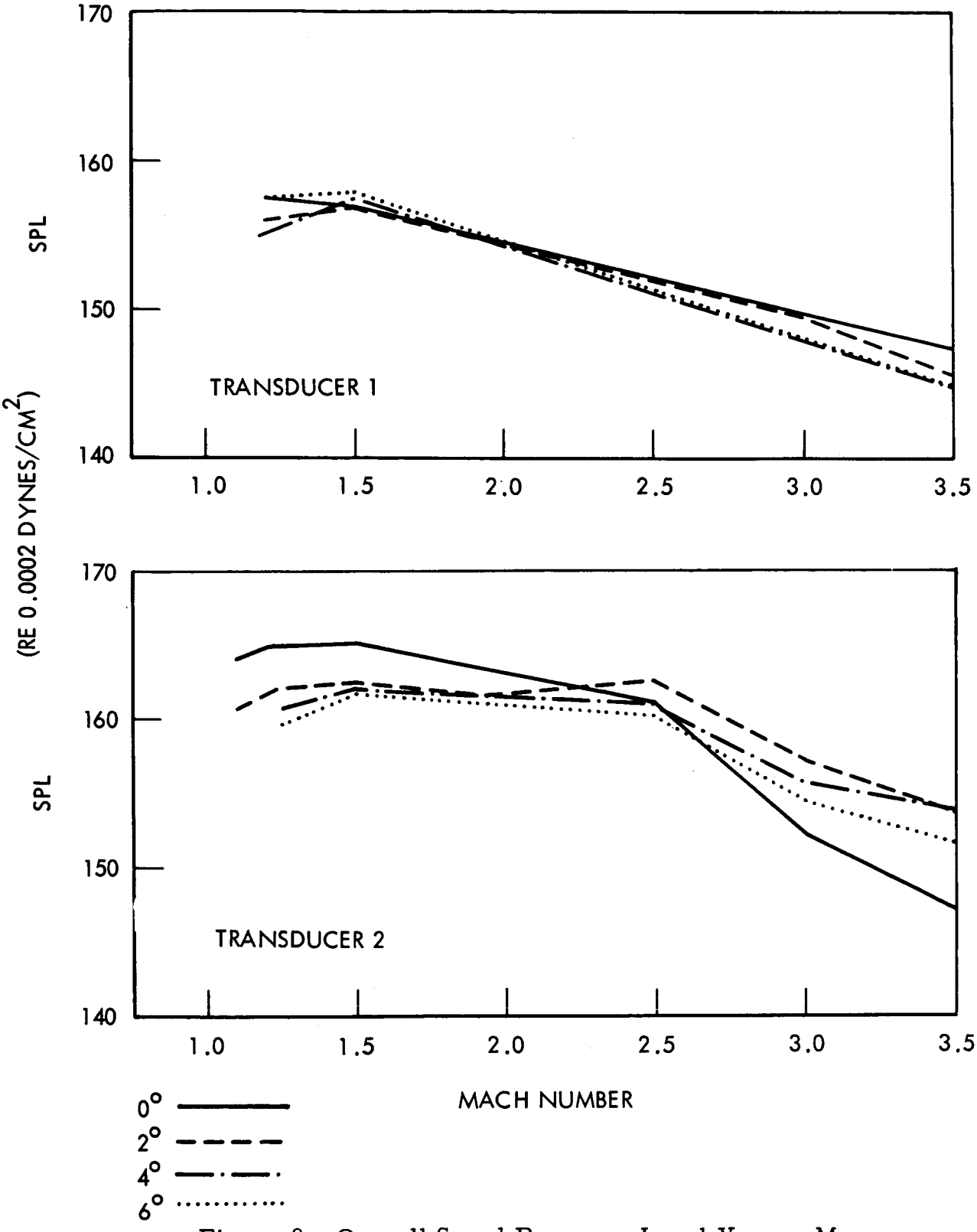

Figure 8. Overall Sound Pressure Level Versus M, Configuration C (M=1.0 to 3.5) (Sheet 1)

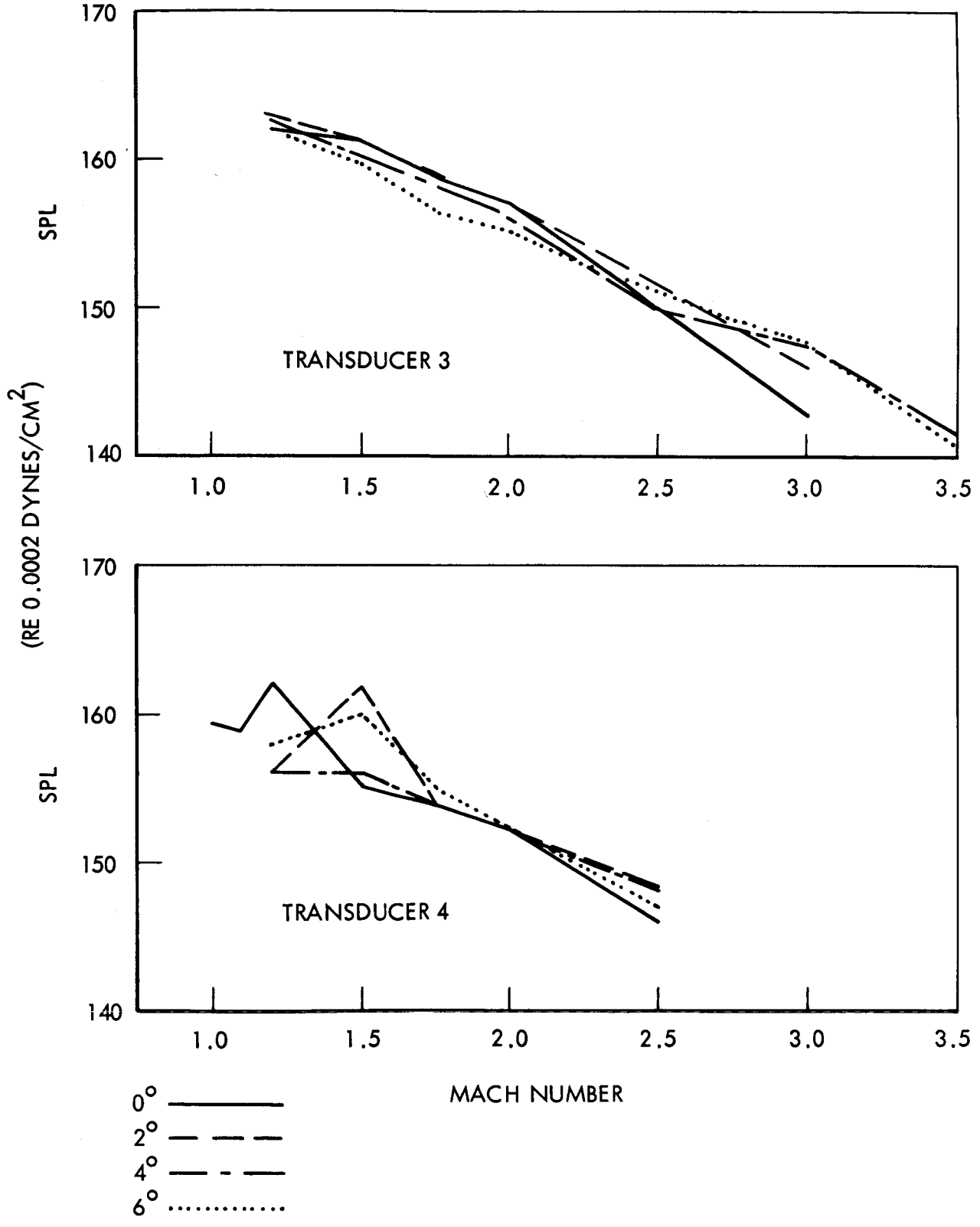

Figure 8. Overall Sound Pressure Level Versus M, Configuration C (M=1.0 to 3.5) (Sheet 2)

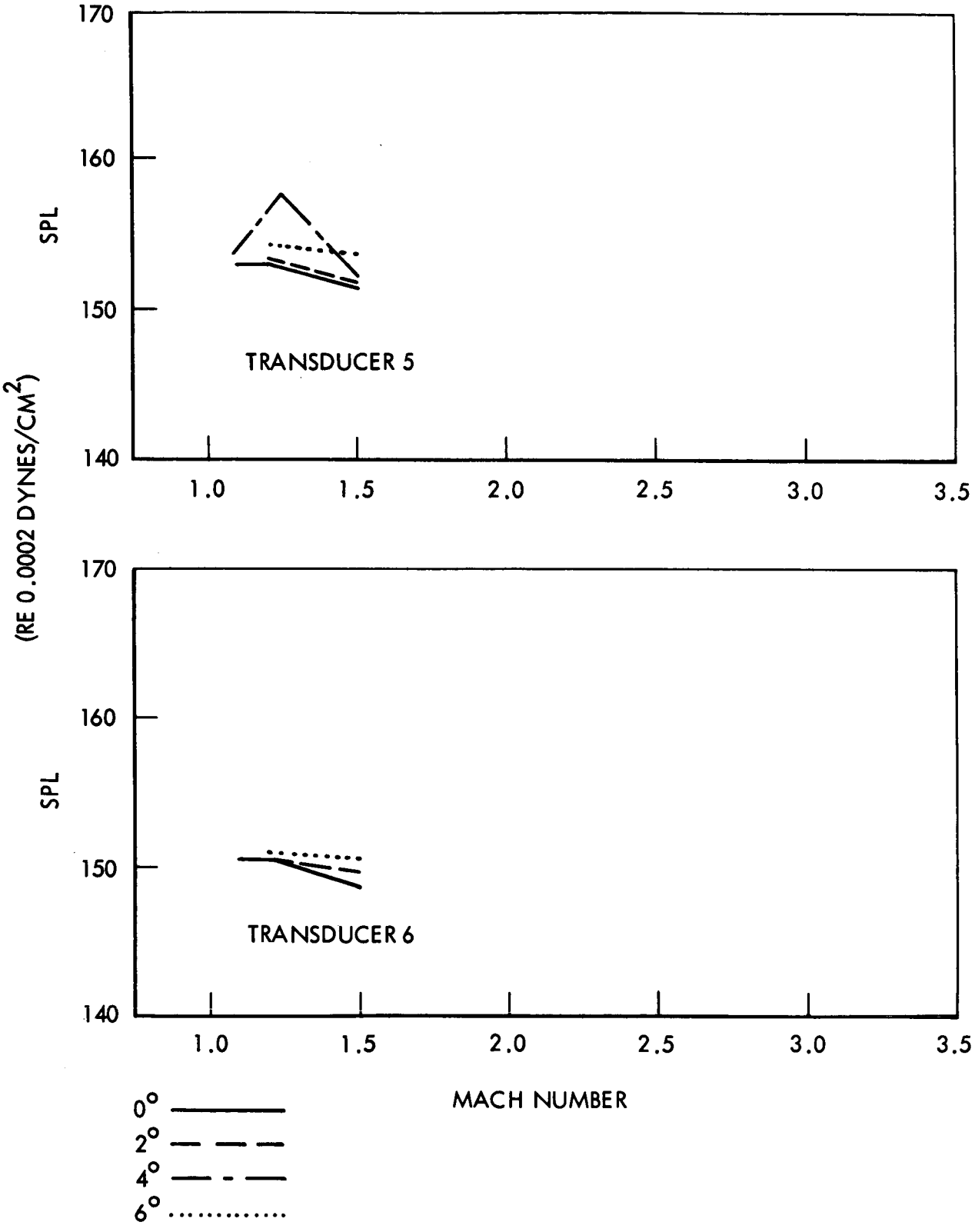

Figure 8. Overall Sound Pressure Level Versus M, Configuration C (M=1.0 to 3.5) (Sheet 3)

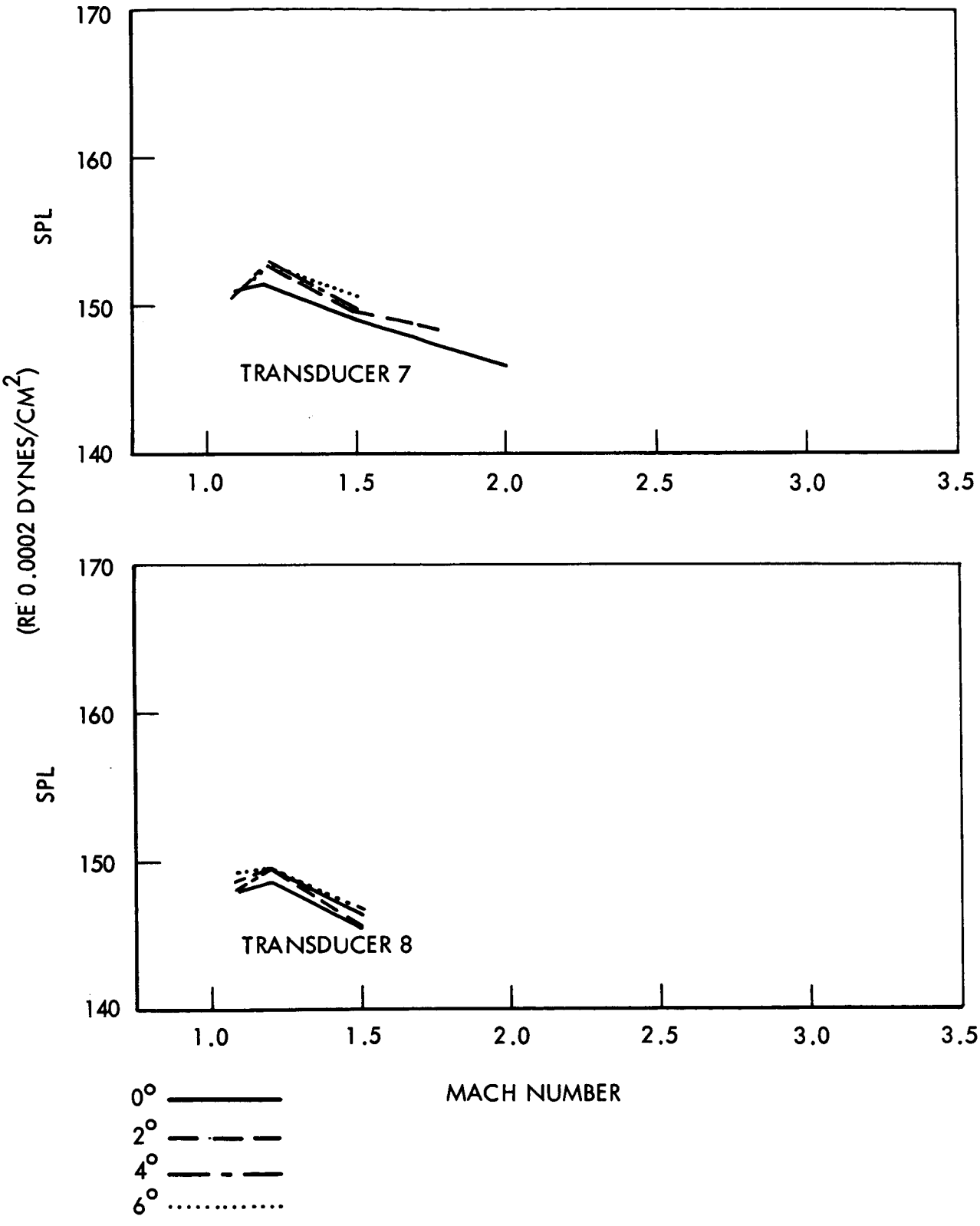

Figure 8. Overall Sound Pressure Level Versus M, Configuration C (M=1.0 to 3.5) (Sheet 4)

CONFIDENTIAL

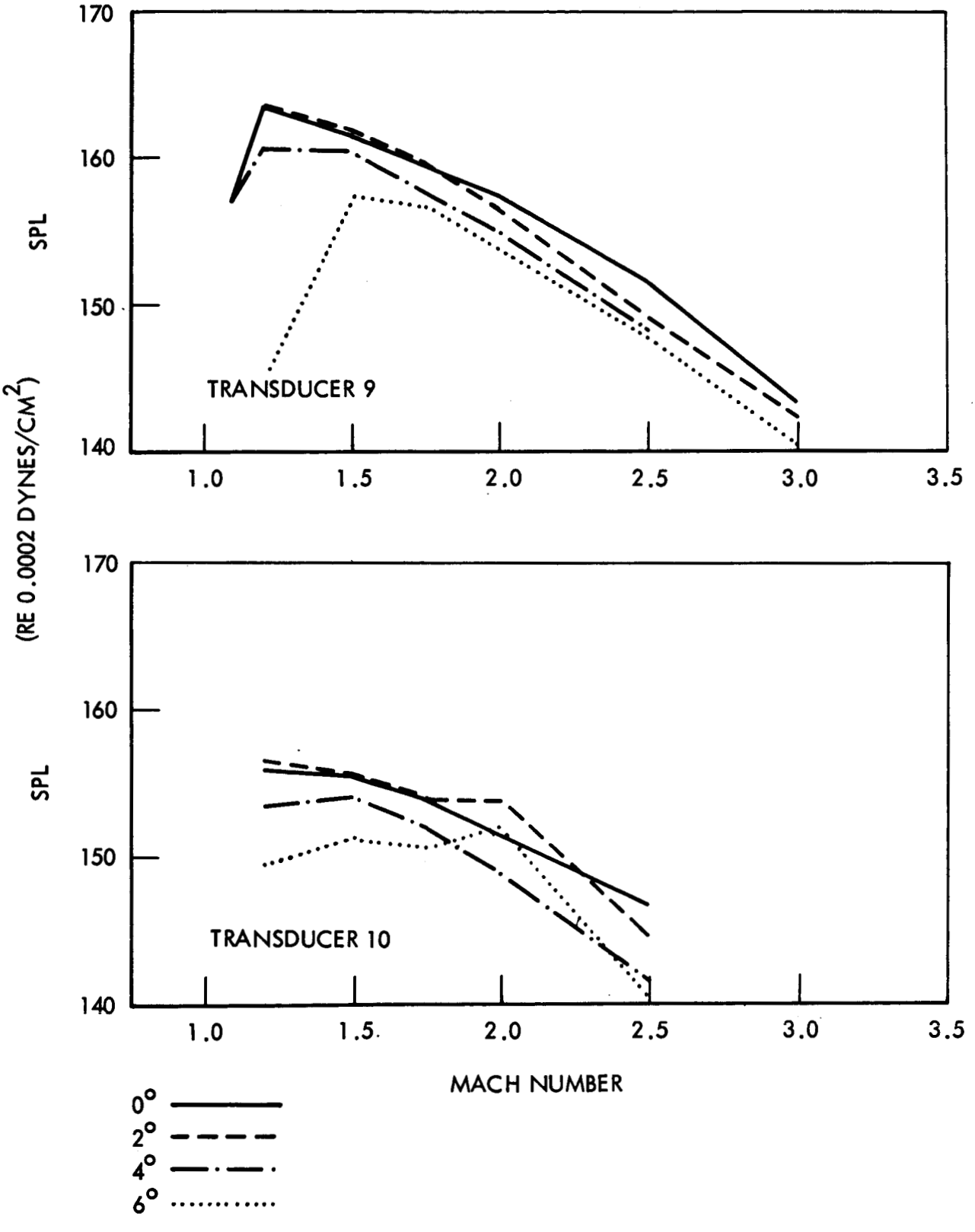

Figure 8. Overall Sound Pressure Level Versus M, Configuration C (M=1.0 to 3.5) (Sheet 5)

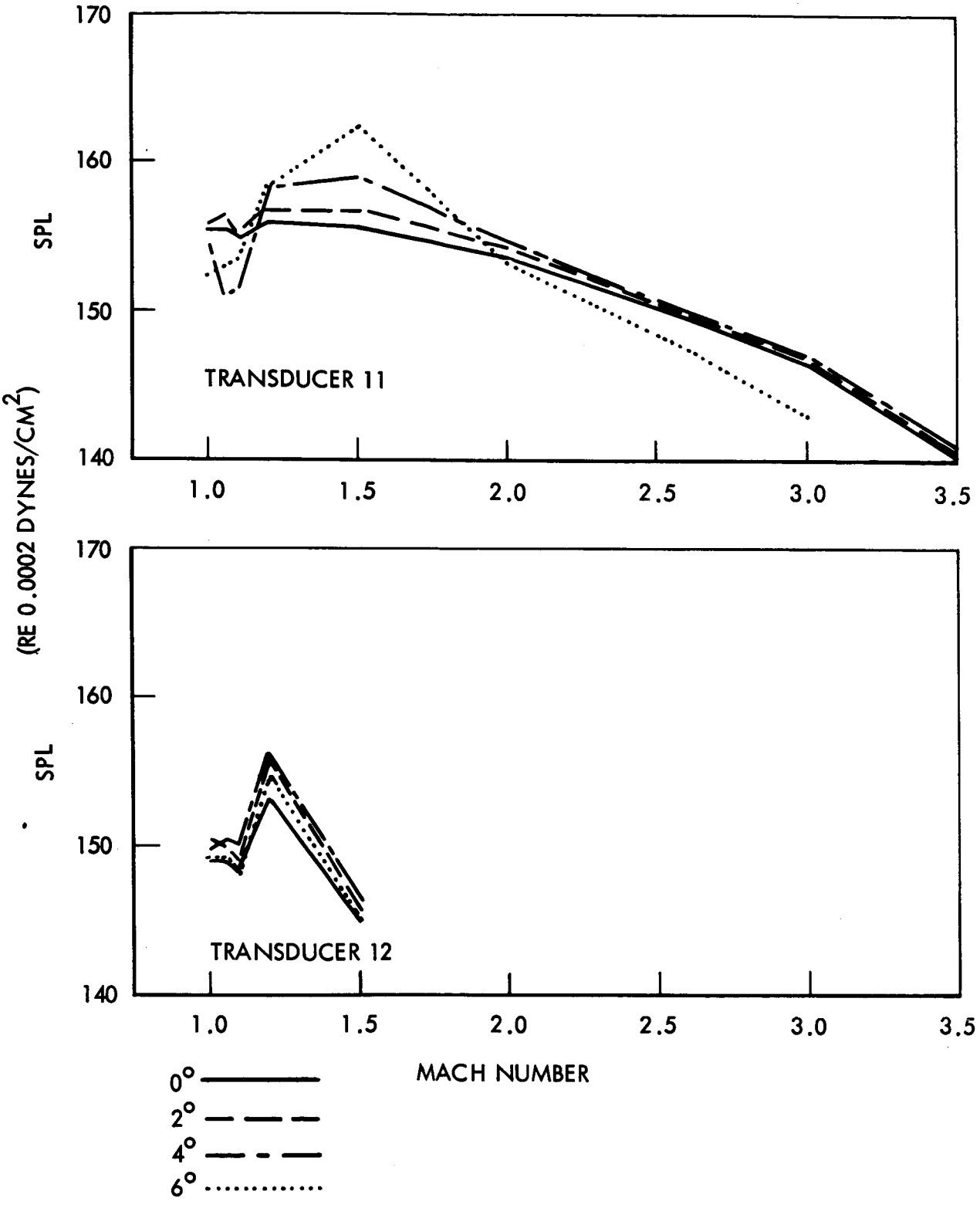

Figure 8. Overall Sound Pressure Level Versus M, Configuration C (M=1.0 to 3.5) (Sheet 6)

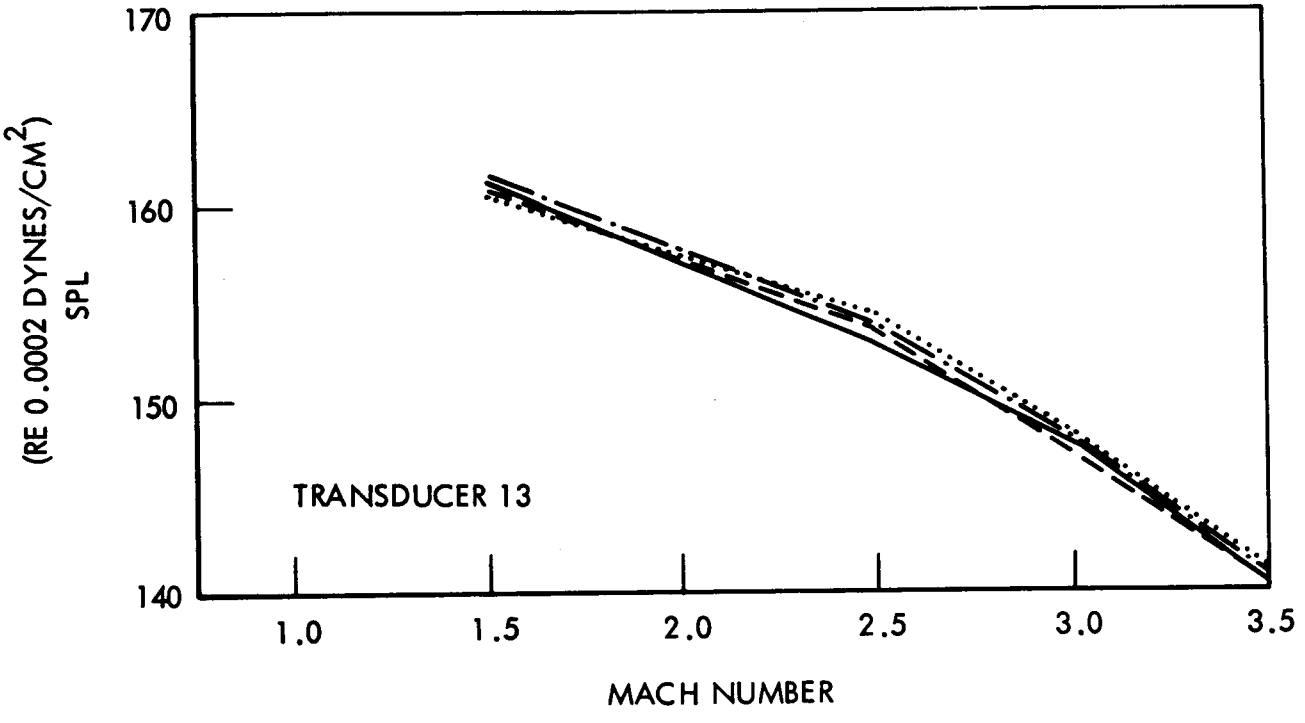

Figure 8. Overall Sound Pressure Level Versus M, Configuration C (M = 1.0 to 3.5) (Sheet 7)

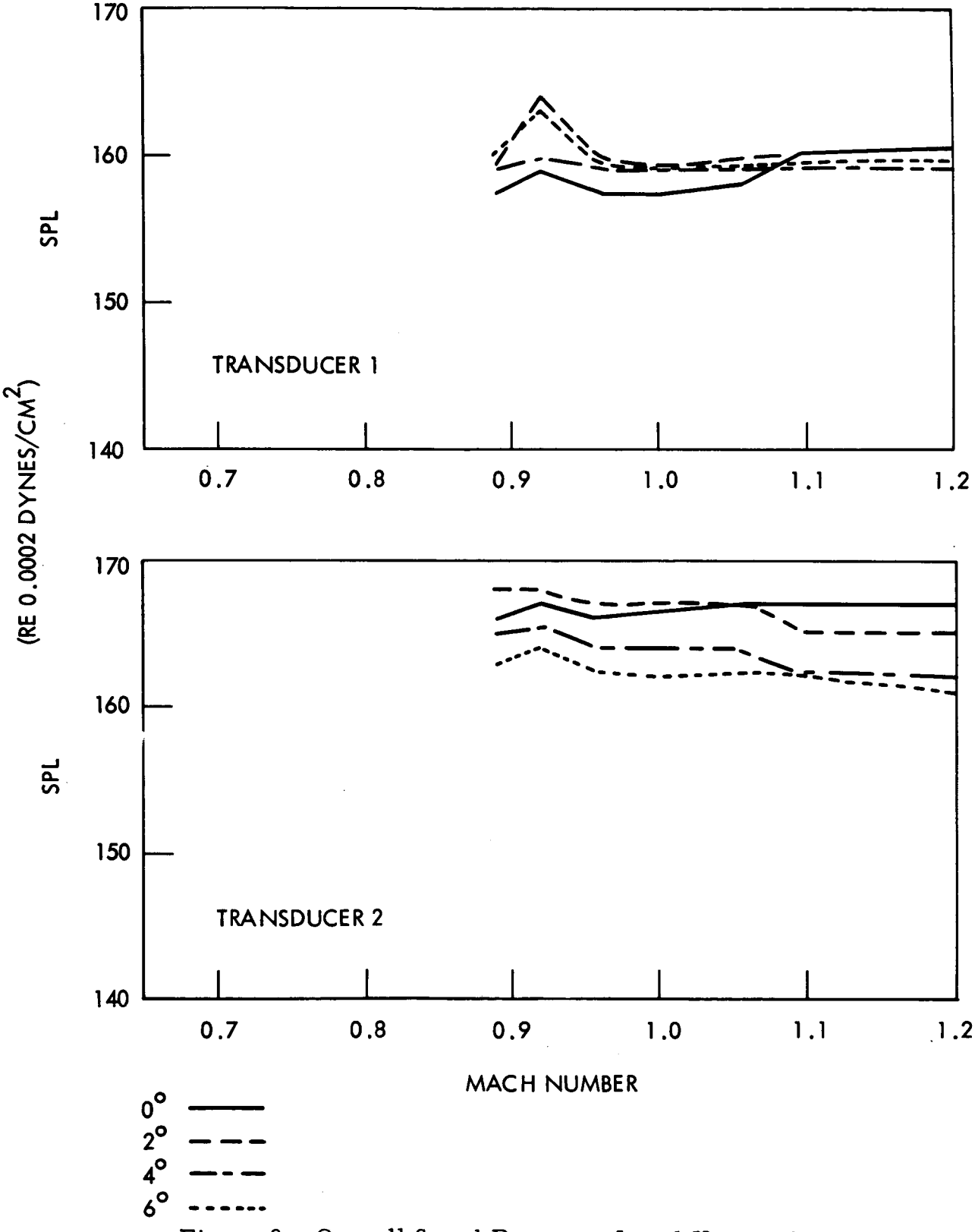

Figure 9. Overall Sound Pressure Level Versus M, Configuration D (M=0.7 to 1.2) (Sheet 1)

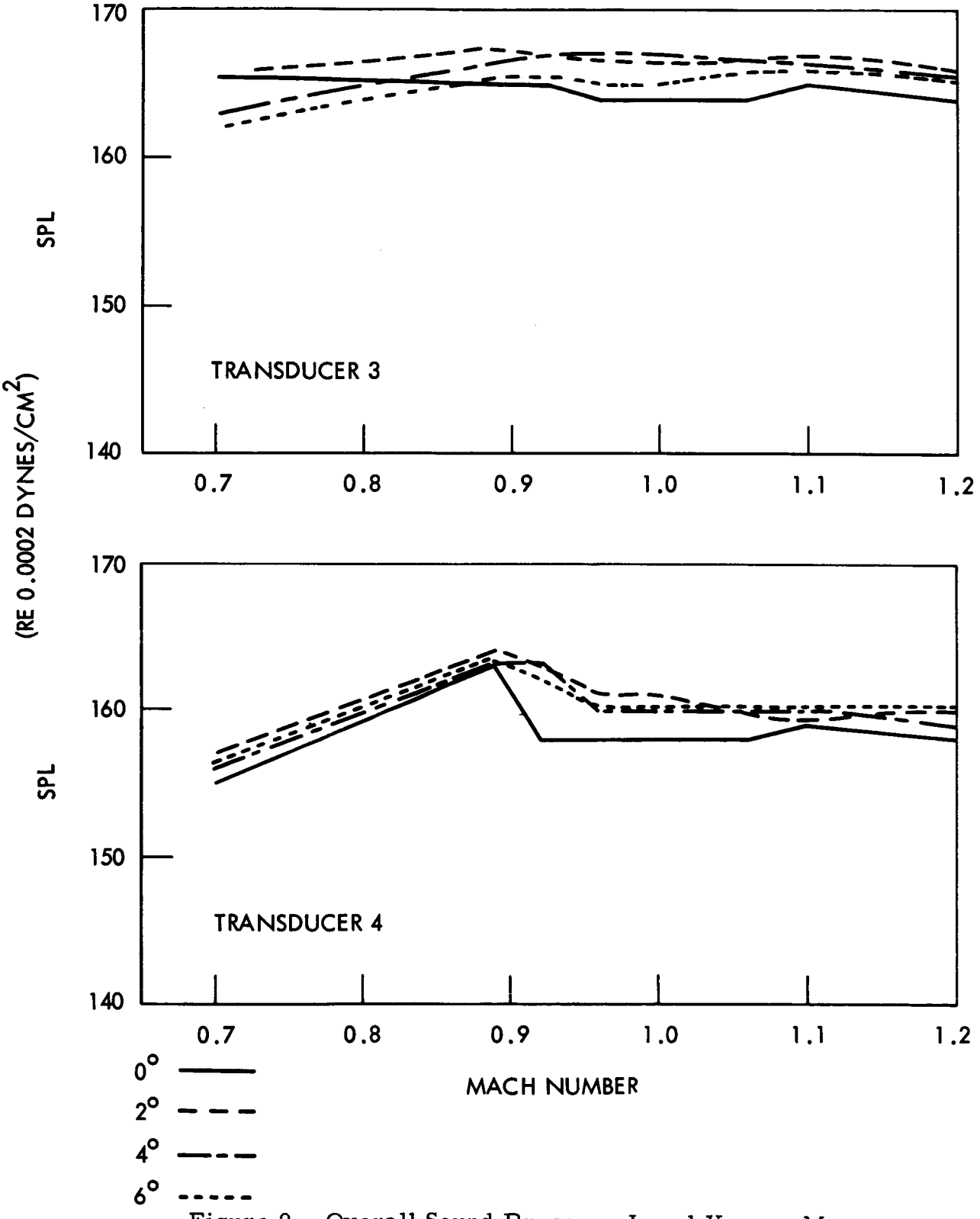

Figure 9. Overall Sound Pressure Level Versus M, Configuration D (M=0.7 to 1.2) (Sheet 2)

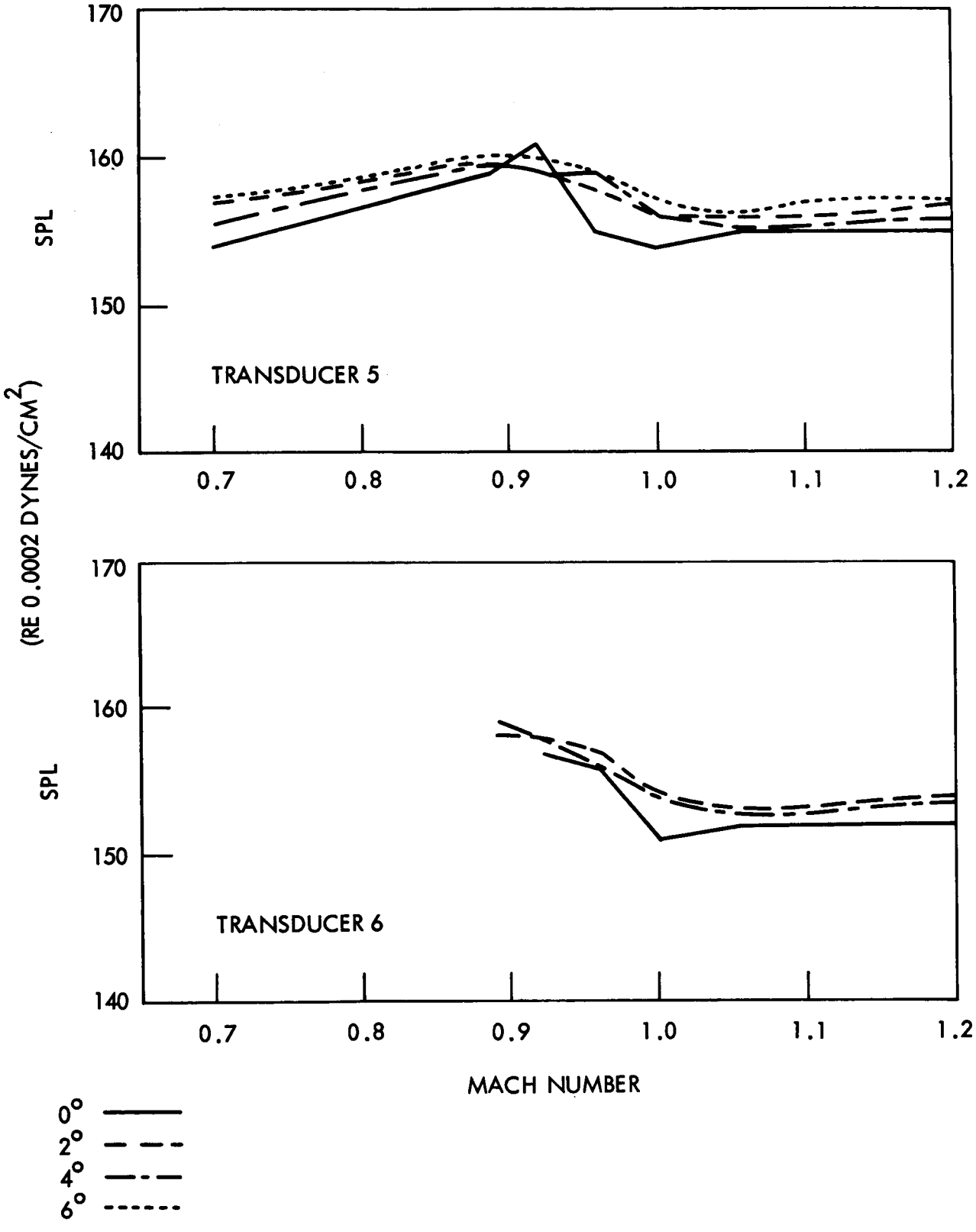

Figure 9. Overall Sound Pressure Level Versus M, Configuration D (M=0.7 to 1.2) (Sheet 3)

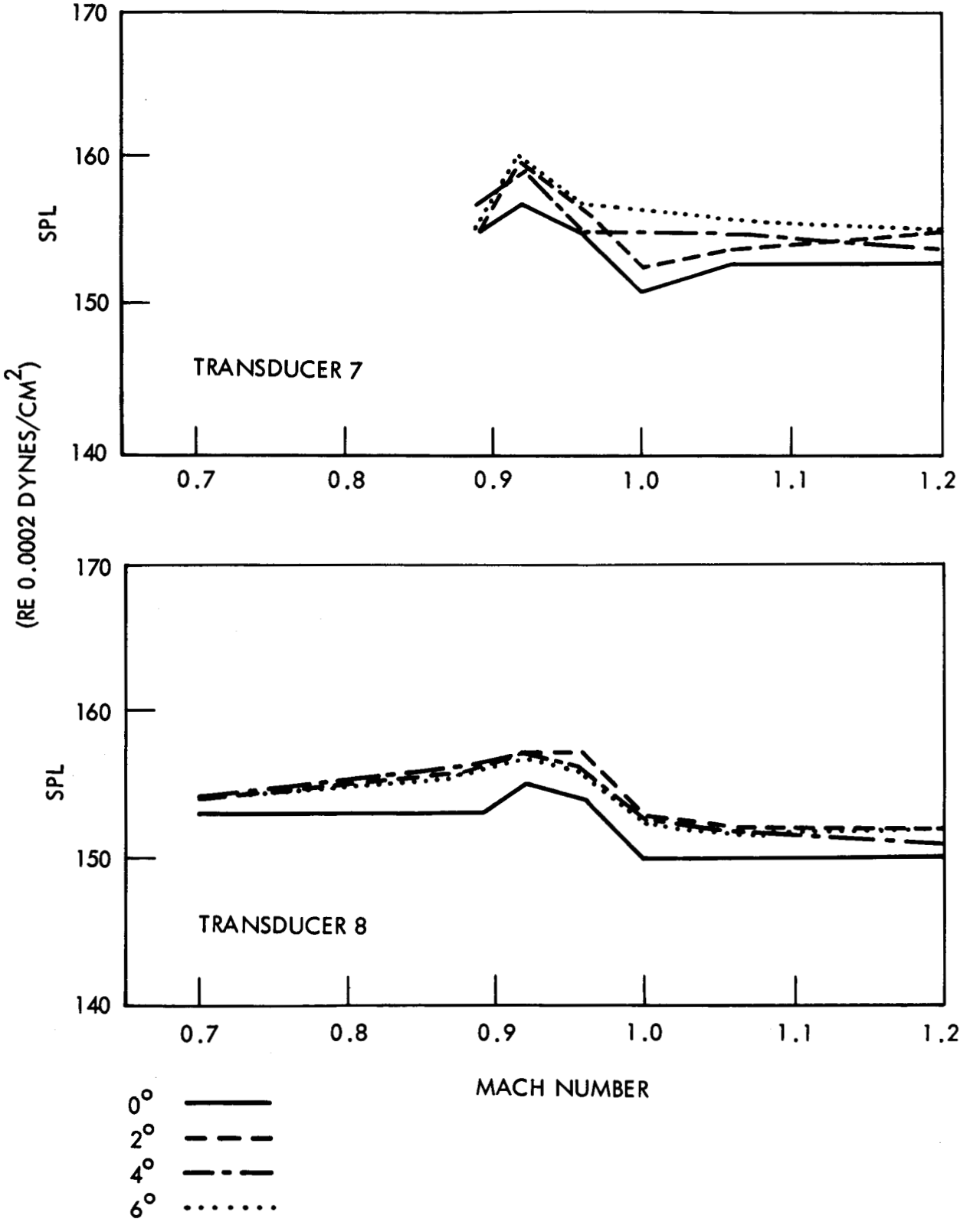

Figure 9. Overall Sound Pressure Level Versus M, Configuration D (M=0.7 to 1.2) (Sheet 4)

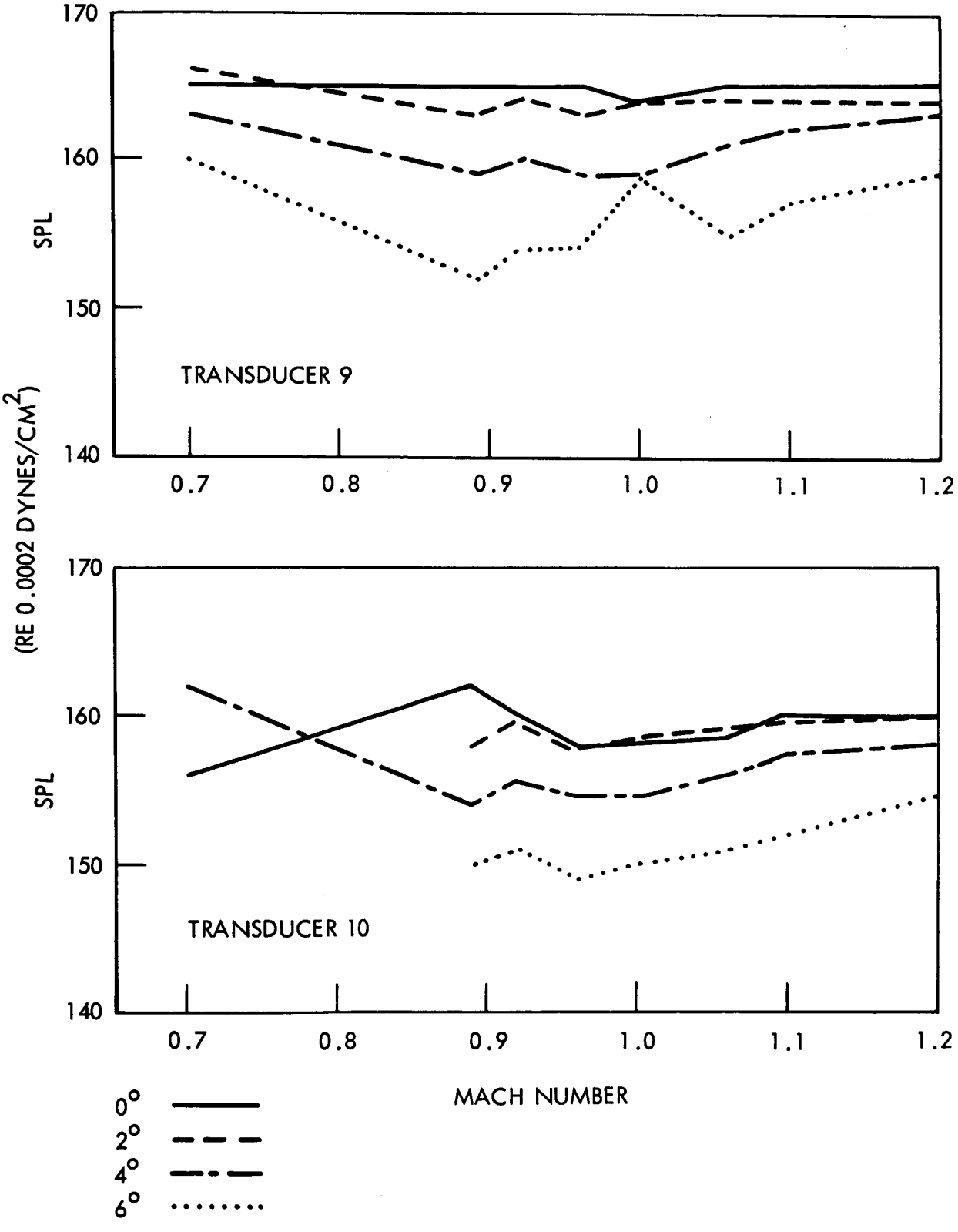

Figure 9. Overall Sound Pressure Level Versus M, Configuration D (M=0.7 to 1.2) (Sheet 5)

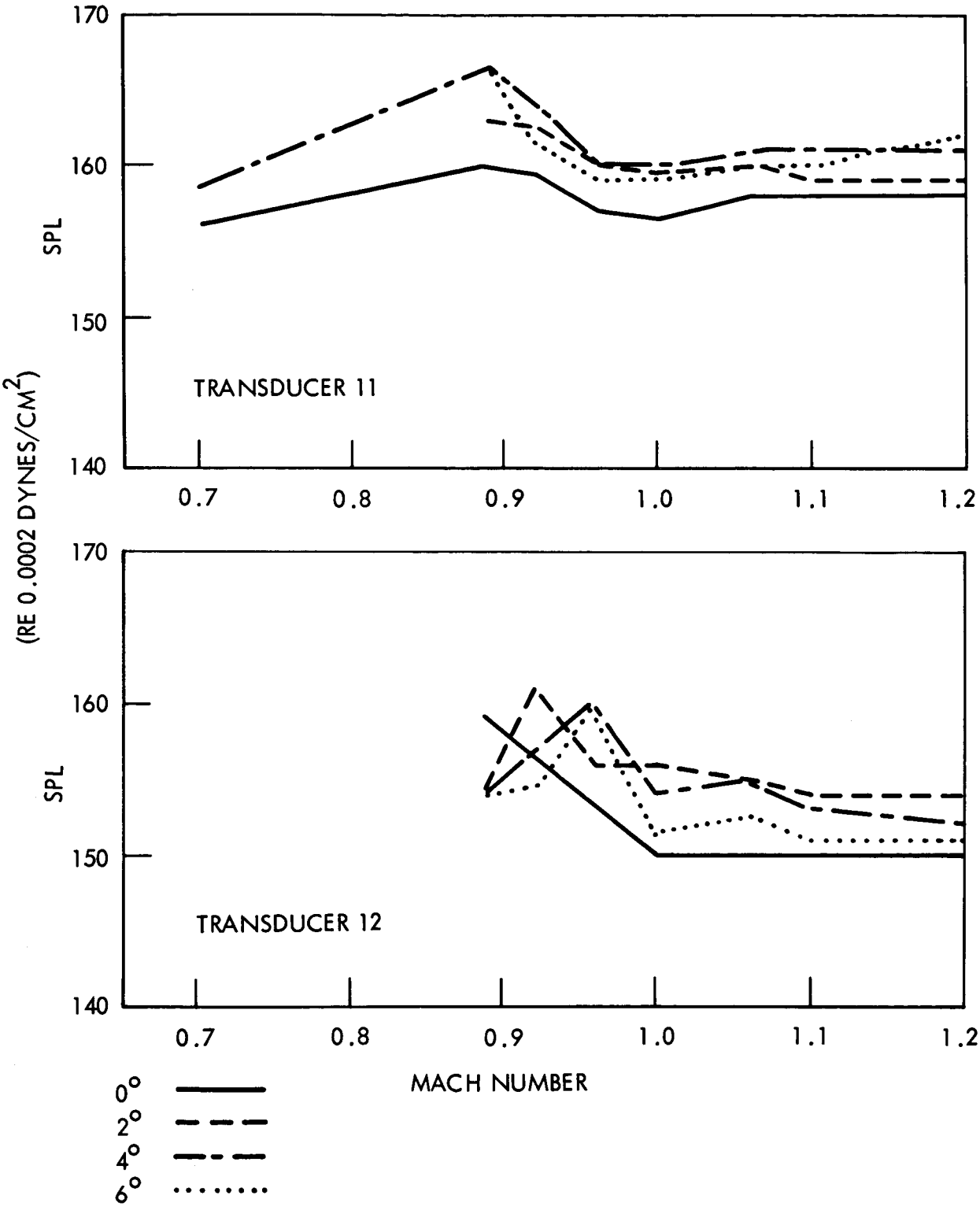

Figure 9. Overall Sound Pressure Level Versus M, Configuration D (M=0.7 to 1.2) (Sheet 6)

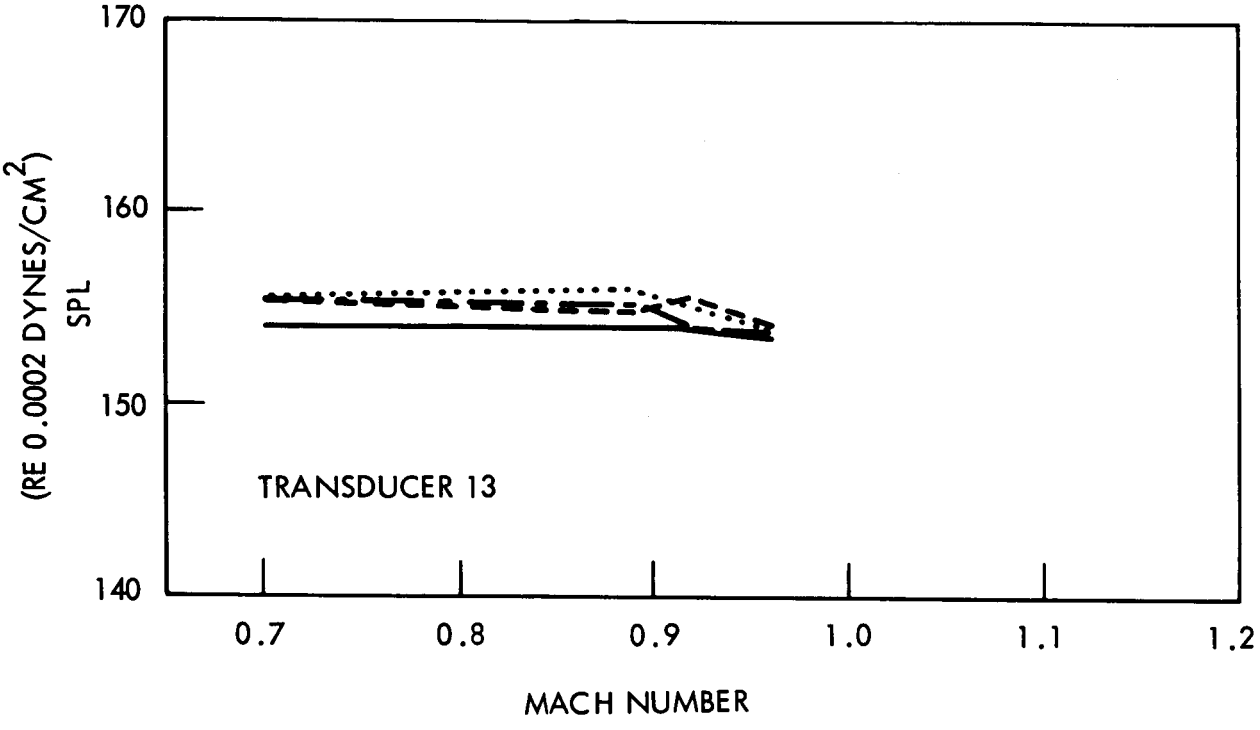

Figure 9. Overall Sound Pressure Level Versus M, Configuration D (M = 0.7 to 1.2) (Sheet 7)

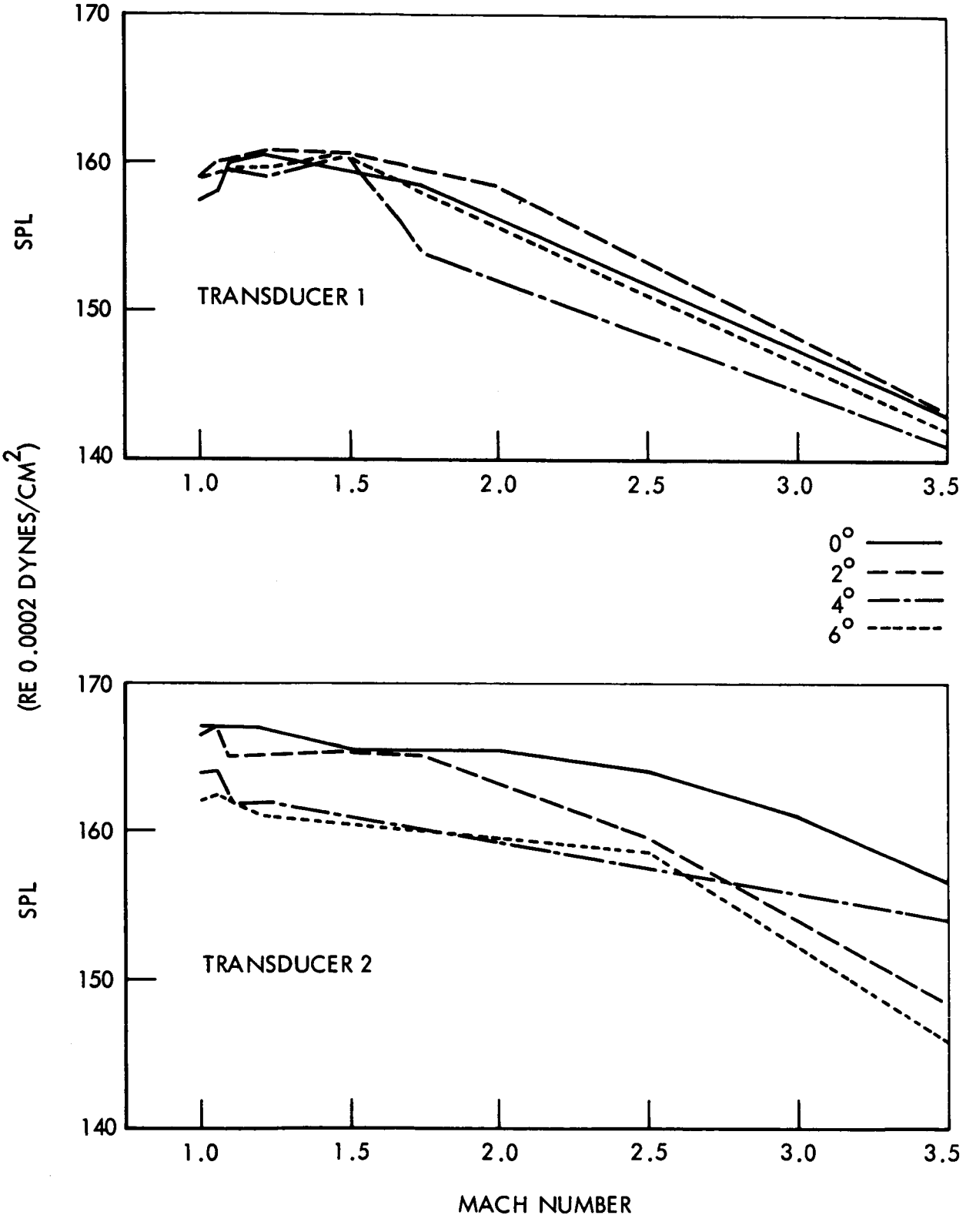

Figure 10. Overall Sound Pressure Level Versus M, Configuration D (M=1.0 to 3.5) (Sheet 1)

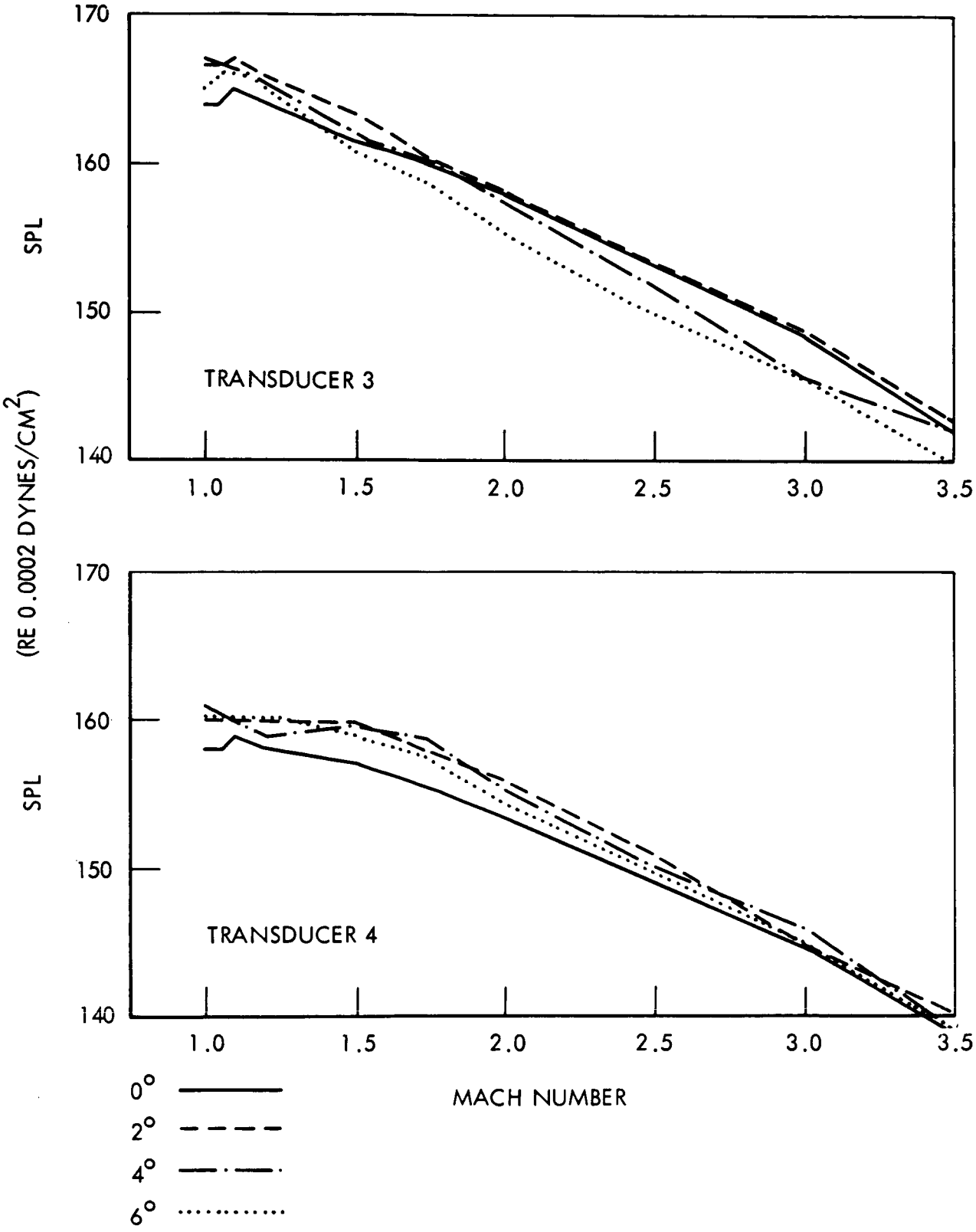

Figure 10. Overall Sound Pressure Level Versus M, Configuration D (M=1.0 to 3.5) (Sheet 2)

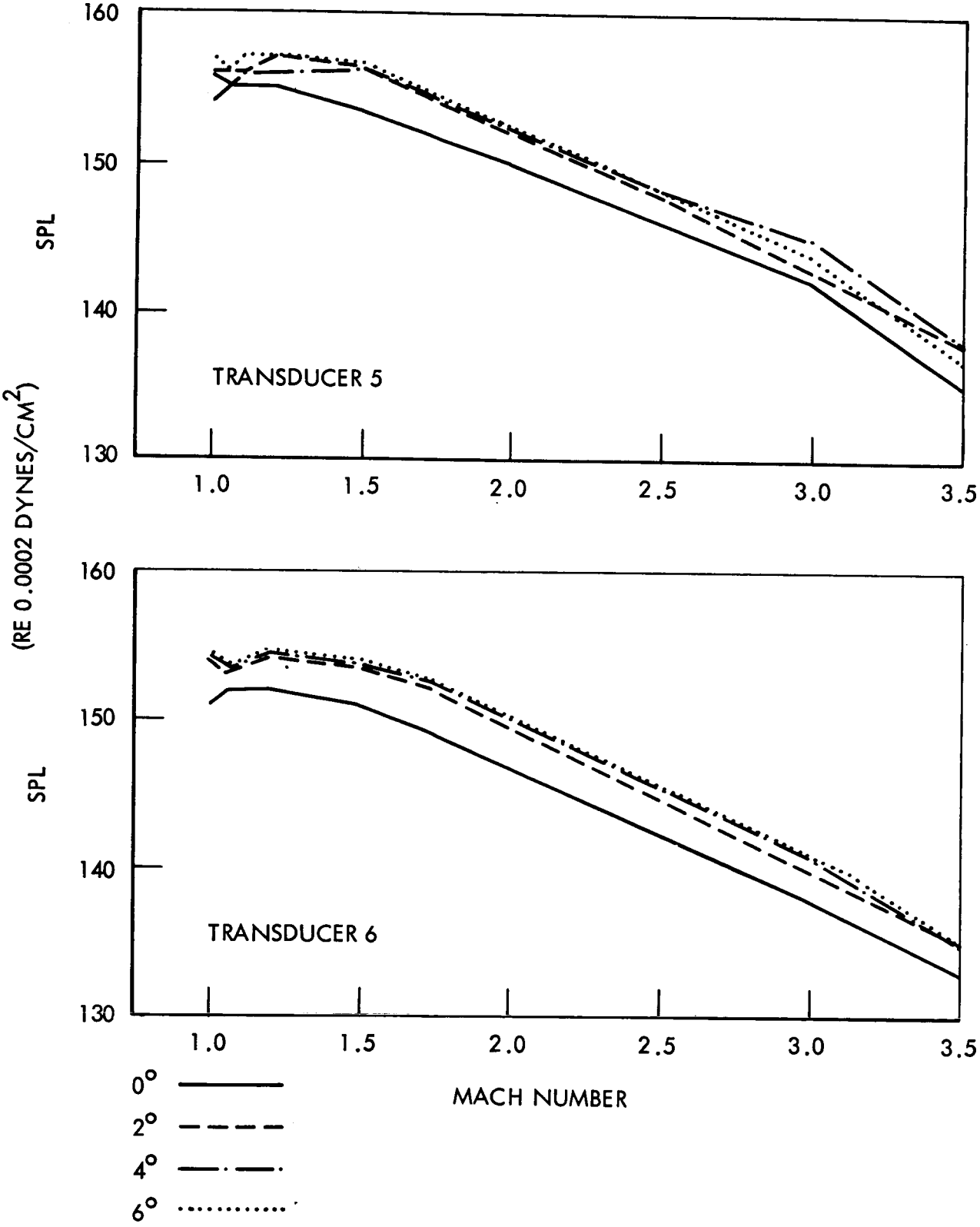

Figure 10. Overall Sound Pressure Level Versus M, Configuration D (M=1.0 to 3.5) (Sheet 3)

CONFIDENTIAL

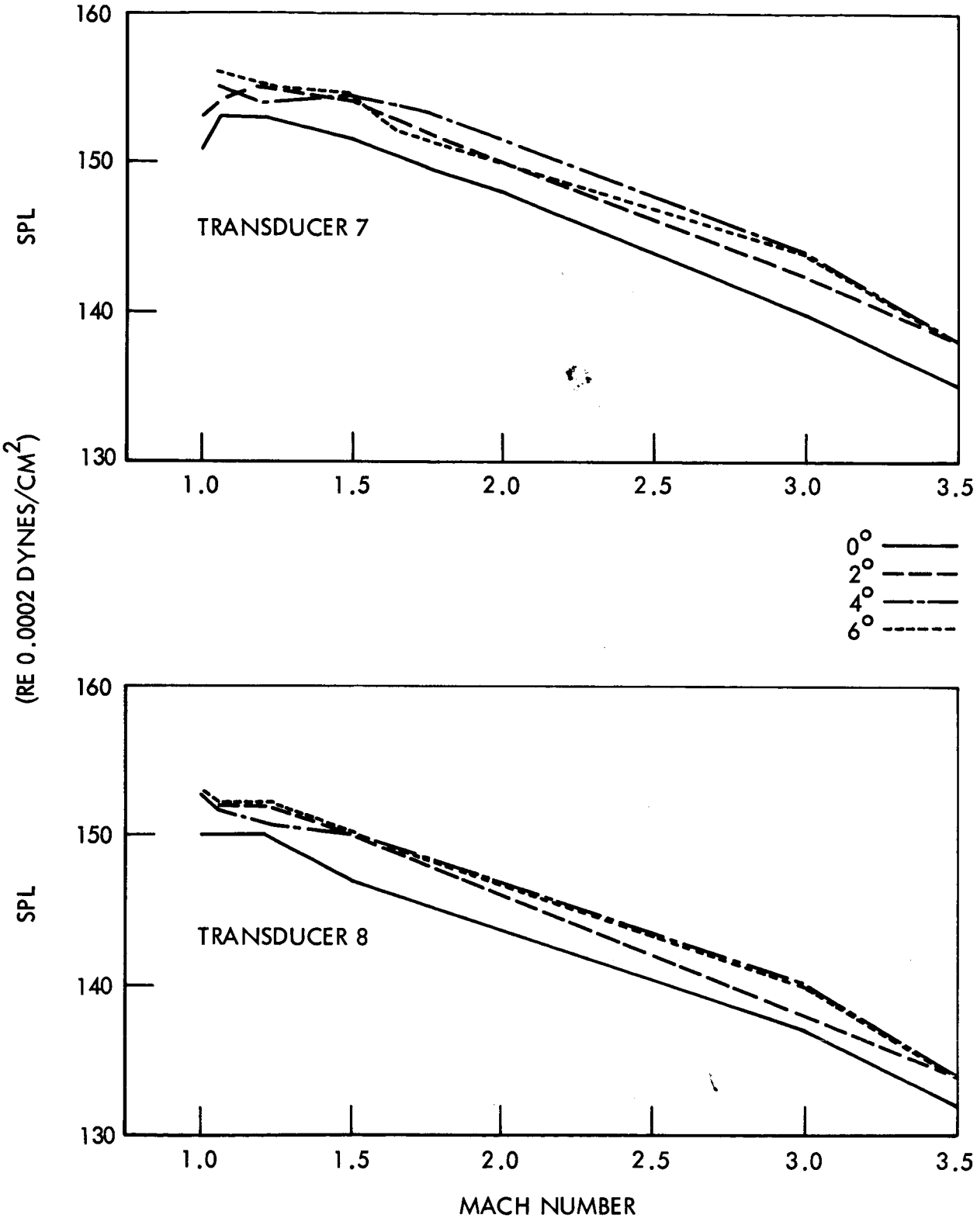

Figure 10. Overall Sound Pressure Level Versus M, Configuration D (M=1.0 to 3.5) (Sheet 4)

CONFIDENTIAL

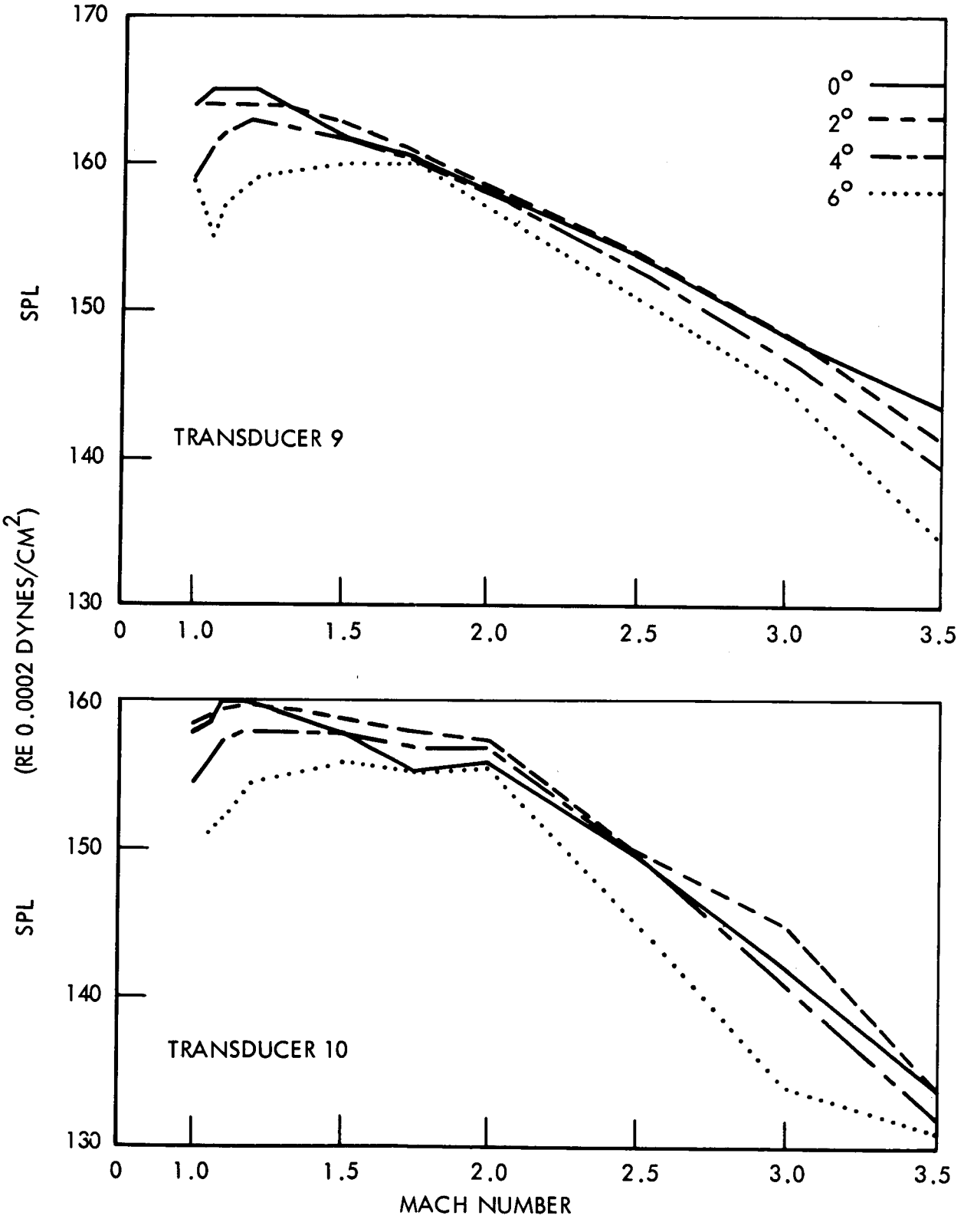

Figure 10. Overall Sound Pressure Level Versus M, Configuration D (M=1.0 to 3.5) (Sheet 5)

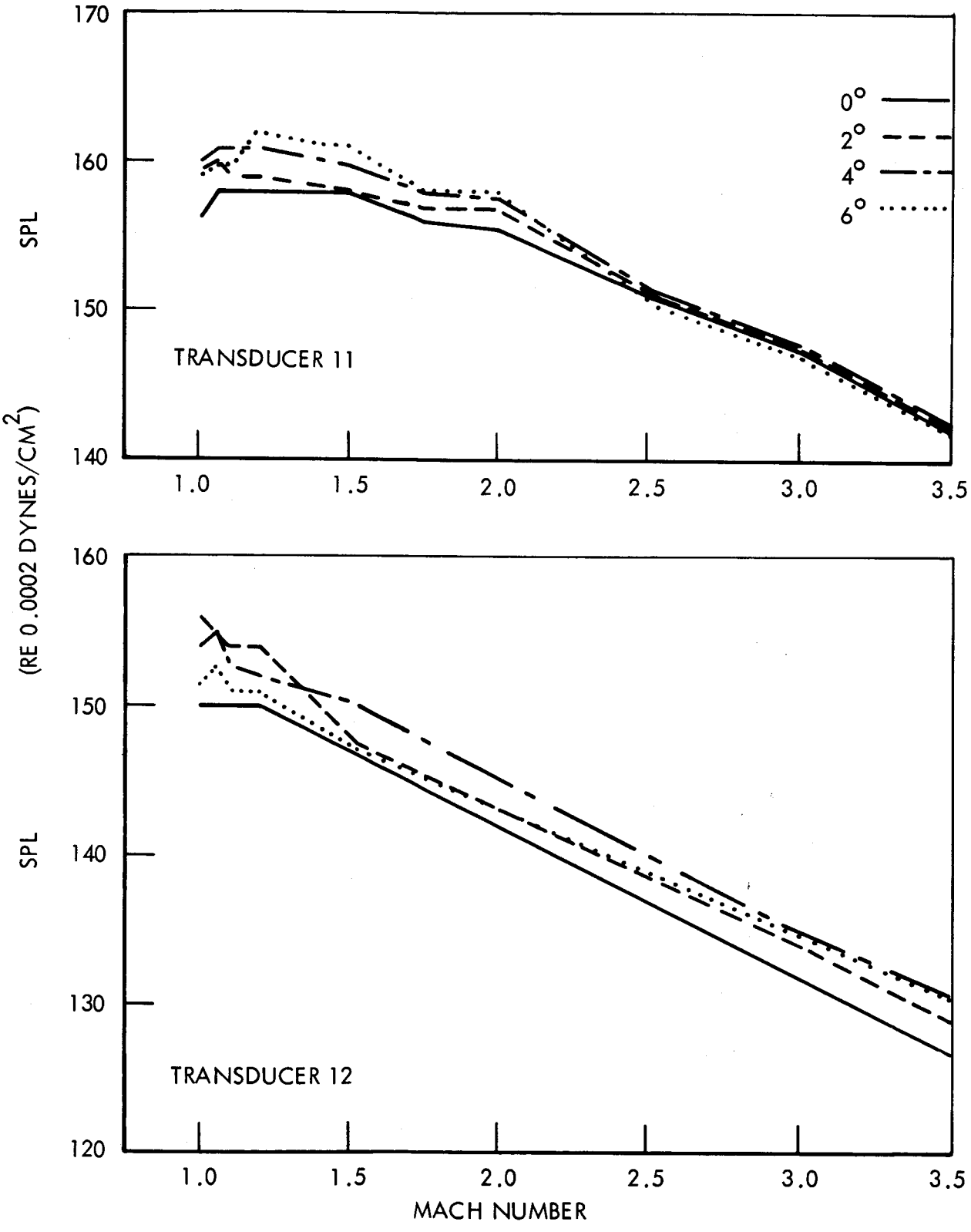

Figure 10. Overall Sound Pressure Level Versus M, Configuration D (M=1.0 to 3.5) (Sheet 6)

CONFIDENTIAL

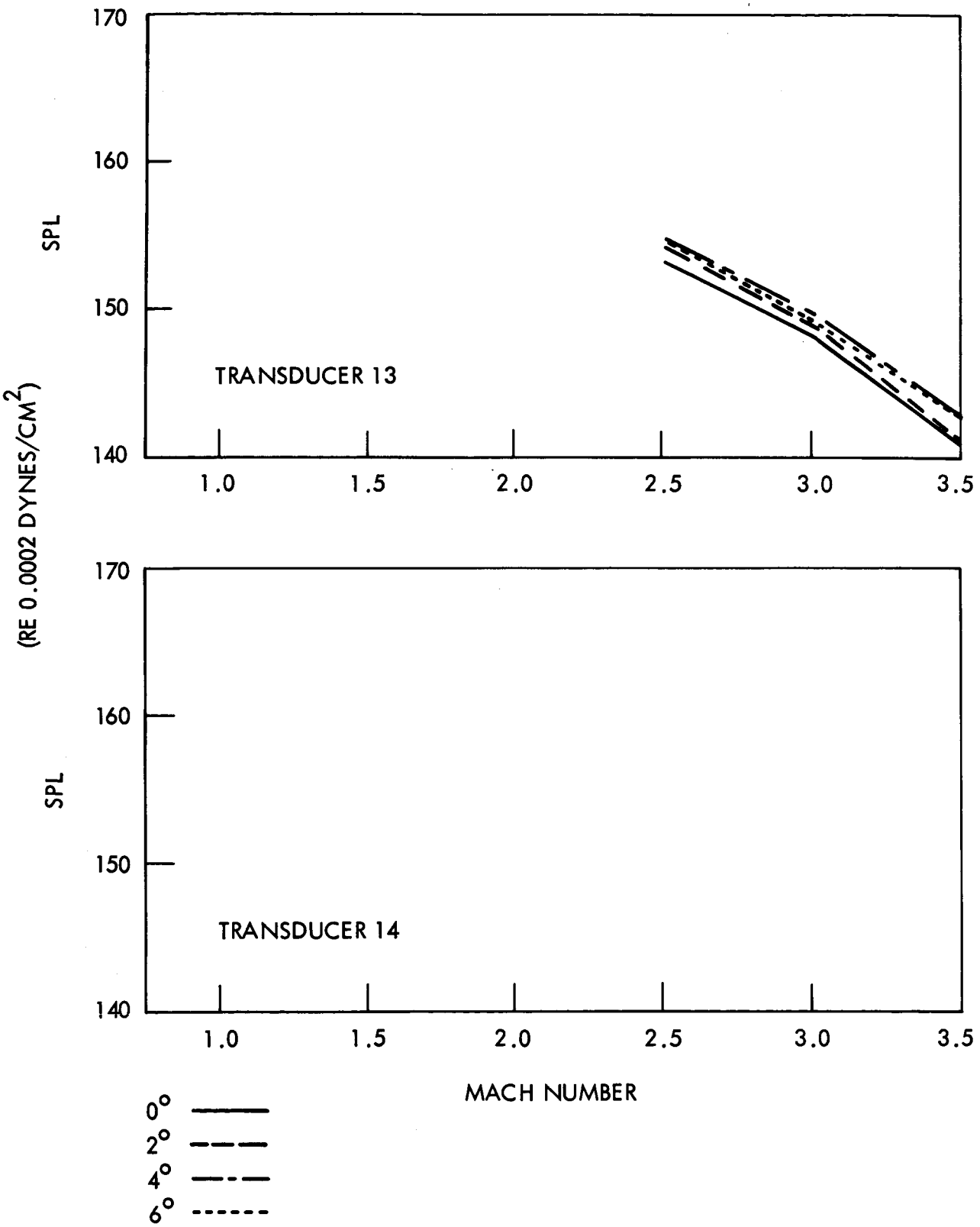

Figure 10. Overall Sound Pressure Level Versus M, Configuration D (M=1.0 to 3.5) (Sheet 7)

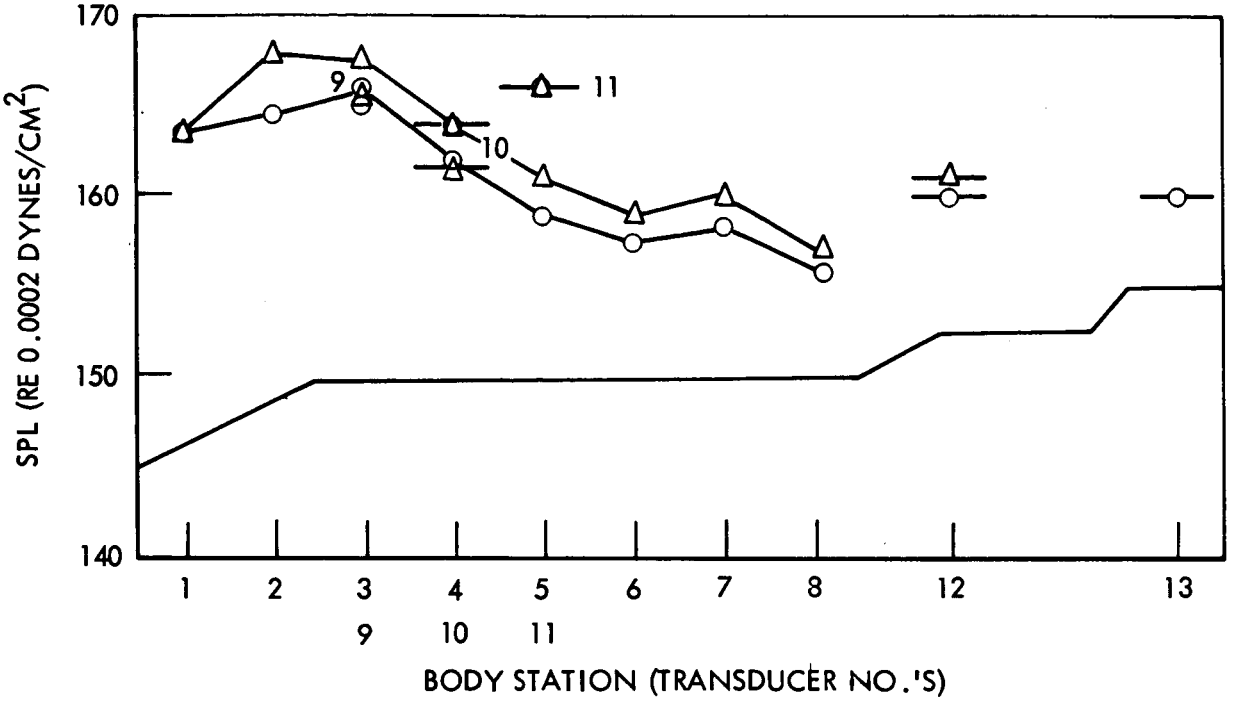

SIMPLE TOWER

TRANS	MACH NO.	ANGLE
1	.70	0
2	1.50	0
3	.70	2
4	.89	6
5	.89	2
6	.89	0
7	.92	6
8	.92	6
9	.70	0
10	.70	2
11	.89	4
12	.92	2
13	1.50	4

TOWER AND WASHER

TRANS	MACH NO.	ANGLE
1	.92	2
2	.92	2
3	.89	2
4	.89	2
5	.92	0
6	.89	2
7	.92	6
8	.92	2
9	.70	2
10	.89	0
11	.89	4
12	.92	2
13	NO DATA POINT	

Figure 11. Maximum Sound Pressure Distribution

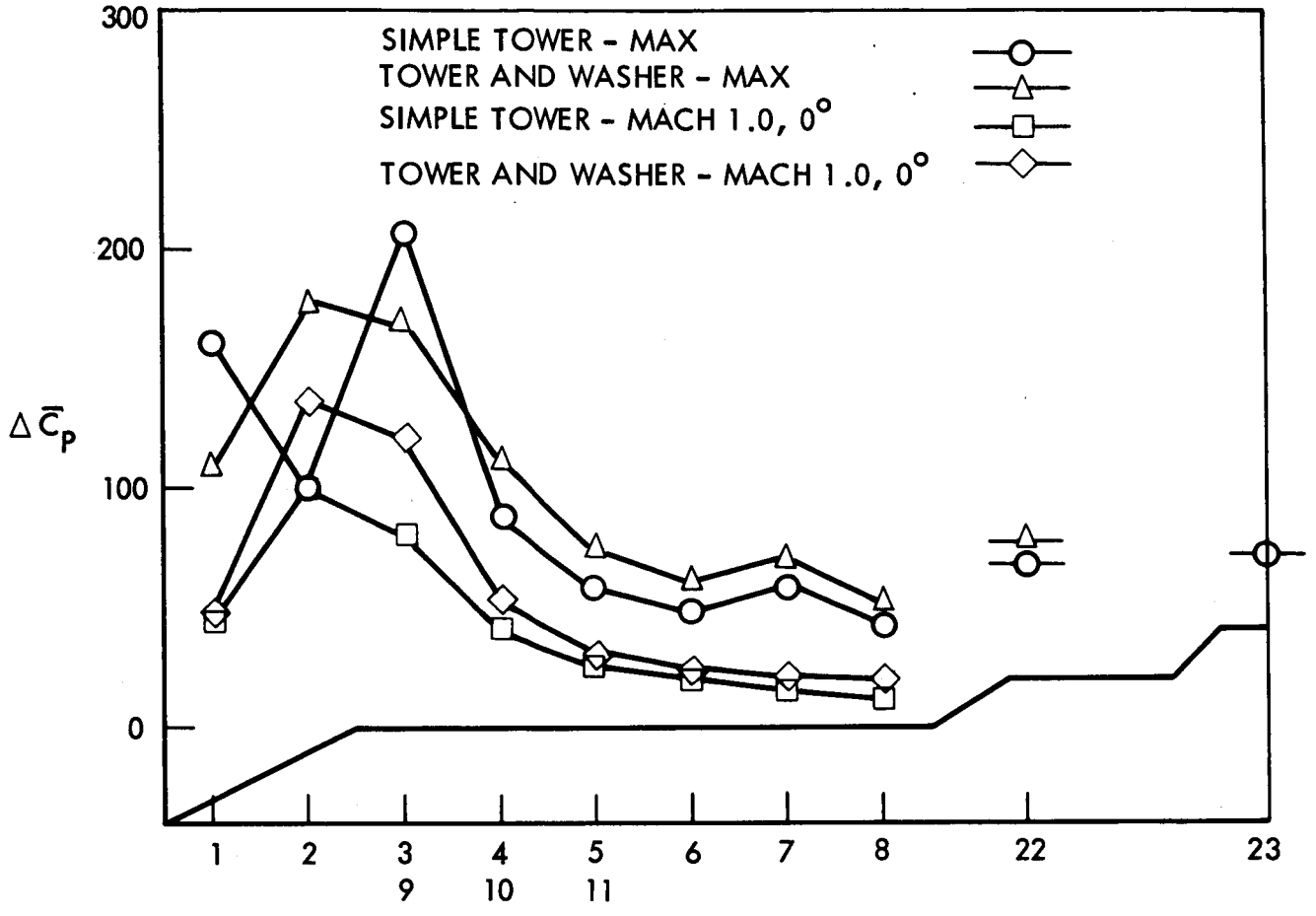

SIMPLE TOWER

TRANS	MACH NO.	ANGLE
1	.70	0
2	1.50	0
3	.70	2
4	.89	6
5	.89	2
6	.89	0
7	.92	6
8	.92	6
9	.70	0
10	.70	2
11	.89	4
12	.92	2
13	1.50	4

TOWER AND WASHER

TRANS	MACH NO.	ANGLE
1	.92	2
2	.92	2
3	.89	2
4	.89	2
5	.92	0
6	.89	2
7	.92	6
8	.92	2
9	.70	2
10	.89	0
11	.89	4
12	.92	2
13	NO DATA POINT	

Figure 12. Transient Pressure Coefficient Distribution

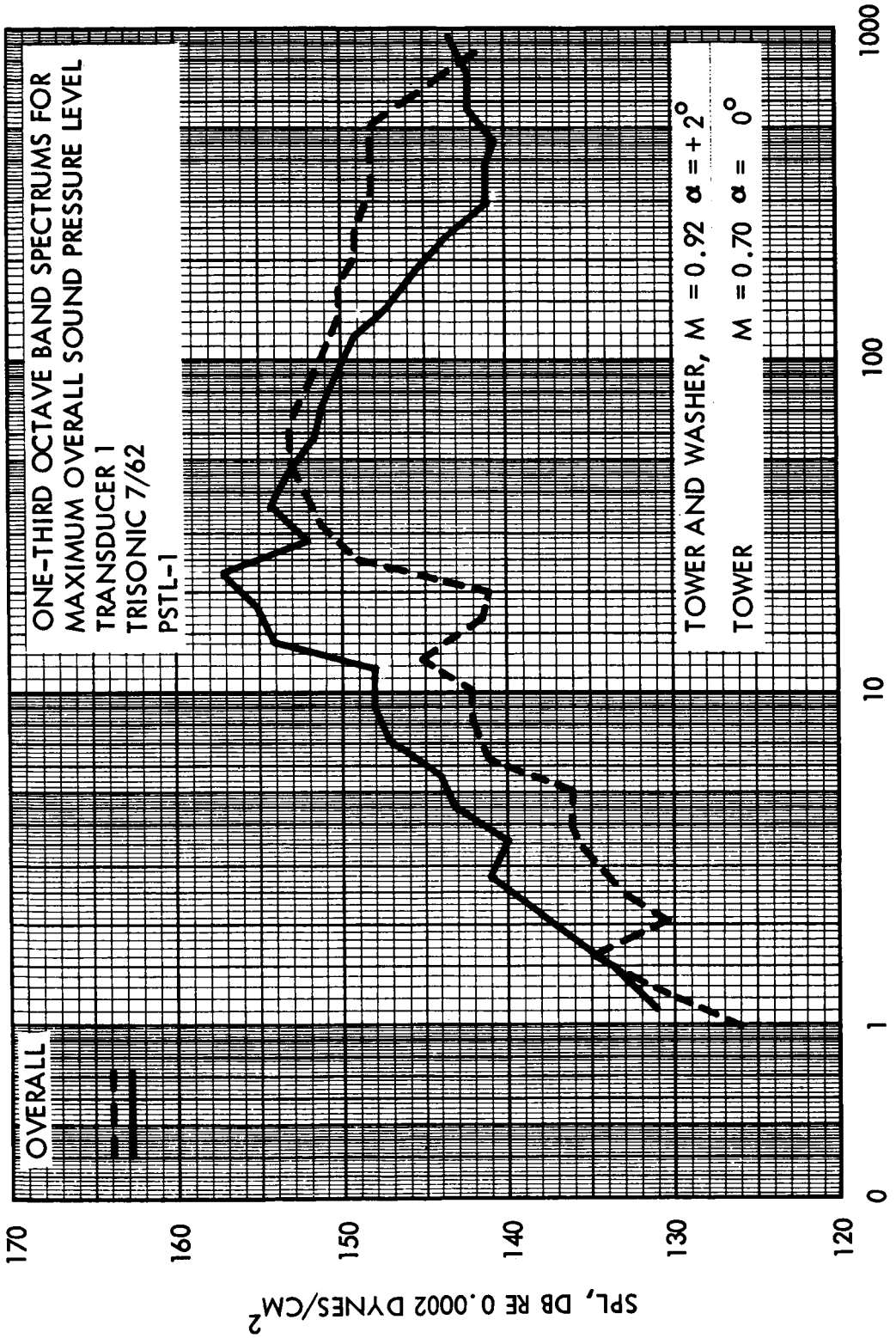

Figure 13. One-Third Octave Band Spectrums of Maximum Sound Pressure Levels (Sheet 1)

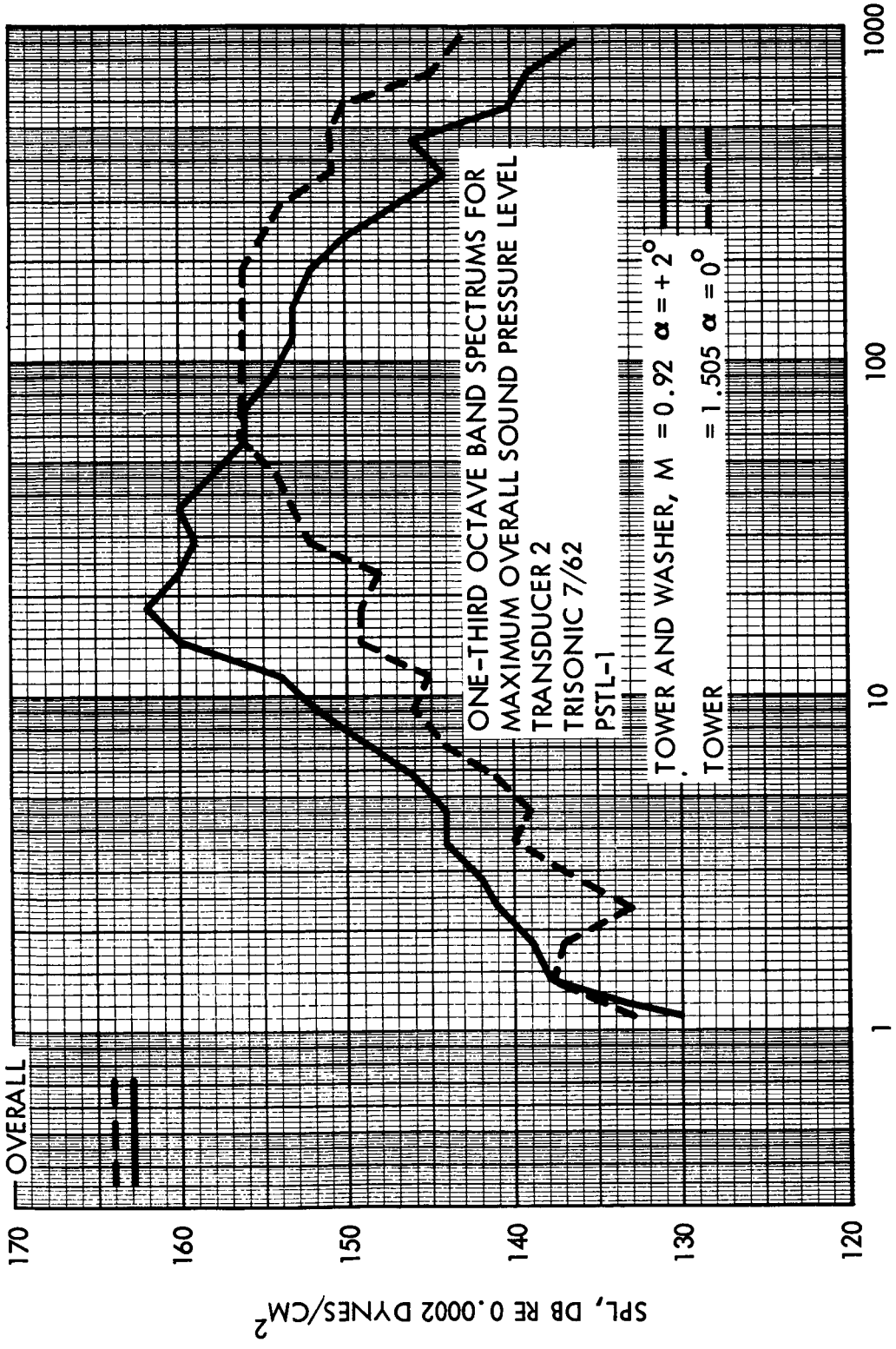

Figure 13. One-Third Octave Band Spectrums of Maximum Sound Pressure Levels (Sheet 2)

CONFIDENTIAL

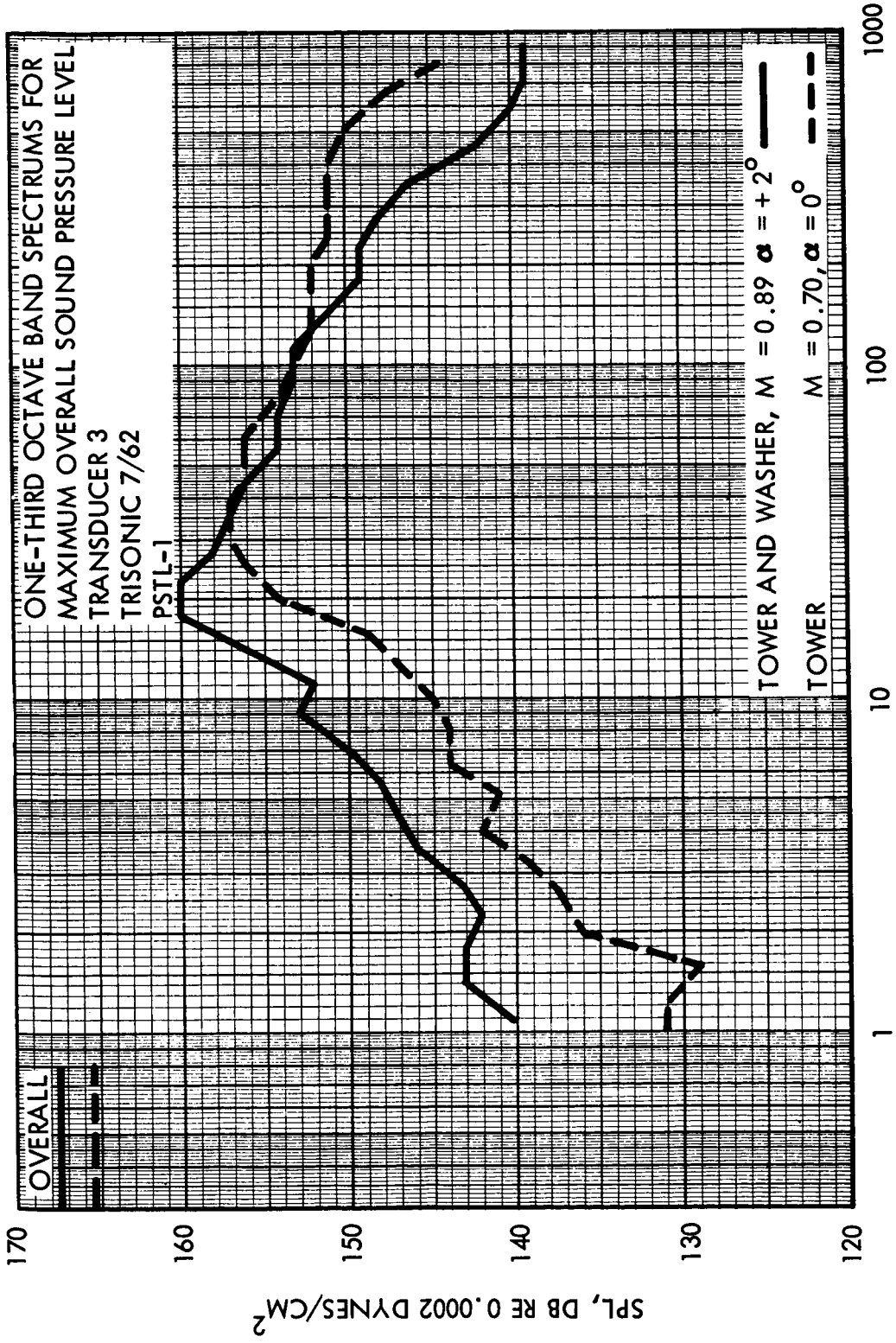

Figure 13. One-Third Octave Band Spectrums of Maximum Sound Pressure Levels (Sheet 3)

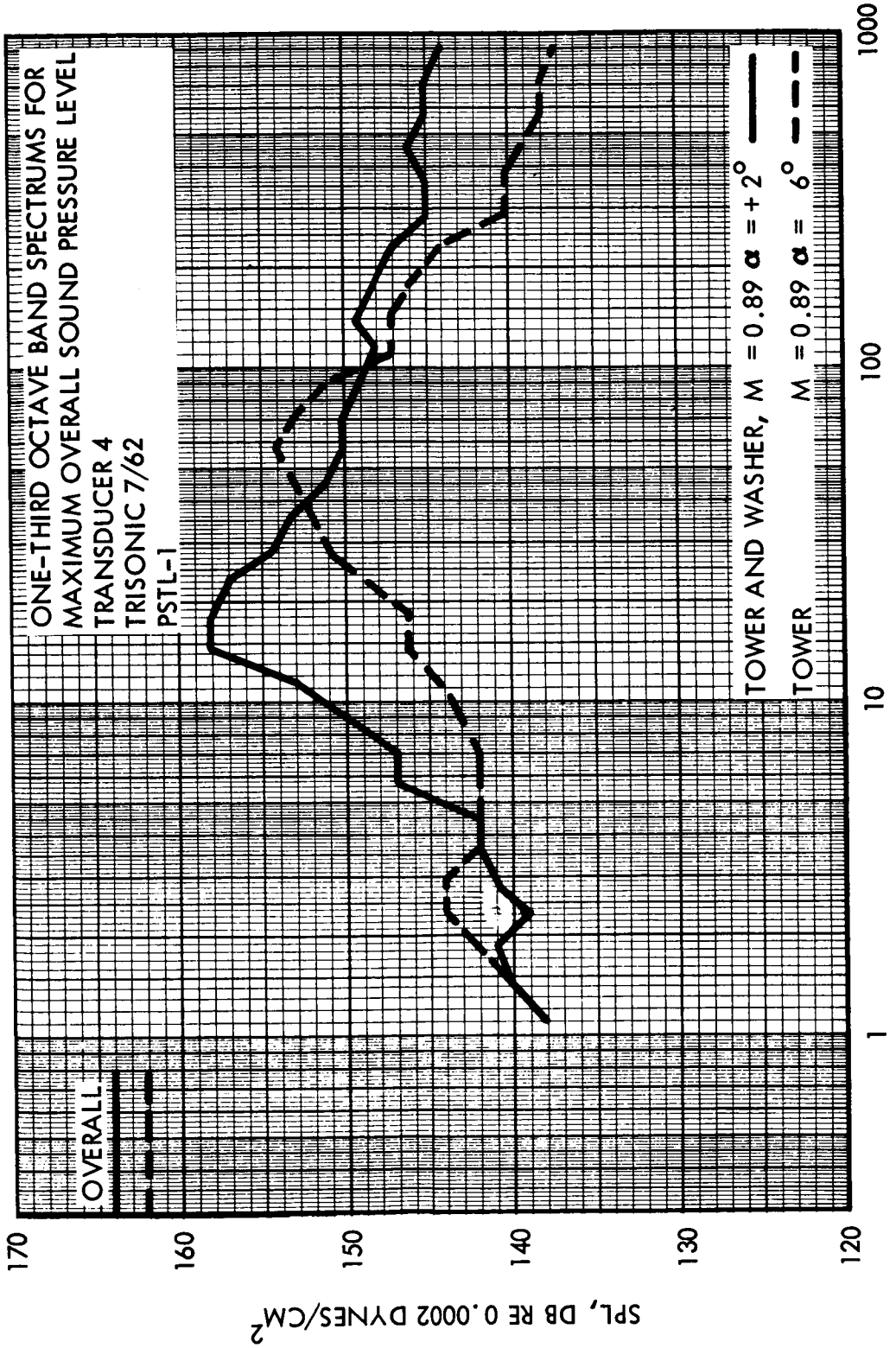

Figure 13. One-Third Octave Band Spectrums of Maximum Sound Pressure Levels (Sheet 4)

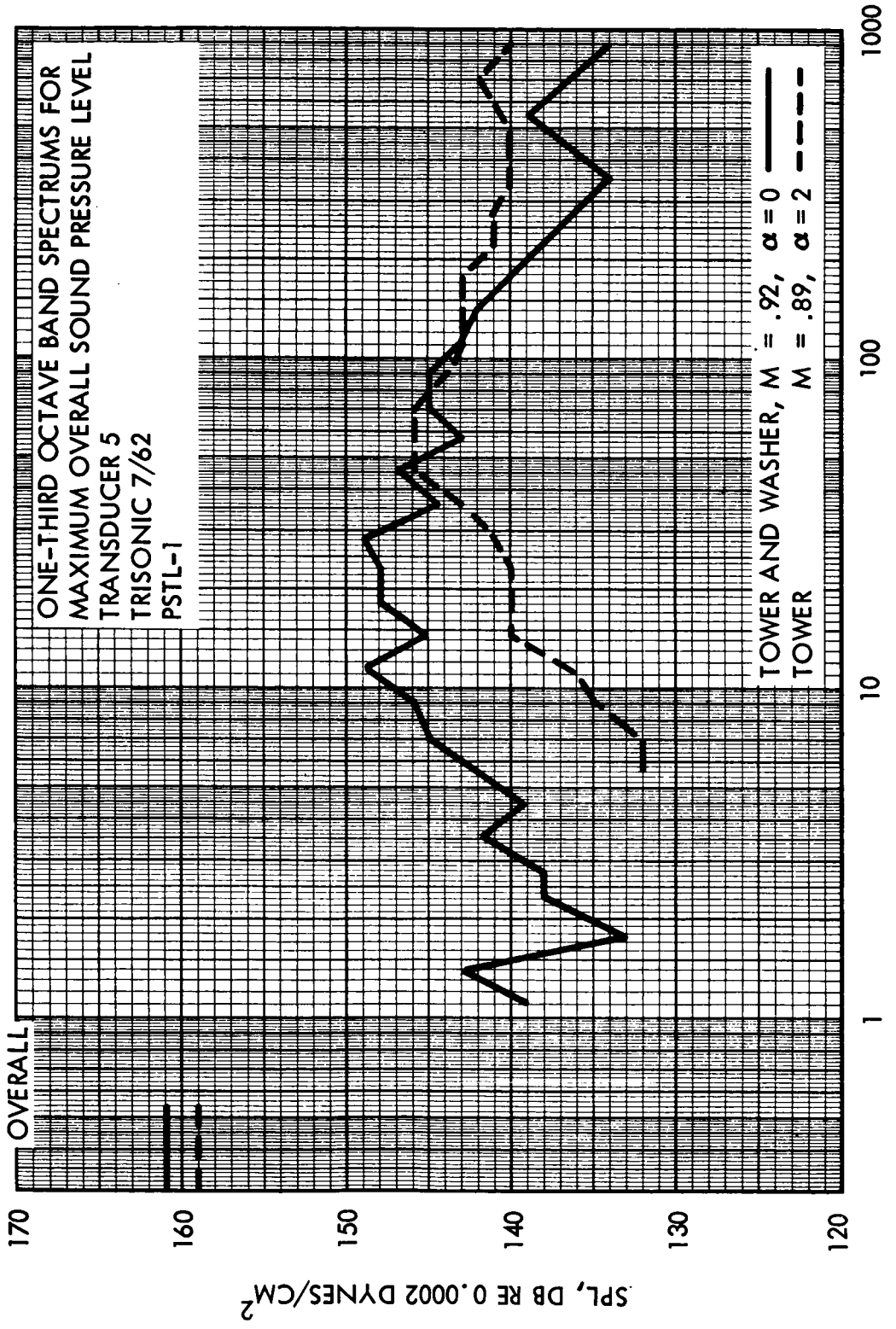

Figure 13. One-Third Octave Band Spectrums of Maximum Sound Pressure Levels (Sheet 5)

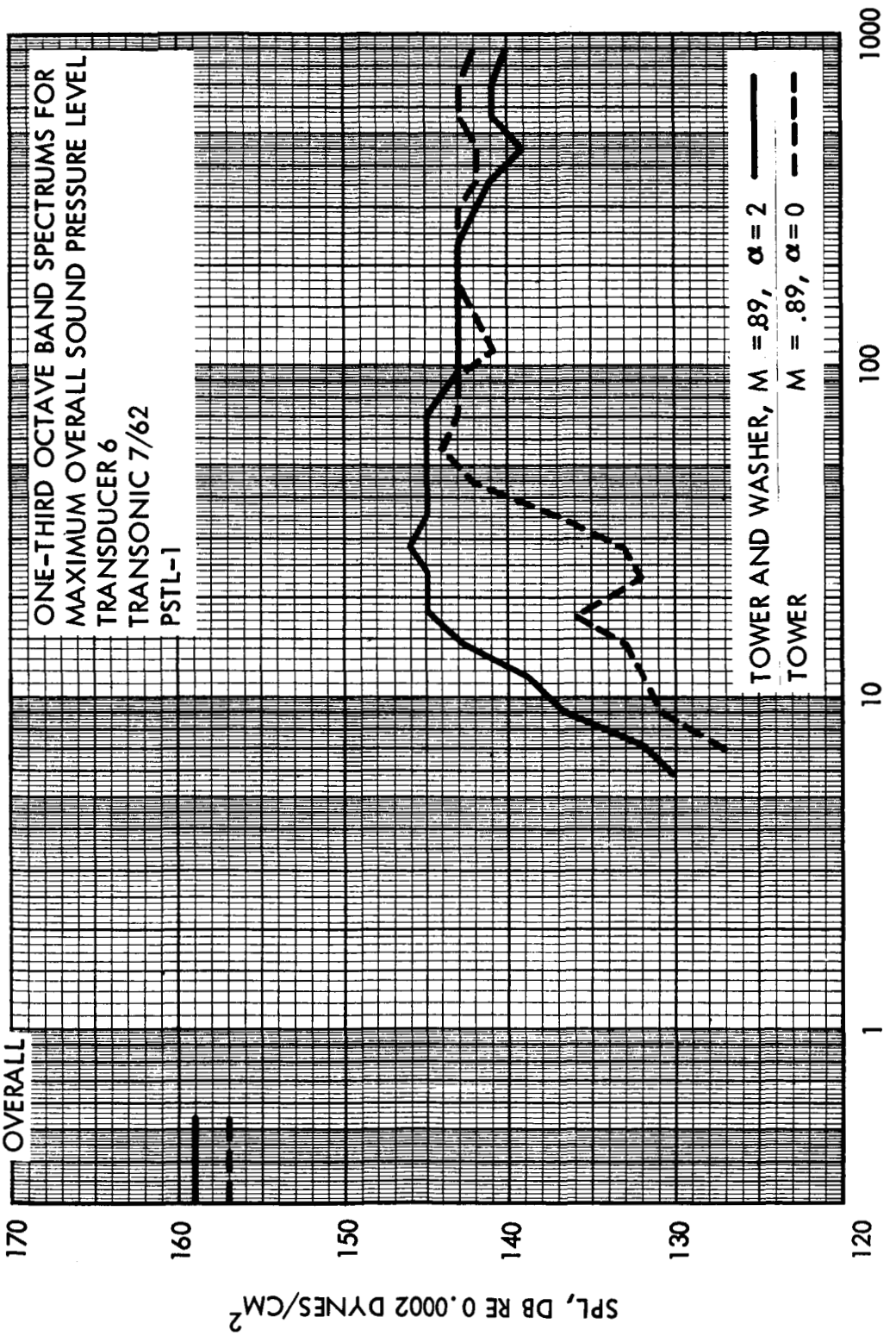

Figure 13. One-Third Octave Band Spectrums of Maximum Sound Pressure Levels (Sheet 6)

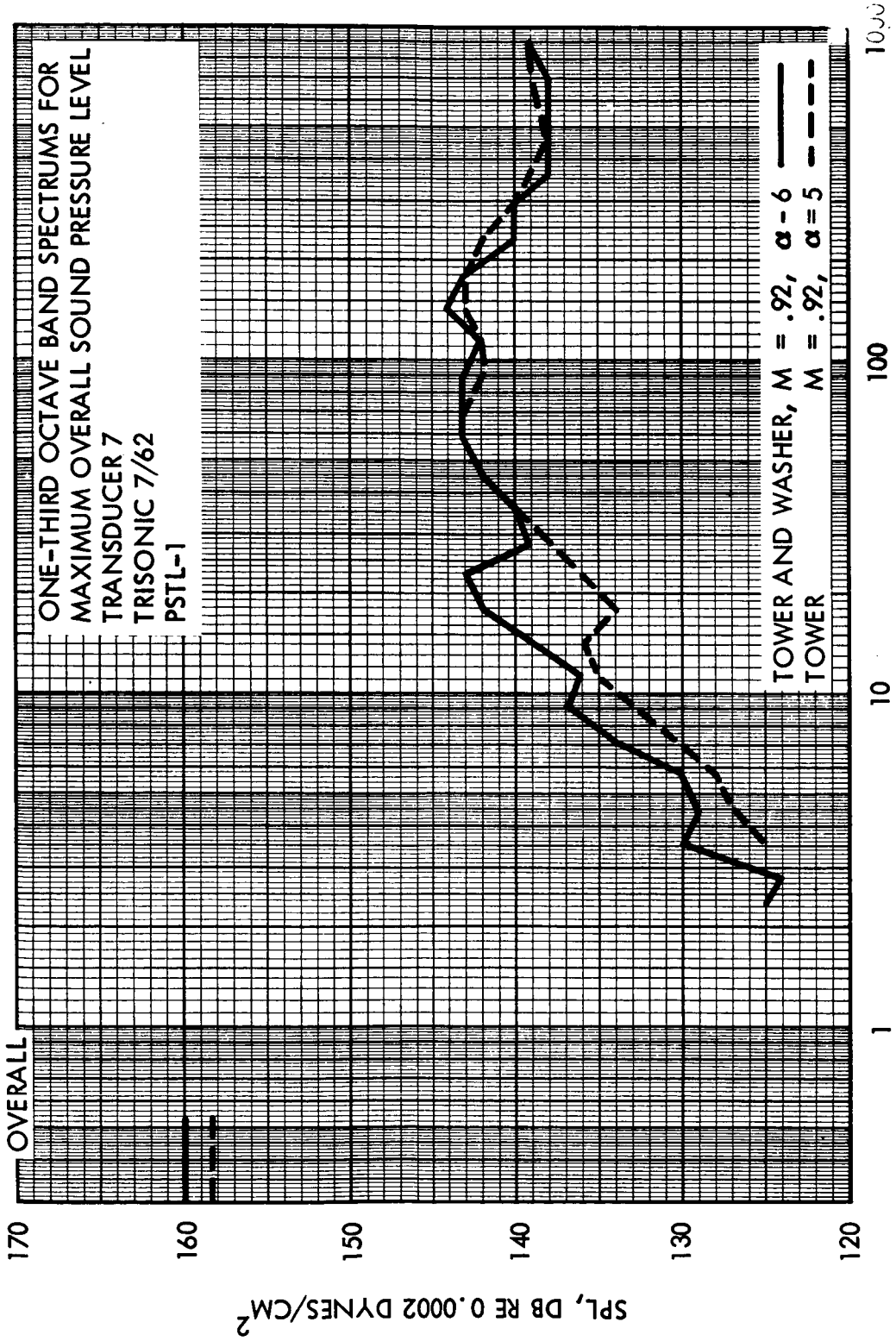

Figure 13. One-Third Octave Band Spectrums of Maximum Sound Pressure Levels (Sheet 7)

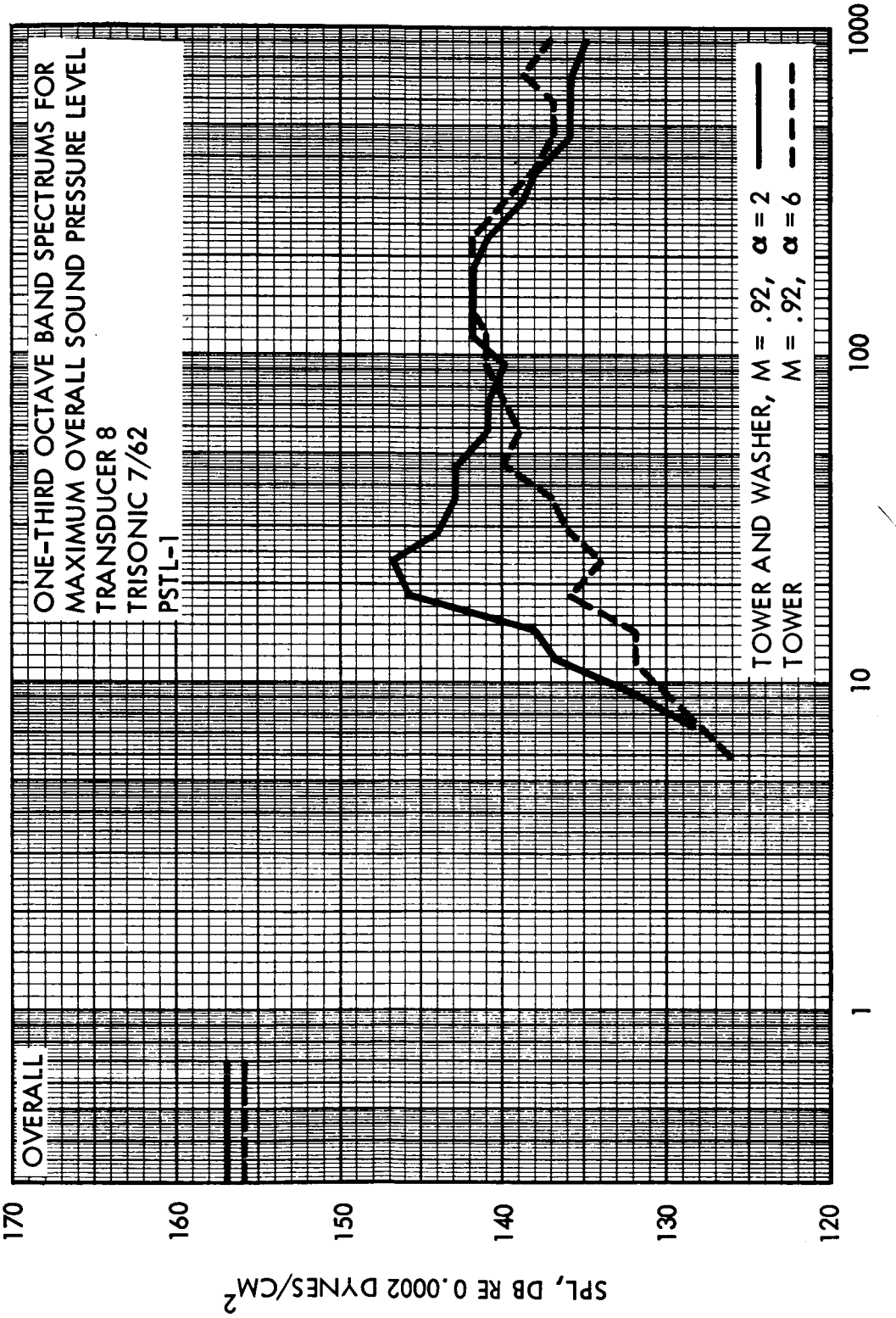

Figure 13. One-Third Octave Band Spectrums of Maximum Sound Pressure Levels (Sheet 8)

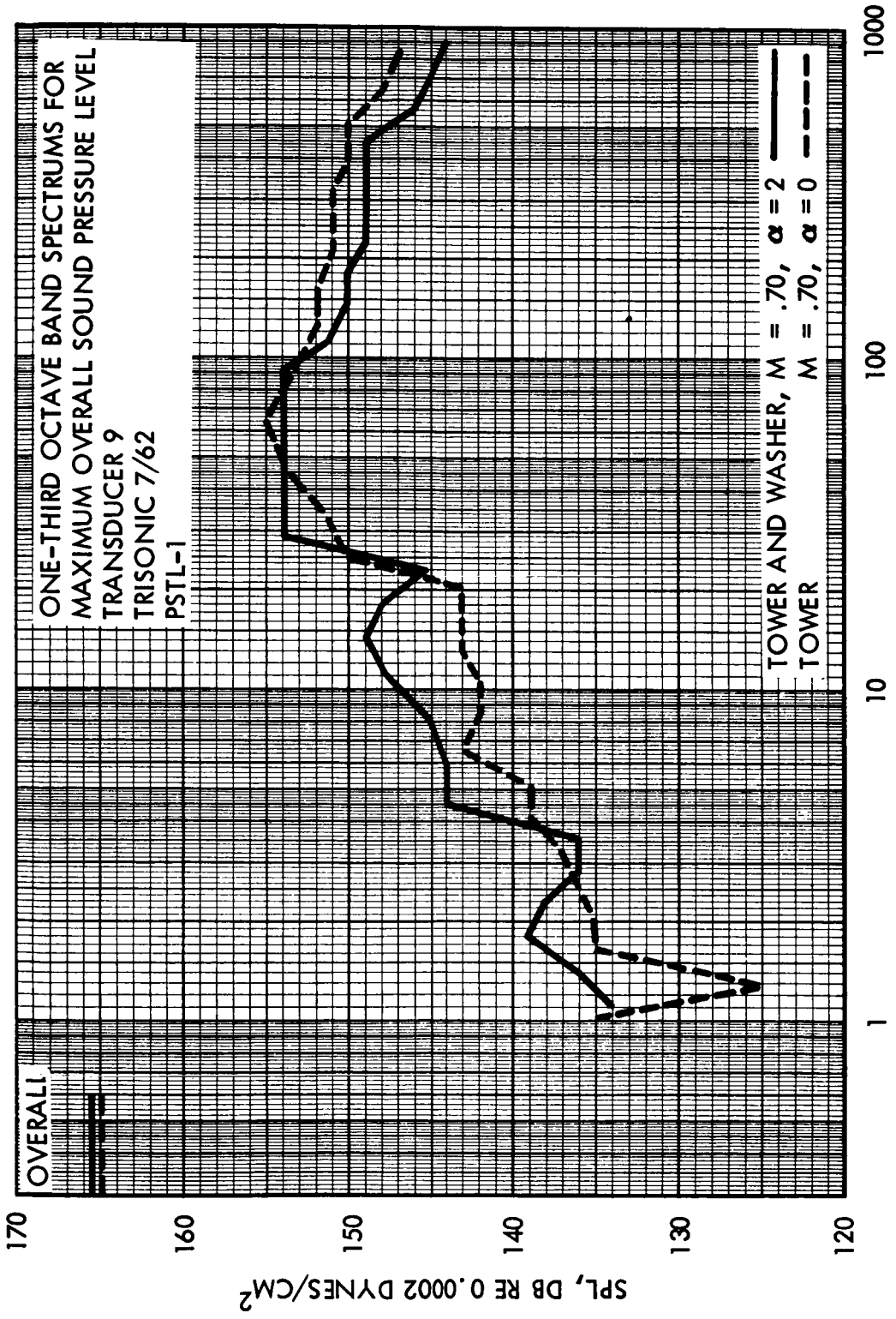

Figure 13. One-Third Octave Band Spectrums of Maximum Sound Pressure Levels (Sheet 9)

CONFIDENTIAL

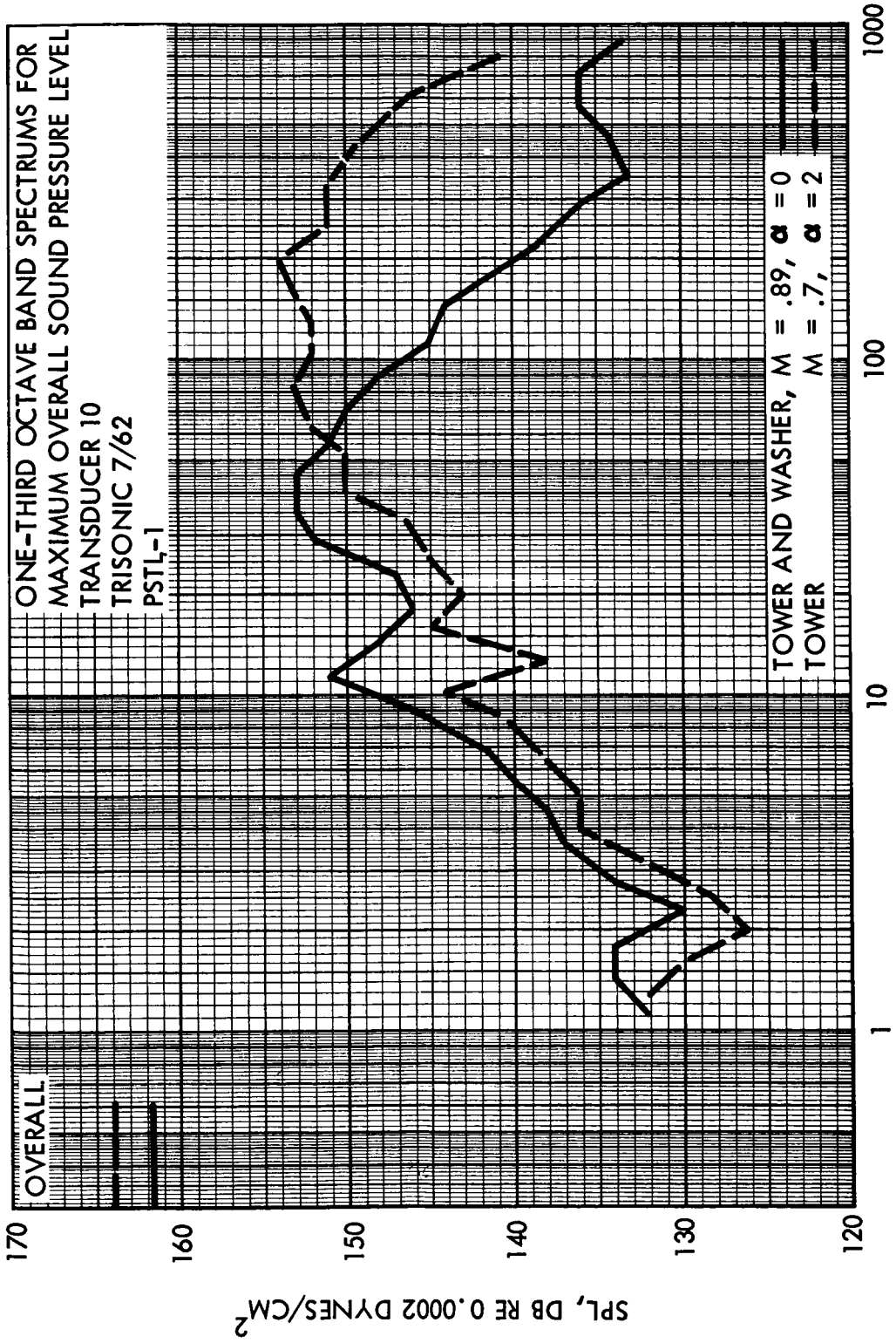

Figure 13. One-Third Octave Band Spectrums of Maximum Sound Pressure Levels (Sheet 10)

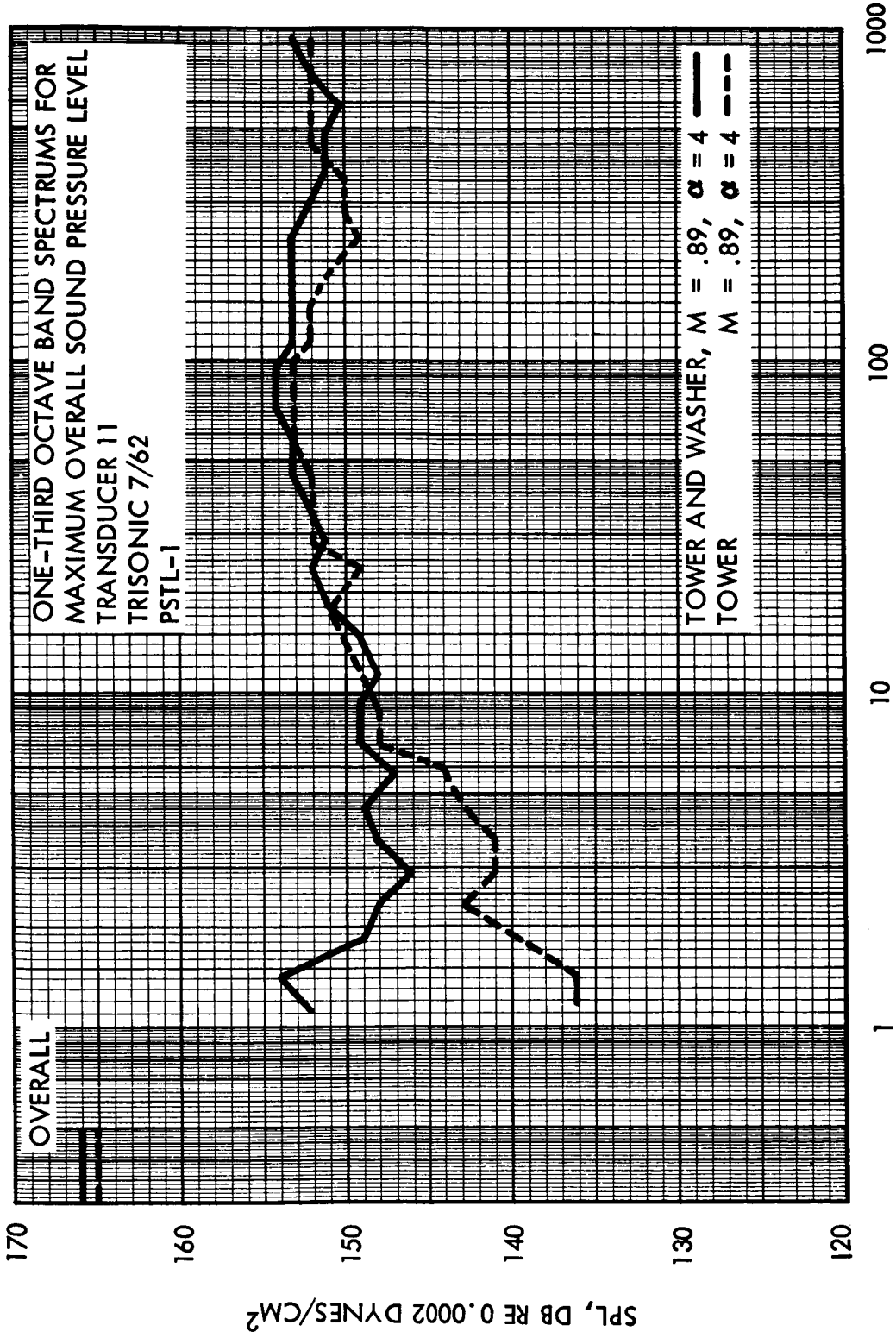

Figure 13. One-Third Octave Band Spectrums of Maximum Sound Pressure Levels (Sheet 11)

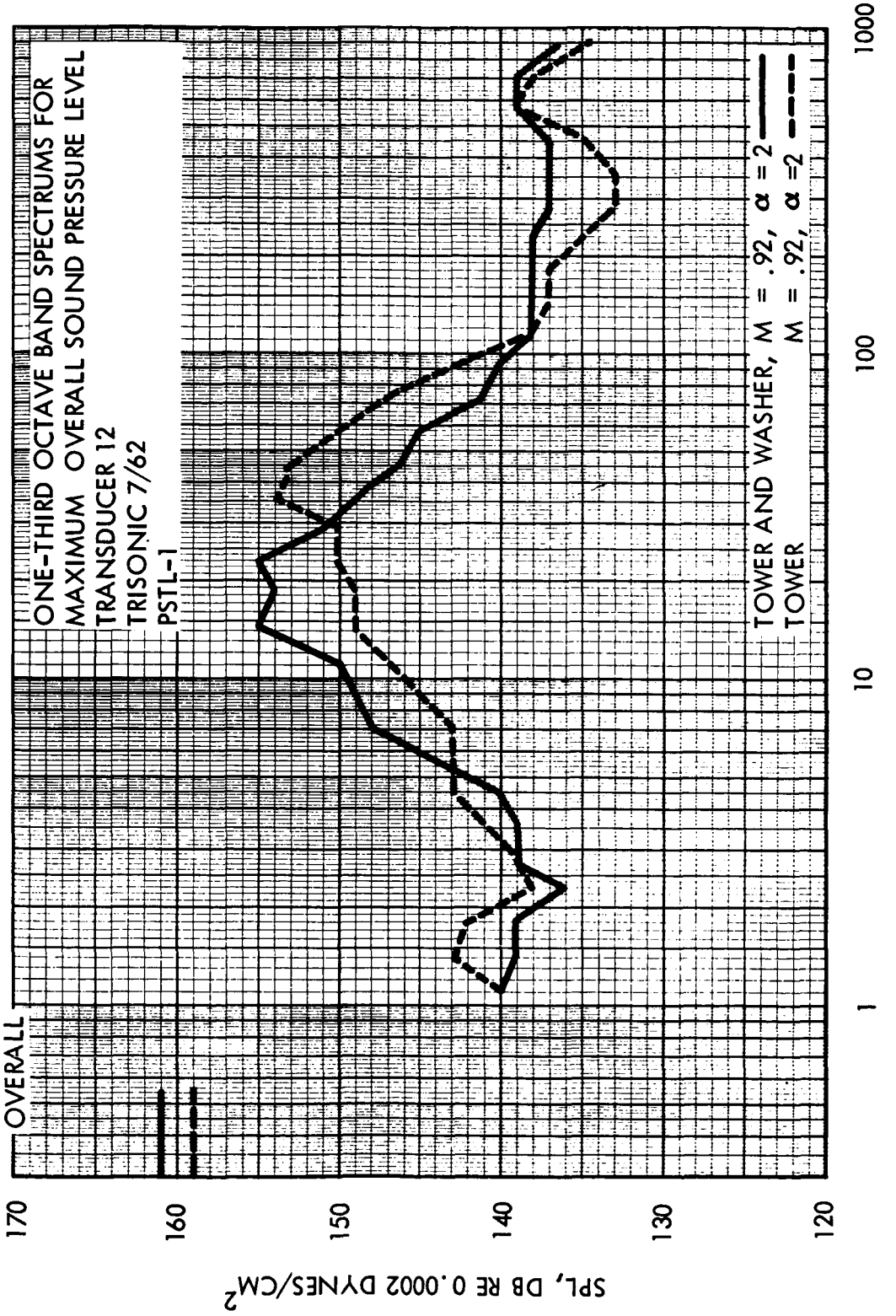

Figure 13. One-Third Octave Band Spectrums of Maximum Sound Pressure Levels (Sheet 12)

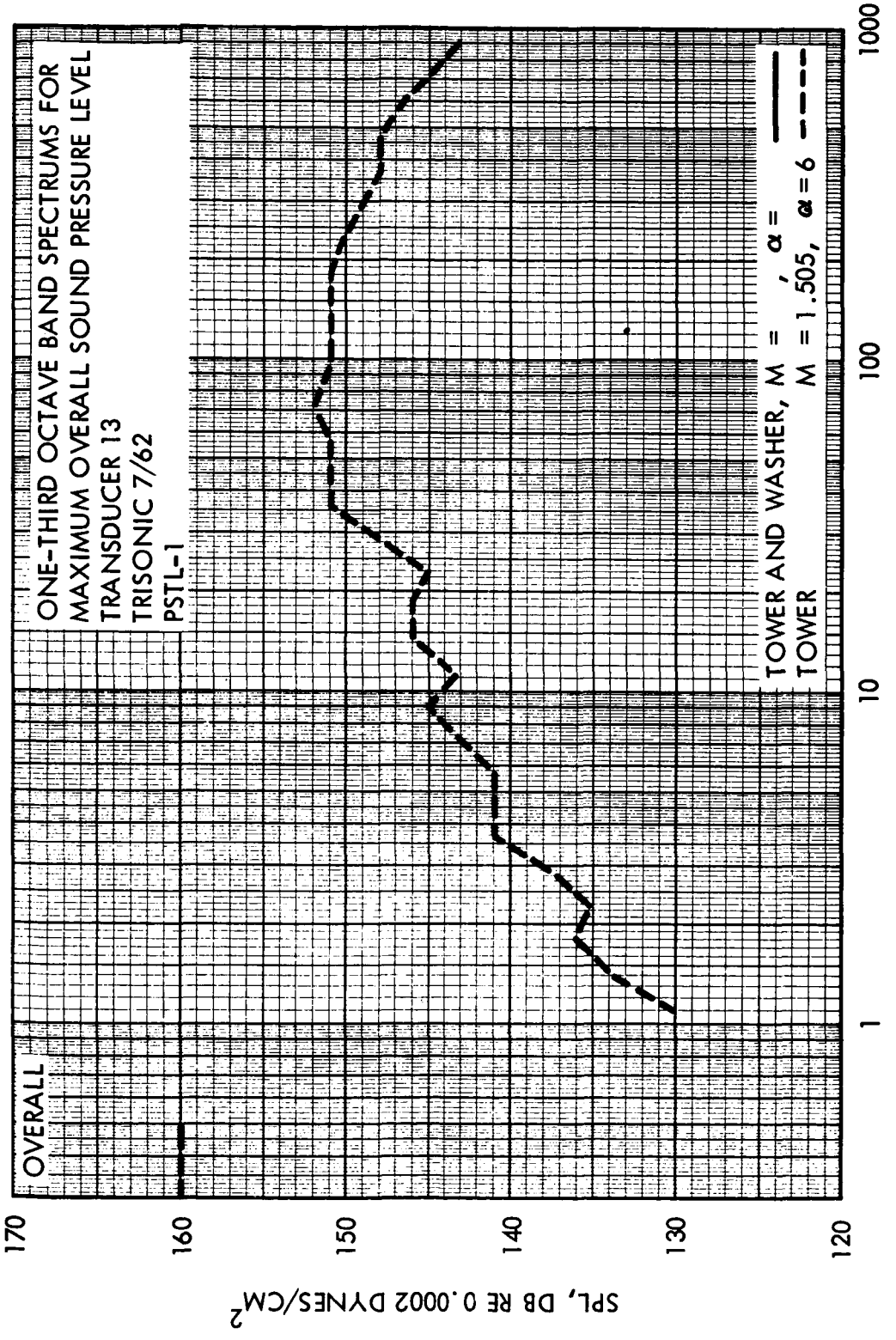

Figure 13. One-Third Octave Band Spectrums of Maximum Sound Pressure Levels (Sheet 13)

CONFIDENTIAL

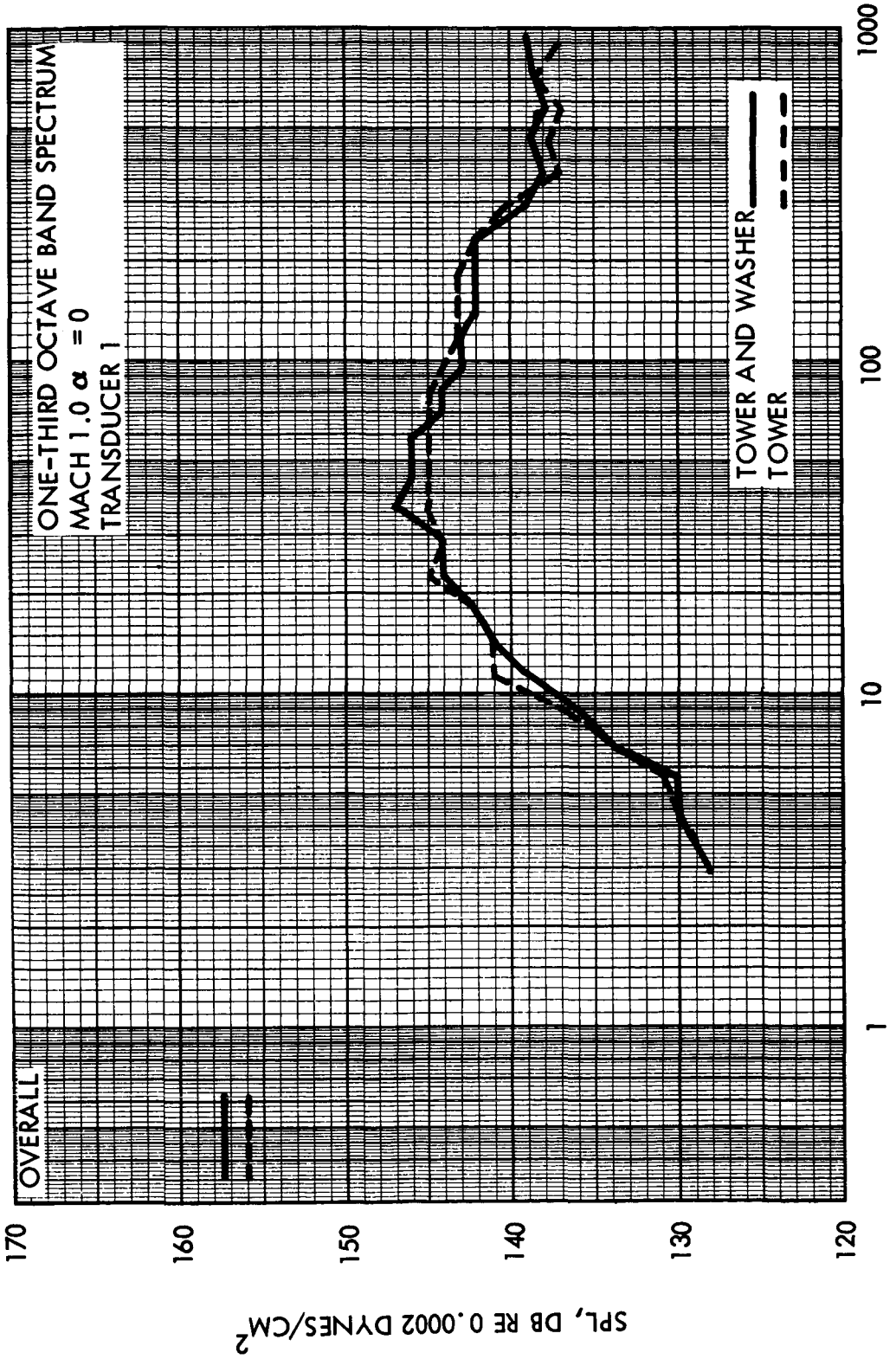

Figure 14. One-Third Octave Band Spectrums of Sound Pressure Level (M=1.0, α=0) (Sheet 1)

CONFIDENTIAL

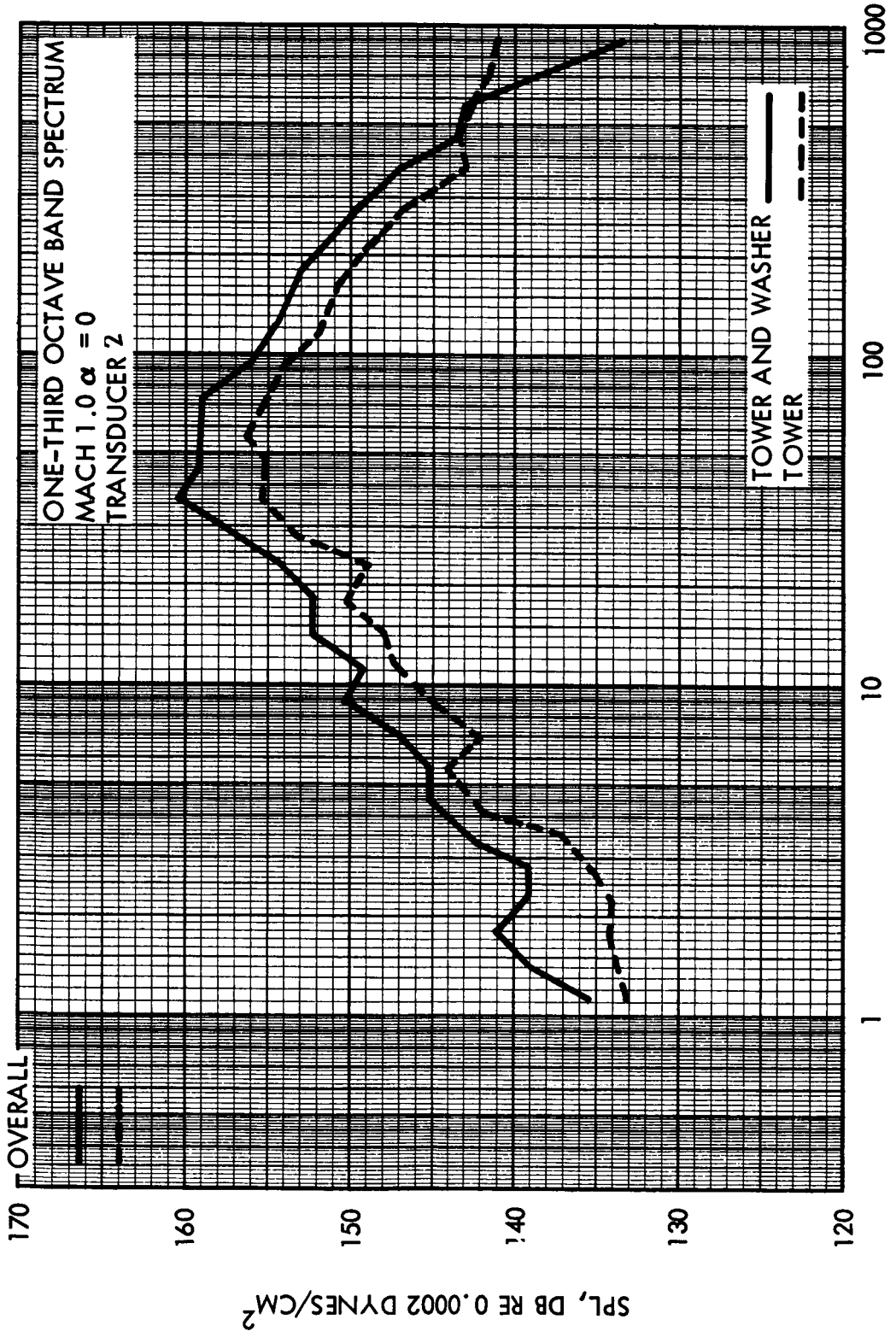

Figure 14. One-Third Octave Band Spectrums of Sound Pressure Level (M=1.0, α=0) (Sheet 2)

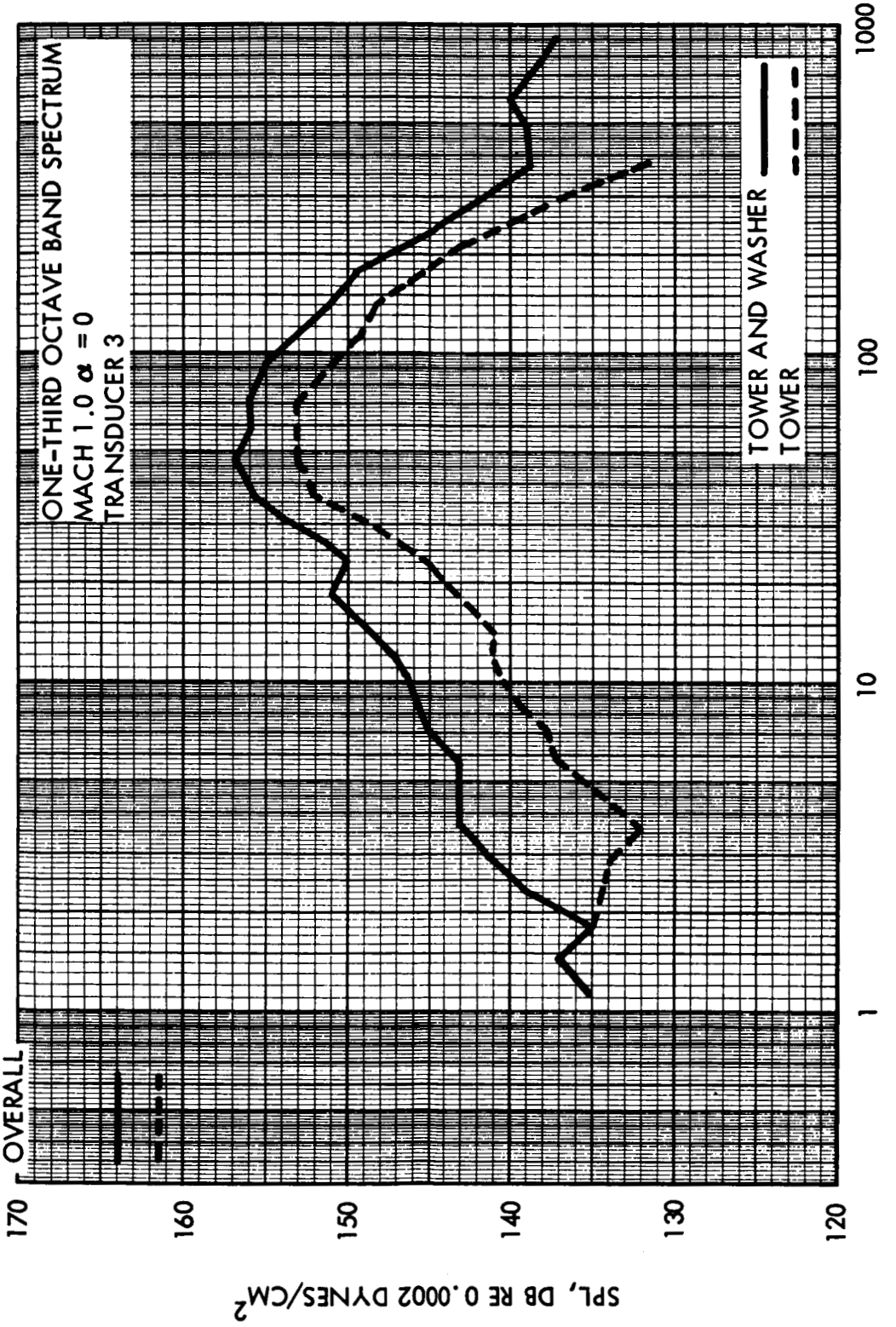

Figure 14. One-Third Octave Band Spectrums of Sound Pressure Level (M=1.0, α=0) (Sheet 3)

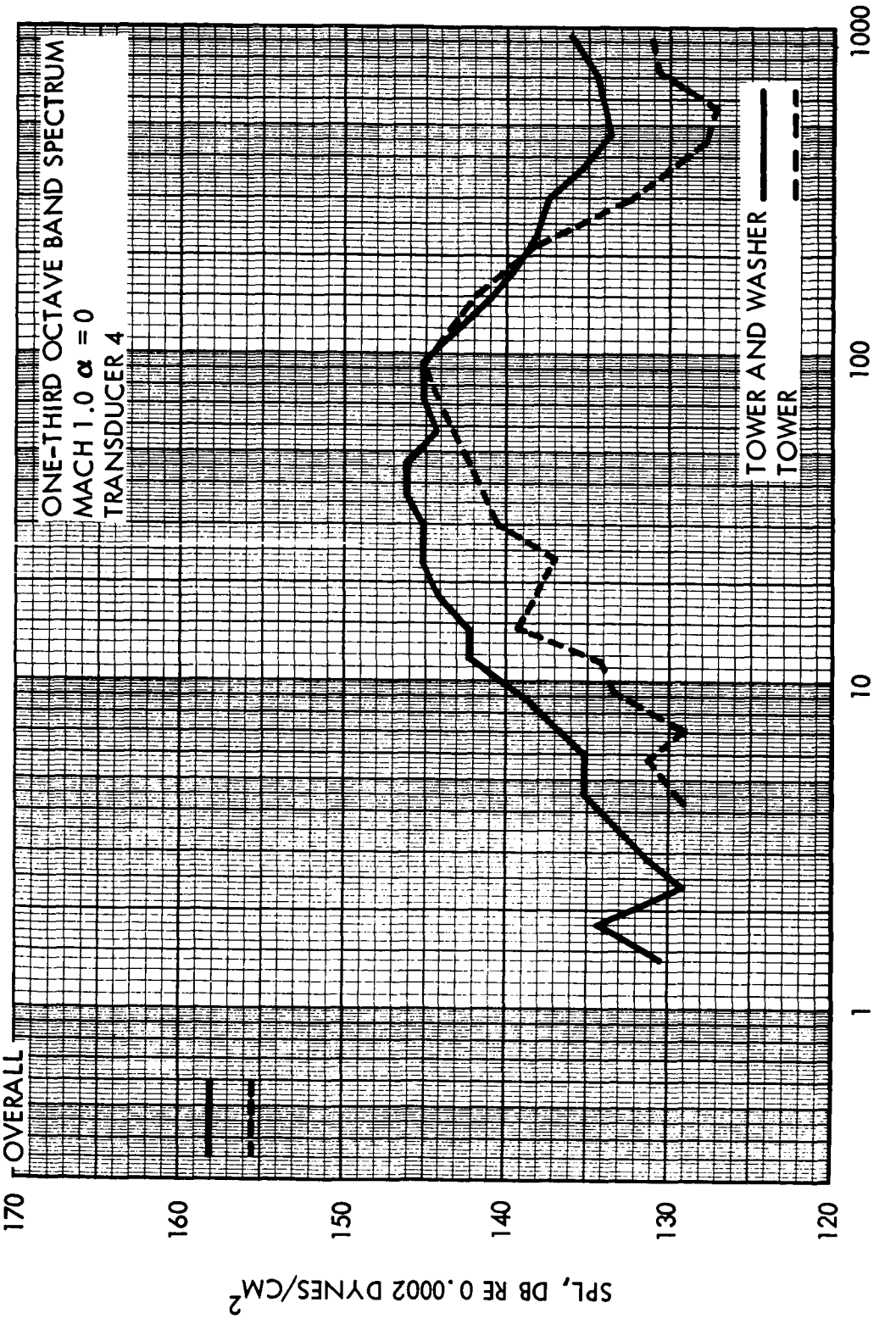

Figure 14. One-Third Octave Band Spectrums of Sound Pressure Level (M=1.0, α=0) (Sheet 4)

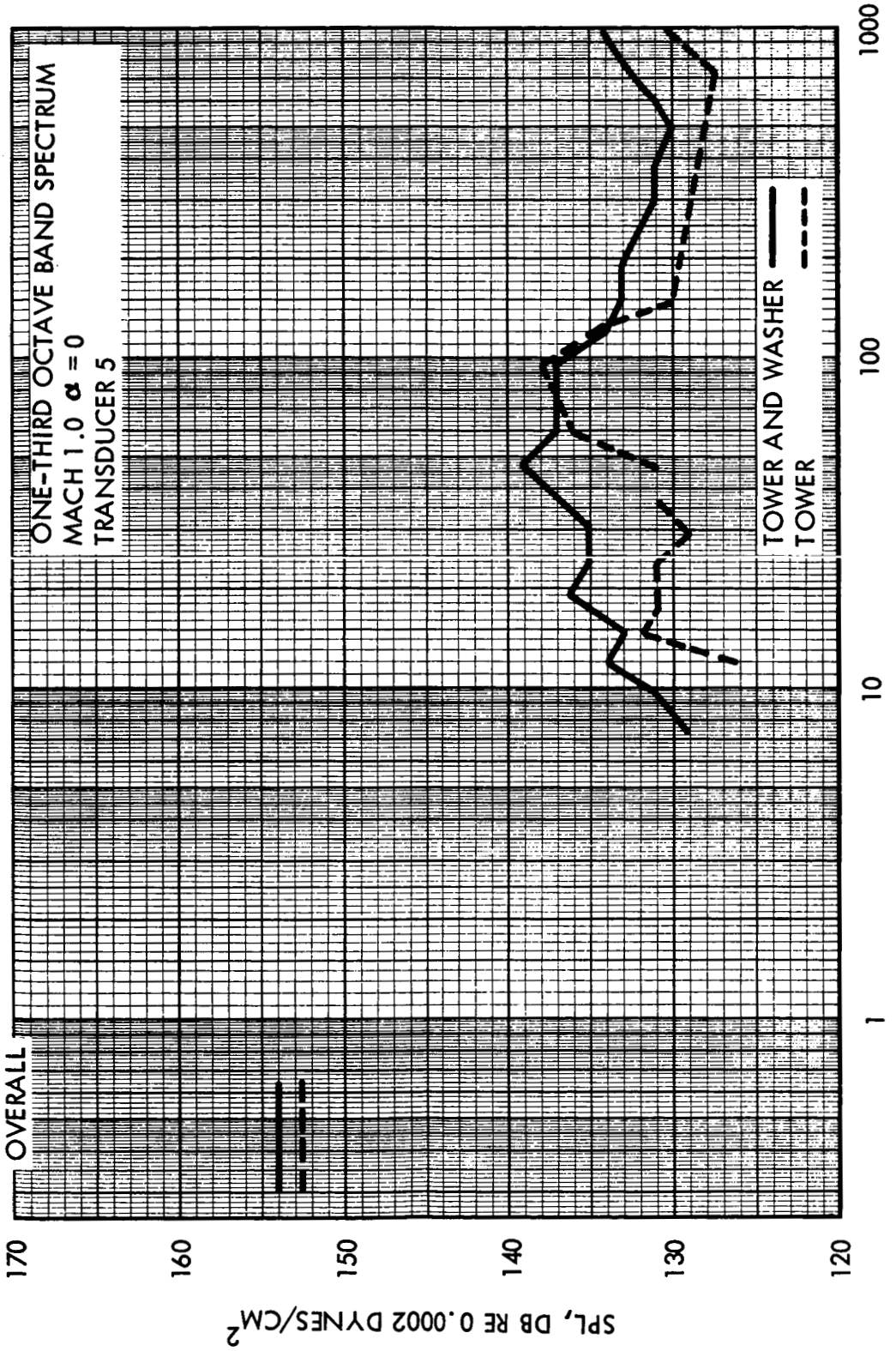

Figure 14. One-Third Octave Band Spectrums of Sound Pressure Level (M=1.0, α=0) (Sheet 5)

CONFIDENTIAL

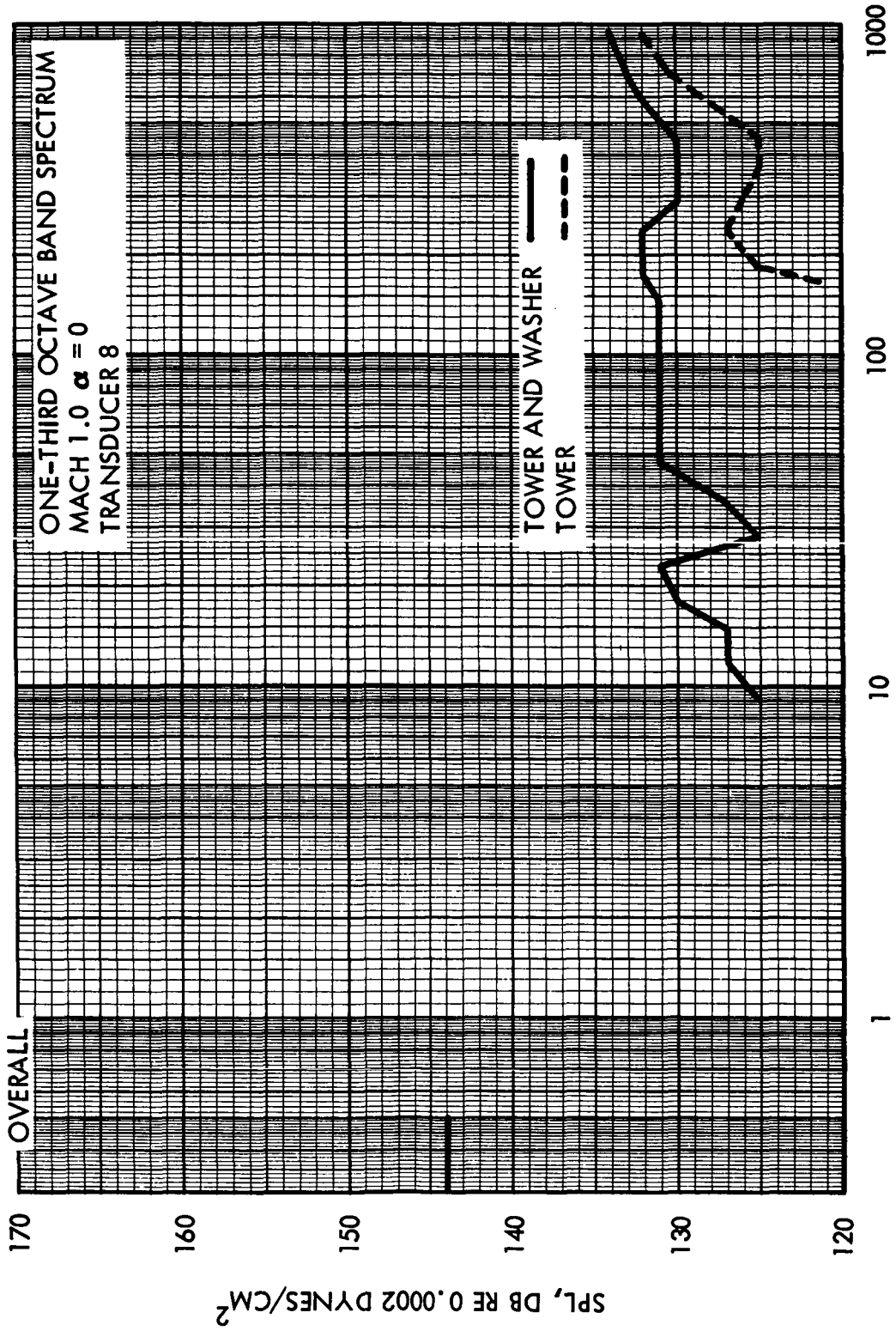

Figure 14. One-Third Octave Band Spectrums of Sound Pressure Level (M=1.0, α=0) (Sheet 6)

CONFIDENTIAL

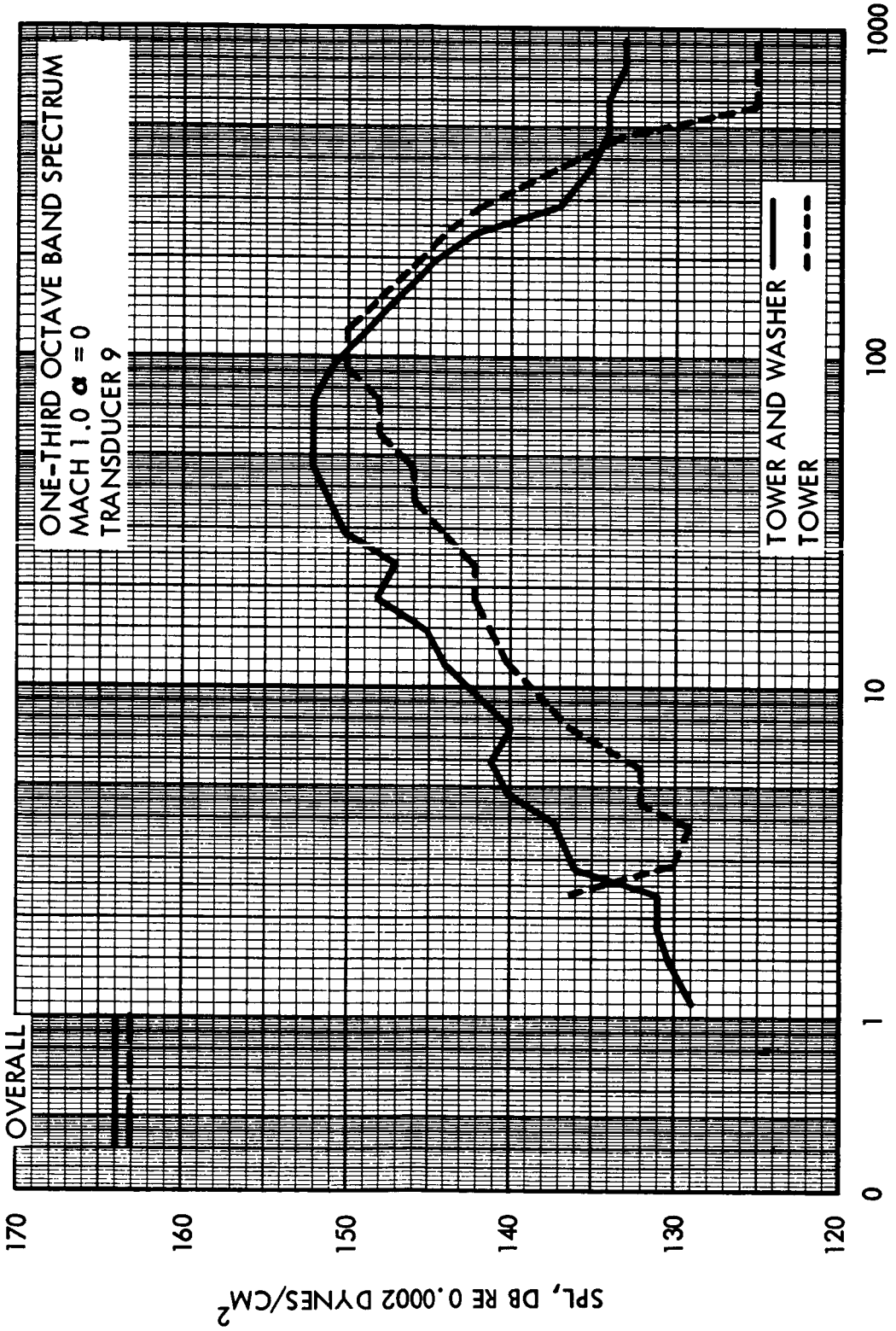

Figure 14. One-Third Octave Band Spectrums of Sound Pressure Level (M=1.0, α=0) (Sheet 7)

CONFIDENTIAL

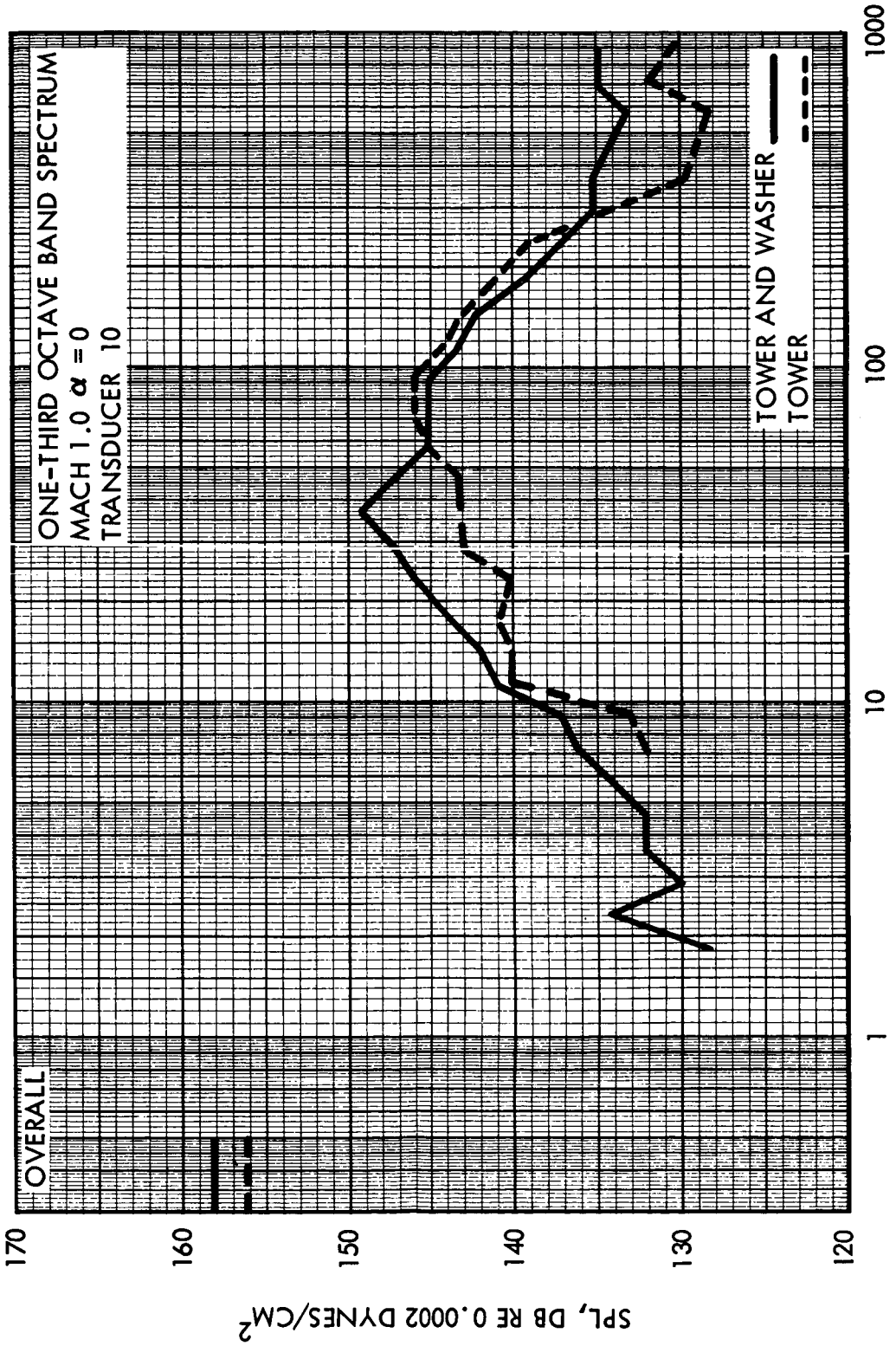

Figure 14. One-Third Octave Band Spectrums of Sound Pressure Level (M=1.0, α=0) (Sheet 8)

CONFIDENTIAL

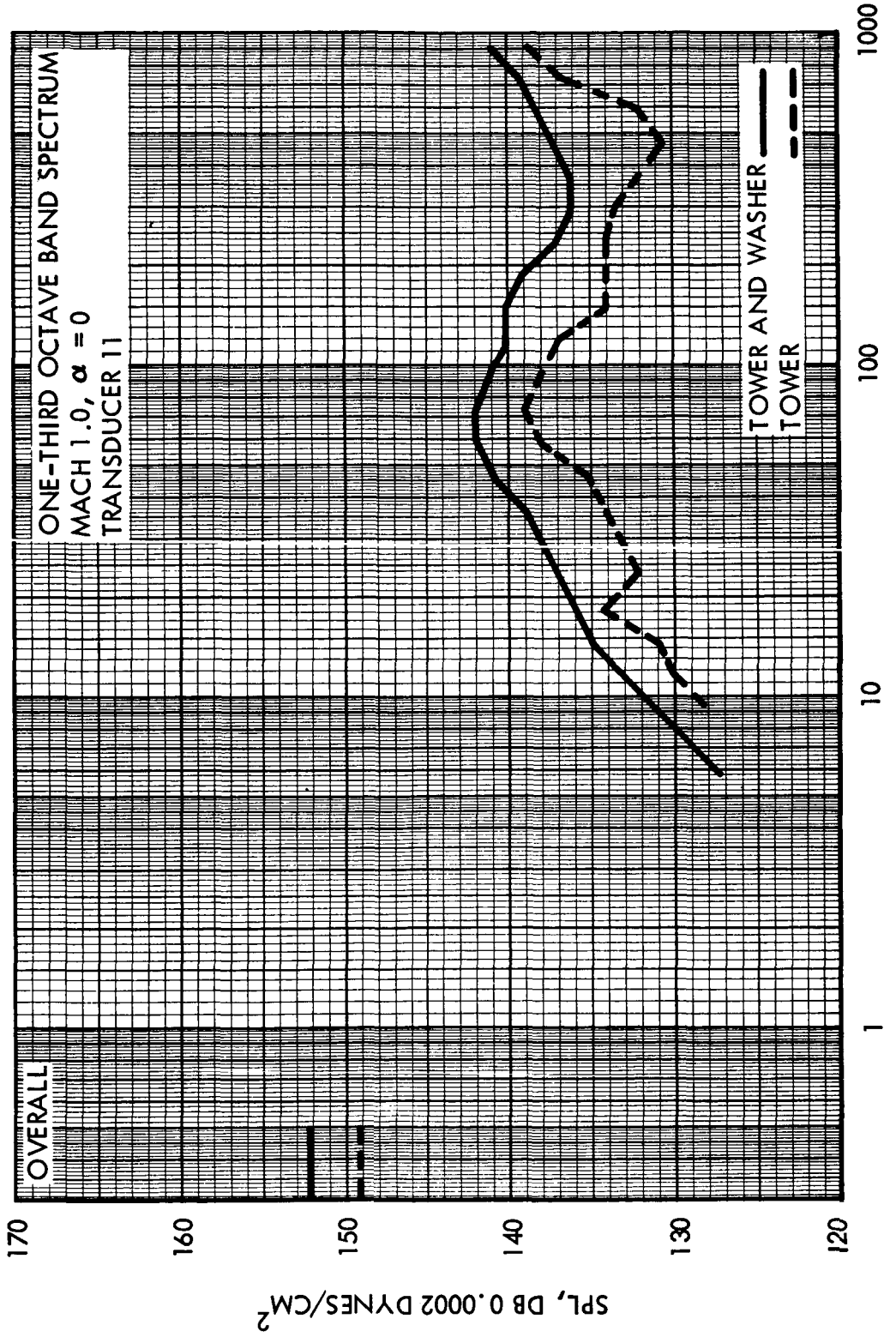

Figure 14. One-Third Octave Band Spectrums of Sound Pressure Level (M=1.0, α=0) (Sheet 9)

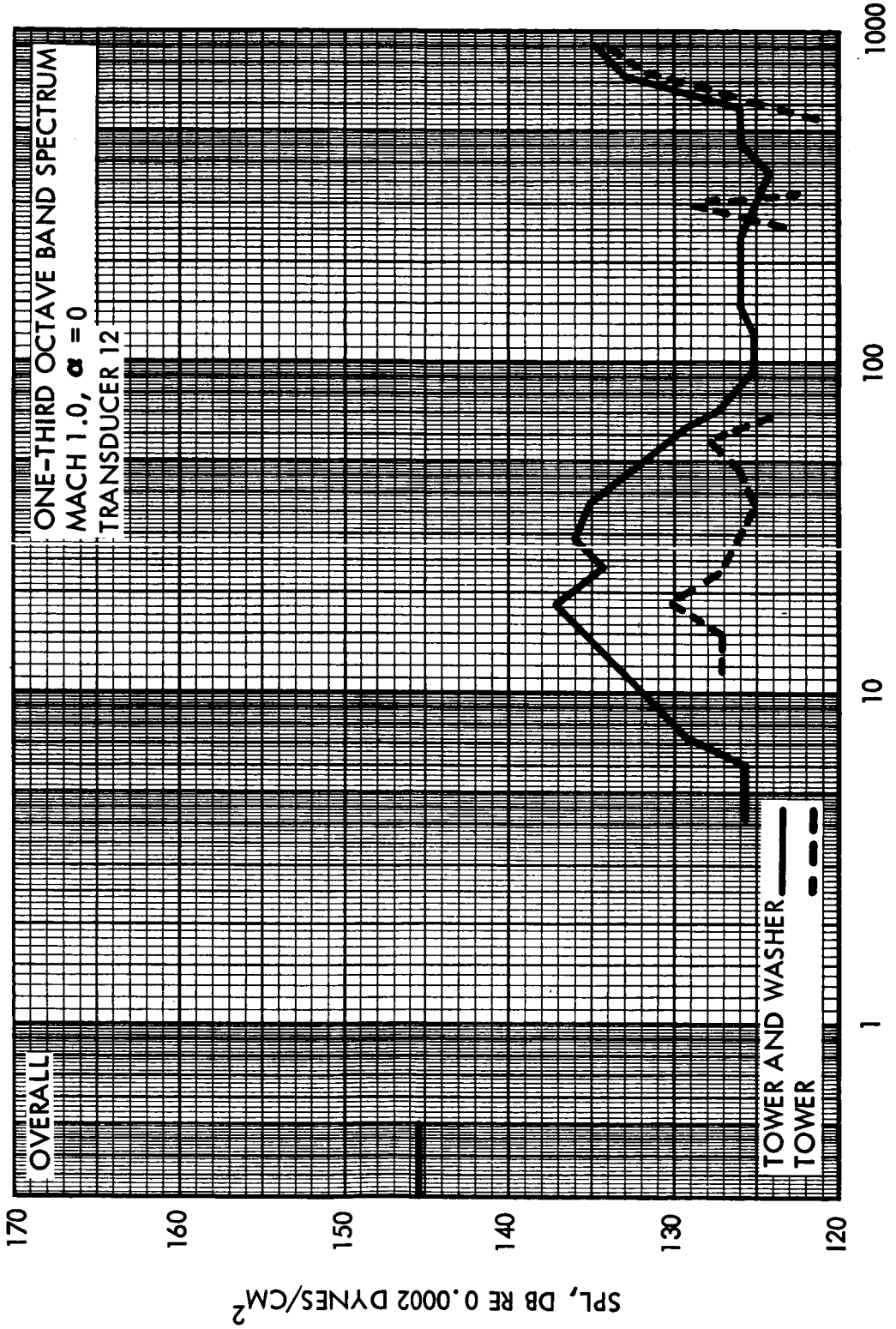

Figure 14. One-Third Octave Band Spectrums of Sound Pressure Level (M=1.0, α=0) (Sheet 10)

CONFIDENTIAL

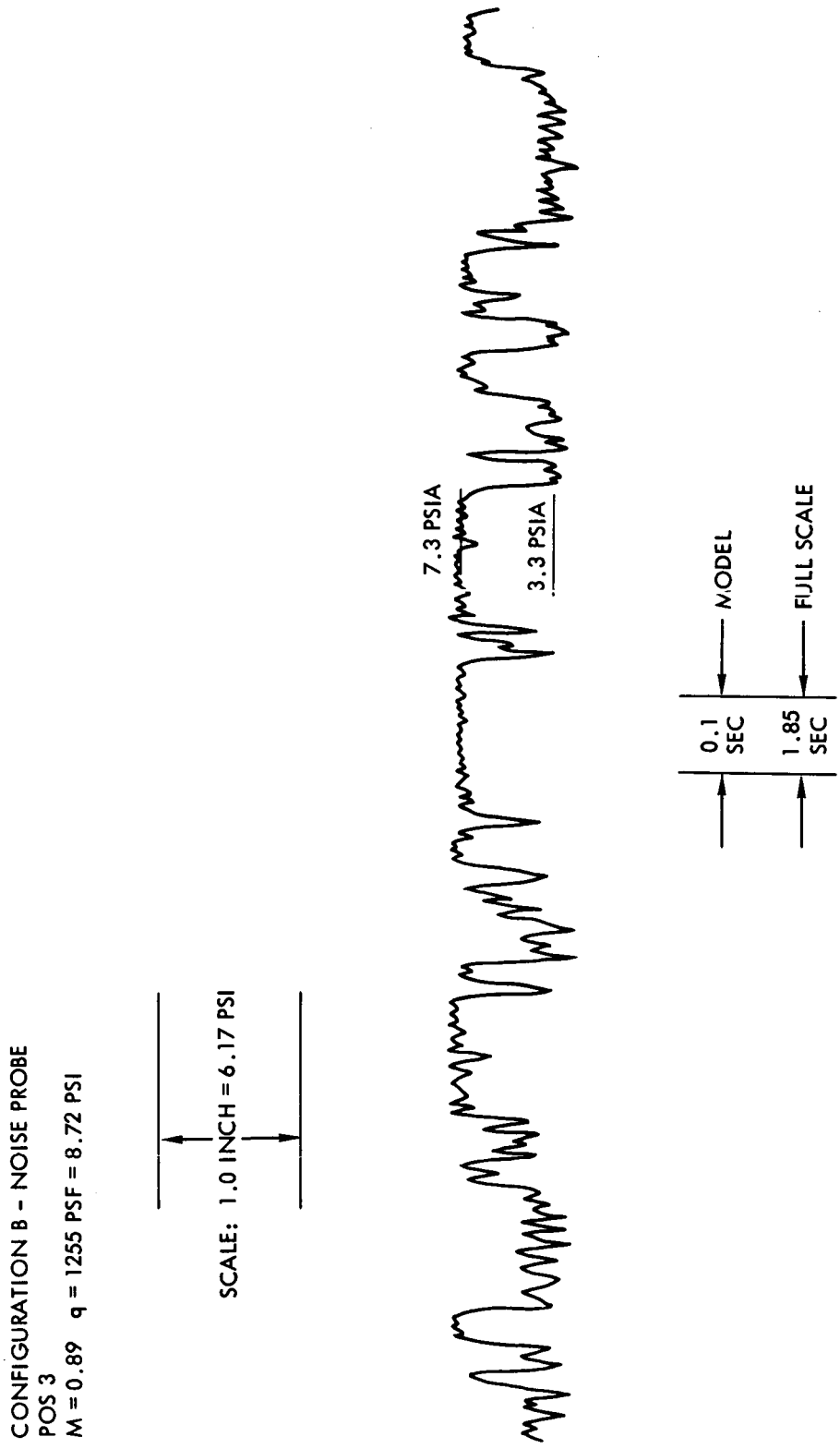

Figure 15. Typical Pressure Fluctuation Due to Boundary Layer Detachment

CONFIDENTIAL

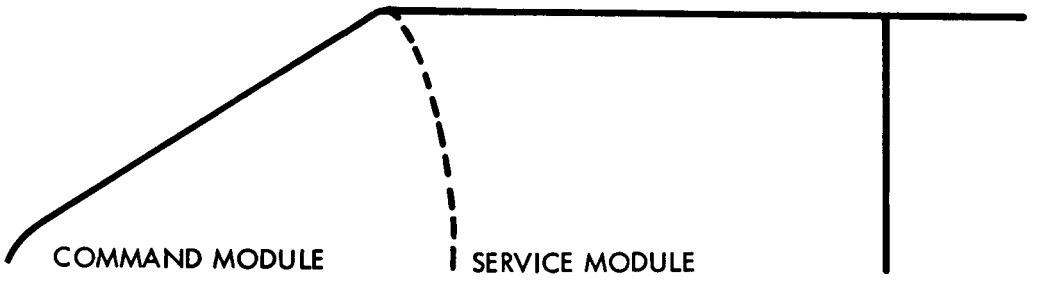

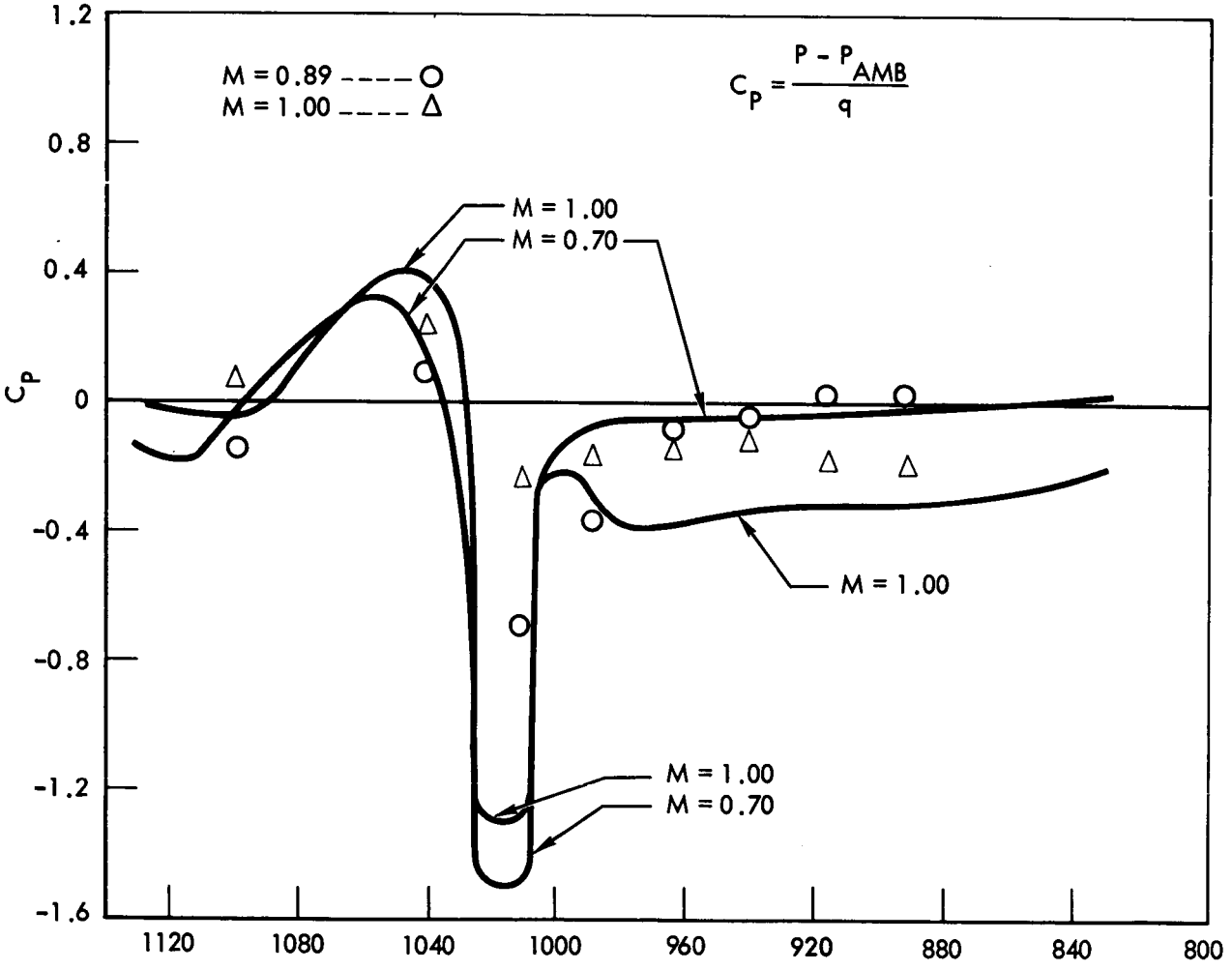

Figure 16. Static Pressure Distribution